NASA Contractor Report 2994

Application of Second-Order Turbulent Modeling to the Prediction of Radiated Aerodynamic Sound

Alan J. Bilanin and Joel E. Hirsh

NASA

NASA Contractor Report 2994

Application of Second-Order Turbulent Modeling to the Prediction of Radiated Aerodynamic Sound

Alan J. Bilanin and Joel E. Hirsh
Aeronautical Research Associates of Princeton, Inc.
Princeton, New Jersey

NASA

National Aeronautics
and Space Administration

Scientific and Technical
Information Office

1978

APPLICATION OF SECOND-ORDER TURBULENT MODELING TO THE PREDICTION OF RADIATED AERODYNAMIC SOUND

Alan J. Bilanin and Joel E. Hirsh

Aeronautical Research Associates of Princeton, Inc.
50 Washington Road, Princeton, New Jersey 08540

SUMMARY

Current formulations of the generation of aerodynamic sound by turbulence all require statistical information with regard to the turbulent flowfield. Second-order closure turbulent modeling in its present form is shown to provide some of this statistical information.

The Ribner[1] formulation of the generation of aerodynamic sound is coupled with predictions of second-order velocity correlations and integral scale to estimate the sound radiated from several complicated jet flows. In particular, it is shown that the sound radiated from a cold swirling jet is greater than from its nonswirling equal thrust counterpart.

The noise radiated from the flowfield of a multitube suppressor is estimated and compared with an equal thrust equal diameter Gaussian jet. It is shown that the multitube concept is indeed quieter.

I.   INTRODUCTION

This report describes an attempt to develop the technology required to predict the aerodynamic noise radiated from general turbulent flowfields. It is but a first attempt at an admittedly very difficult problem. The difficulties are associated with our quite limited description of turbulence. Nevertheless, it is shown that advanced turbulent transport theory, namely second-order closure turbulence theory, does indeed provide new insight into the aerodynamic sound generation problem. It is also suggested that second-order closure modeling does provide a framework or backbone upon which can be built a more complete turbulence theory, which is directly suited to be coupled with accepted formulations of the aerodynamic generation problem. The most popular of these are the theories of Ribner,[1] Lighthill,[2] Lilley[3] and most recently that of Yates.[4]

What is offered by second-order closure turbulence theory is a method of computing certain statistical turbulent quantities

under fairly general circumstances. A deficiency, in our opinion, of several models currently being used to estimate the sound radiated from a turbulent jet, is that the model utilizes turbulent assumptions or methodology which are only applicable to one fluid geometry, namely a jet. The introduction of other jets, heat or swirl, may result in the modification of the turbulence and, thereby, make predictions from these models of limited usefulness. It is for this reason that a truly uniform and general approach to computation of turbulent transport and resulting generation of aerodynamic sound is sought.

This report is organized as follows. In Section II, we argue why at least a second-order closure turbulence theory is needed to compute turbulent quantities to be utilized to estimate the aerodynamic generation of sound. In Section III, we show some predictions of turbulent properties made by second-order closure theory and comparison with data. A simple acoustic model suggested by Ribner[1] is reviewed in Section IV, and modifications and assumptions required to utilize predictions made from second-order closure theory are detailed. In Section V, predictions of the noise radiated in cold jets are given. Included here are predictions for jets which have swirl as well as a multitube jet configuration. The effect of heat and swirl on turbulent jet structures is investigated in Section VI. Finally in Section VII, conclusions are offered.

NOMENCLATURE

a_o	reference speed of sound
A	axial parameter, see Eq. (14)
b	turbulent model constant
D	jet diameter
N	swirl parameter, see Eq. (14)
P	acoustic power radiated in the ϕ direction per unit solid angle
q	r.m.s. turbulence level, $\sqrt{\overline{u_i' u_i'}}$
r, θ, z	circular cylindrical coordinate system
t	time
U_i	velocity components in a Cartesian coordinate system
u,v,w	velocity components in a r, θ, z coordinate system
r_p	radius of primary jet

v_c turbulent model constant

x_i Cartesian coordinates

α swirl angle

ρ density

π pressure

ν kinematic viscosity

Λ turbulent integral scale parameter

II. SECOND-ORDER CLOSURE TURBULENT TRANSPORT THEORY (INCOMPRESSIBLE FLOW)

Second-order turbulent closure theory is a model by which one can compute the ensemble average mean components of velocity $\overline{U}_i$, as well as the second-order turbulent velocity correlations $\overline{u_i u_i}$. The derivation of the second-order closure model is straightforward and is detailed briefly below.

The dynamics of an incompressible fluid are governed by the continuity equation and the momentum equations

$$\frac{\partial U_i}{\partial x_i} = 0 \qquad (1)$$

$$\frac{\partial U_i}{\partial t} + U_j \frac{\partial U_i}{\partial x_j} = -\frac{1}{\rho} \frac{\partial \pi}{\partial x_i} + \nu \frac{\partial^2 U_i}{\partial x_j \partial x_j} \qquad (2)$$

Assuming the velocities and pressure can be split as the sum of an ensemble average mean and a fluctuation

$$U_i = \overline{U}_i + u_i'$$

$$\pi = \overline{\pi} + p' \qquad (3)$$

there results upon substitution into Eqs. (1) and (2) and ensemble averaging

$$\frac{\partial \overline{U}_i}{\partial x_i} = 0 \qquad (4)$$

$$\frac{\partial \overline{U}_i}{\partial t} + \overline{U}_j \frac{\partial \overline{U}_i}{\partial x_j} = -\frac{1}{\rho}\frac{\partial \overline{\pi}}{\partial x_i} - \frac{\partial}{\partial x_j}\overline{u_i' u_j'} + \nu \frac{\partial^2 \overline{U}_i}{\partial x_i \partial x_j} \qquad (5)$$

equations for the mean velocity and pressure. The momentum equations, however, contain unknown second-order velocity correlations known as Reynolds stresses $-\overline{u_i' u_j'}$. Solution of Eqs. (4) and (5) cannot be attempted until a specification of $\overline{u_i' u_j'}$ is made. The essence of first-order closure, K theory or eddy viscosity theory is an attempt to specify $\overline{u_i' u_j'}$ as a function of mean flow gradients and mean flow length scales.

Second-order closure theory derives independent equations for these second-order velocity correlations. The procedure for doing this is as follows. The splitting of variables into mean and fluctuation is substituted into Eq. (2), and Eq. (5) is subtracted from this result. The remainder is then multiplied by u_j' and ensemble averaged. The above procedure is then repeated interchanging i for j and then it can be shown that the second-order velocity correlations must satisfy

$$\frac{\partial}{\partial t}\overline{u_i' u_j'} + \overline{U}_k \frac{\partial}{\partial x_k}\overline{u_i' u_j'} = \underbrace{-\overline{u_i' u_k'}\frac{\partial \overline{U}_j}{\partial x_k} - \overline{u_j' u_k'}\frac{\partial \overline{U}_i}{x_k}}_{\text{production}}$$

$$\underbrace{-\frac{\partial}{\partial x_k}(\overline{u_k' u_i' u_j'}) - \frac{1}{\rho}\left(\frac{\partial \overline{u_i' p}}{\partial x_j} + \frac{\partial \overline{u_j' p}}{\partial x_i}\right)}_{\substack{\text{velocity and pressure} \\ \text{diffusion}}}$$

$$+ \underbrace{\nu \frac{\partial^2 \overline{u_i' u_j'}}{\partial x_k^2}}_{\substack{\text{viscous} \\ \text{diffusion}}} + \underbrace{\overline{\frac{p'}{\rho}\left(\frac{\partial u_i'}{\partial x_j} + \frac{\partial u_j'}{\partial x_i}\right)}}_{\substack{\text{pressure strain} \\ \text{correlation}}}$$

$$\underbrace{- 2\nu \overline{\frac{\partial u_i'}{\partial x_k}\frac{\partial u_j'}{\partial x_k}}}_{\text{dissipation}} \qquad (6)$$

Note now that there appears third-order and some second-order correlations which themselves need independent equations. In principle third-order correlation equations could be developed but the spirit of second-order closure is to model these third-order

4

and second-order correlations in terms of known second-order correlations. The success of the second-order theory is dependent upon two assumptions:

1. The Reynolds stress equations are not extremely sensitive to inaccuracies introduced by the replacement of exact terms with modeled ones.

2. Reasonable physically motivated models can be developed for the terms which must be replaced.

These assumption are apparently justified, since it has been demonstrated over the years that the second-order closure model has predicted turbulent transport in a variety of high Reynolds number flowfields. The details of the modeling as well as comparisons of the turbulent model with data may be found in Ref. 5. Here, we simply give the terms to be modeled and the terms which replace them.

Pressure - velocity diffusion

$$- \frac{\partial}{\partial x_k} \overline{u_k' u_i' u_j'} - \frac{1}{\rho} \left(\frac{\partial \overline{u_i' p}}{\partial x_j} + \frac{\partial \overline{u_j' p}}{\partial x_i} \right) = v_c \frac{\partial}{\partial x_k} \left(q \Lambda \frac{\partial \overline{u_i' u_j'}}{\partial x_k} \right) \quad (7)$$

where v_c has been determined to be 0.3, $q = \overline{u_i' u_i'}$ and Λ is the turbulent macroscale or integral scale variable.

Pressure strain correlation

$$\overline{\frac{p'}{\rho} \left(\frac{\partial u_i'}{\partial x_j} + \frac{\partial u_j'}{\partial x_i} \right)} = \frac{q}{\Lambda} \left(\overline{u_i' u_j'} - \delta_{ij} \frac{q^2}{3} \right) \quad (8)$$

where this term contains the mechanisms by which the energy components attempt to redistribute energy between themselves.

Dissipation

$$\nu \overline{\frac{\partial u_i'}{\partial x_k} \frac{\partial u_j}{\partial x_k}} = \delta_{ij} \frac{bq^3}{3\Lambda} \quad (9)$$

where b has been determined to be equal to 0.125. The dissipation here is for high Reynolds numbers and is assumed to be isotropic. Upon substitution of these modeled terms the equations governing the dynamics of the second-order correlations become

5

$$\frac{\partial \overline{u_i' u_j'}}{\partial t} + \overline{U}_k \frac{\partial \overline{u_i' u_j'}}{\partial x_k} = - \overline{u_i' u_k'} \frac{\partial \overline{U}_j}{\partial x_k} - \overline{u_j' u_k'} \frac{\partial \overline{U}_i}{\partial x_k}$$

$$+ \nu_c \frac{\partial}{\partial x_k} q\Lambda \frac{\partial \overline{u_i' u_j'}}{\partial x_k} - \frac{q}{\Lambda}\left(\overline{u_i' u_j'} - \delta_{ij}\, \frac{q^2}{3}\right)$$

$$+ \nu \frac{\partial^2 \overline{u_i' u_j'}}{\partial x_k^2} - \delta_{ij}\, \frac{2bq^3}{3} \qquad (10)$$

The turbulent integral scale parameter Λ is determined from

$$\frac{\partial \Lambda}{\partial t} + \overline{U}_k \frac{\partial \Lambda}{\partial x_k} = -1.8\, \frac{\Lambda}{q^2}\, \overline{u_i u_k} \frac{\partial \overline{U}_i}{\partial x_k} + 0.6\, q$$

$$+ \nu_c \frac{\partial}{\partial x_k}\left(q\Lambda \frac{\partial \Lambda}{\partial x_k}\right) - \frac{0.375}{q}\left(\frac{\partial q\Lambda}{\partial x_k}\right)^2 \qquad (11)$$

The details of the derivation of this relationship is given in Ref. 5.

Equations (4), (5), (10) and (11) along with appropriate boundary conditions are then solved numerically for the quantities $\overline{U}_i$, $\overline{u_i' u_j'}$ and Λ .

Before proceeding to obtain solutions for turbulent flowfields relevant to the aerodynamic sound generation problem, we can show that second-order closure turbulent modeling does contain physics that might be lost in K or eddy viscosity theories. We do this by asking if second-order closure can be simplified under some limiting process to define an eddy viscosity model. The conditions under which an eddy viscosity can be expected to be valid have been argued by Donaldson.[6] Briefly, eddy viscosity concepts are restricted to high Reynolds number flows, where second-order correlations can track their equilibrium values, and the effects of diffusion of correlations can be neglected. If we now consider a nonspreading cylindrical jet with swirl, where the coordinates are r, θ, z with velocity components u, v, w , with $\overline{U} = 0$, $\overline{V} = \overline{V(r)}$ and $\overline{W} = \overline{W(r)}$ and take the high Reynolds number, nondiffusive superequilibrium limit of Eq. (10), there results

$$4\overline{uv}\tilde{V} - \frac{q}{\Lambda}\left(\overline{uu} - \frac{1}{3}q^2\right) - \frac{2bq^3}{3\Lambda} = 0$$

$$2\tilde{V}(\overline{vv} - \overline{uu}) - r\overline{uu}\frac{\partial\tilde{V}}{\partial r} - \frac{q}{\Lambda}\overline{uv} = 0$$

$$2\tilde{V}\tilde{v}\tilde{w} - \frac{\overline{uu}}{r}\frac{\partial W}{\partial r} - \frac{q}{\Lambda}\tilde{u}\tilde{w} = 0$$

$$-4\tilde{V}\overline{uv} - 2r\overline{uv}\frac{\partial\tilde{V}}{\partial r} - \frac{q}{\Lambda}\left(\overline{vv} - \frac{1}{3}q^2\right) - \frac{2bq^3}{3\Lambda} = 0$$

$$-2\tilde{V}\tilde{u}\tilde{w} - \frac{\overline{uv}}{r}\frac{\partial W}{\partial r} - r\tilde{u}\tilde{w}\frac{\partial V}{\partial r} - \frac{q}{\Lambda}\tilde{v}\tilde{w} = 0$$

$$-2r\tilde{u}\tilde{w}\frac{\partial W}{\partial r} - \frac{q}{\Lambda}\left(\overline{ww} - \frac{1}{3}q^2\right) - \frac{2bq^3}{3\Lambda} = 0 \qquad (12)$$

where $\tilde{V} = V(r)/r$, $\tilde{W} = W(r)/r$, $\tilde{u}\tilde{w} = \overline{uw}/r$ and $\tilde{v}\tilde{w} = \overline{vw}/r$.
Assume the velocity correlations are of the form

$$\overline{u_i u_j} = \Lambda^2 \left(r\frac{\partial\tilde{V}}{\partial r}\right)^2 U_i U_j \qquad (13)$$

where $U_i U_j$ is a dimensionless number (turbulent correlation
coefficient). Then, substituting into Eq. (12) yields a nonlinear
system of algebraic equations for $U_i U_j$. The solution of this
system is dependent upon two parameters

$$N = \frac{\tilde{V}}{\left(r\frac{\partial\tilde{V}}{\partial r}\right)} \qquad \text{the swirl parameter}$$

$$A = \frac{\frac{\partial W}{\partial r}}{\left(r\frac{\partial\tilde{V}}{\partial r}\right)} \qquad \text{the axial parameter} \qquad (14)$$

Solutions for $QQ = U_i U_i$ are shown in Fig. 1. Values of $QQ < 0$
denote regions where turbulence is damped. With no swirl , $N = 0$
and it may be shown that $q^2 = 2\Lambda^2 (\partial W/\partial r)^2$ and, therefore, axial
shear is always destabilizing. This analysis[7] has been used pre-
viously to explain the laminar central region in aircraft vortices.
It has been shown that the swirl can in fact suppress the produc-
tion of turbulence in the viscous core, thereby reducing the dis-
persal of smoke which is seeded into the vortex for visualization
purposes.

As can be seen, the turbulent velocity correlation coefficient
which is related to the eddy viscosity has a strong dependence on
the parameters A and N which in turn are functions of mean flow
gradients. It would appear unlikely that the functional form of
an eddy viscosity could be chosen to include flow stability without

7
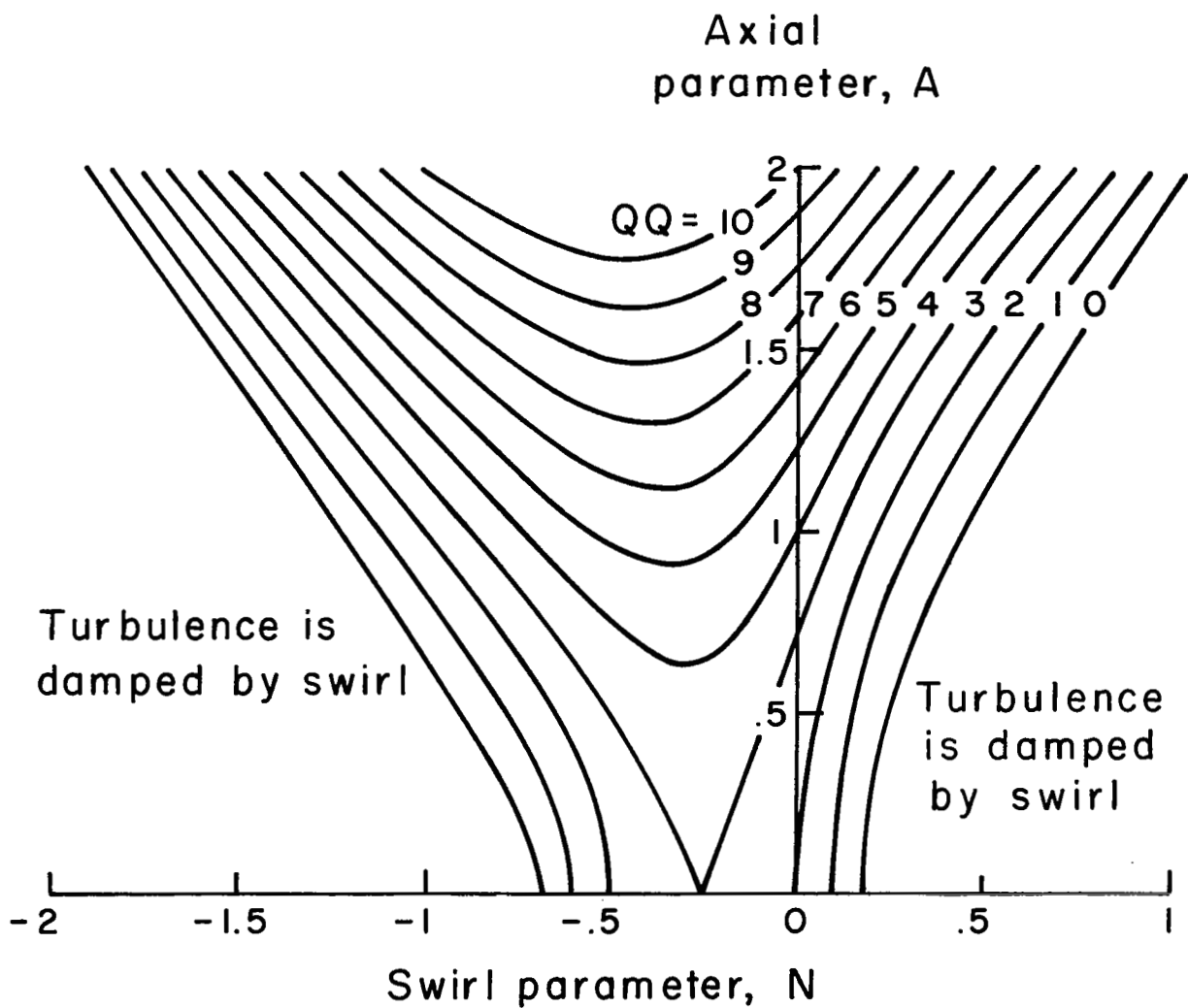
Figure 1. Isopleths of constant QQ showing the dependence on

$$N = \tilde{V}\Big/\Big(r\,\frac{\partial \tilde{\tilde{V}}}{\partial r}\Big) \quad \text{and} \quad A = \frac{\partial W}{\partial r}\Big/\Big(r\,\frac{\partial \tilde{V}}{\partial r}\Big) \quad (\text{Ref. 7})$$

resorting to a second-order closure model initially. It is to be expected, based on the results shown in Fig. 1, that when swirl is added to a jet significant changes in jet structure will result.

Second-order turbulent modeling provides a method to compute the evolution of turbulent flowfields. Flow variables which are obtained are the mean velocity components as well as the second-order velocity correlations and the turbulent macroscale parameter Λ. In the next section, we will show a comparison between predictions made by the second-order closure model and measured turbulent data.

III. COMPARISON WITH JET DATA

Over the years several computer codes have been developed to solve the second-order closure model equations for various flow geometries. Here, we will present results from TDV (three-dimensional vortex) a code developed by Sullivan[8] to compute the decay of an axisymmetric vortex. The streamwise direction is z which is the marching direction, and r is the radial coordinate. We will use the code to predict the evolution of an axisymmetric turbulent jet and make comparisons with Wygnanski and Fiedler[9] data.

At $z = 0$ the axial velocity profile was taken to be a Gaussian and the code was run with the axial velocity held fixed until the second-order velocity correlations establish themselves. The integral scale parameter Λ was taken to be constant during this time. The mean variables were then unlocked and solutions were computed to 112 diameters downstream. Figures 2-7 display second-order closure results compared with Wygnanski and Fiedler data and other theoretical results.

The mean axial velocity distribution across the jet is shown in Fig. 2, at $z = 42$ and 57 diameters downstream of the nozzle. The Wygnanski and Fiedler data is presented as a composite of this data at $z = 40$, 50 and 60 diameters, since all of this data falls on the same solid curve. The velocity scale in this figure is the maximum axial velocity in each axial station and the abscissa is the distance from the axis of symmetry normalized by the distance from the nozzle. The agreement with the Wygnanski and Fielder data is excellent except at values of $r/z > 0.15$. This error is due to the fact that the computational procedure requires that the solution asymtote to a small but finite value of W as $r \to \infty$. In the calculation shown in Fig. 2, this value was taken to be W/W_{max} ($z = 0$) = 0.005. A calculation with W/W_{max} ($z = 0$) asymptoting to 0.02 as $r \to \infty$ gave an error approximately four times as large for $r/z > 0.15$ but excellent agreement for $r/z < 0.15$.

The variation of the fields with downstream distance is
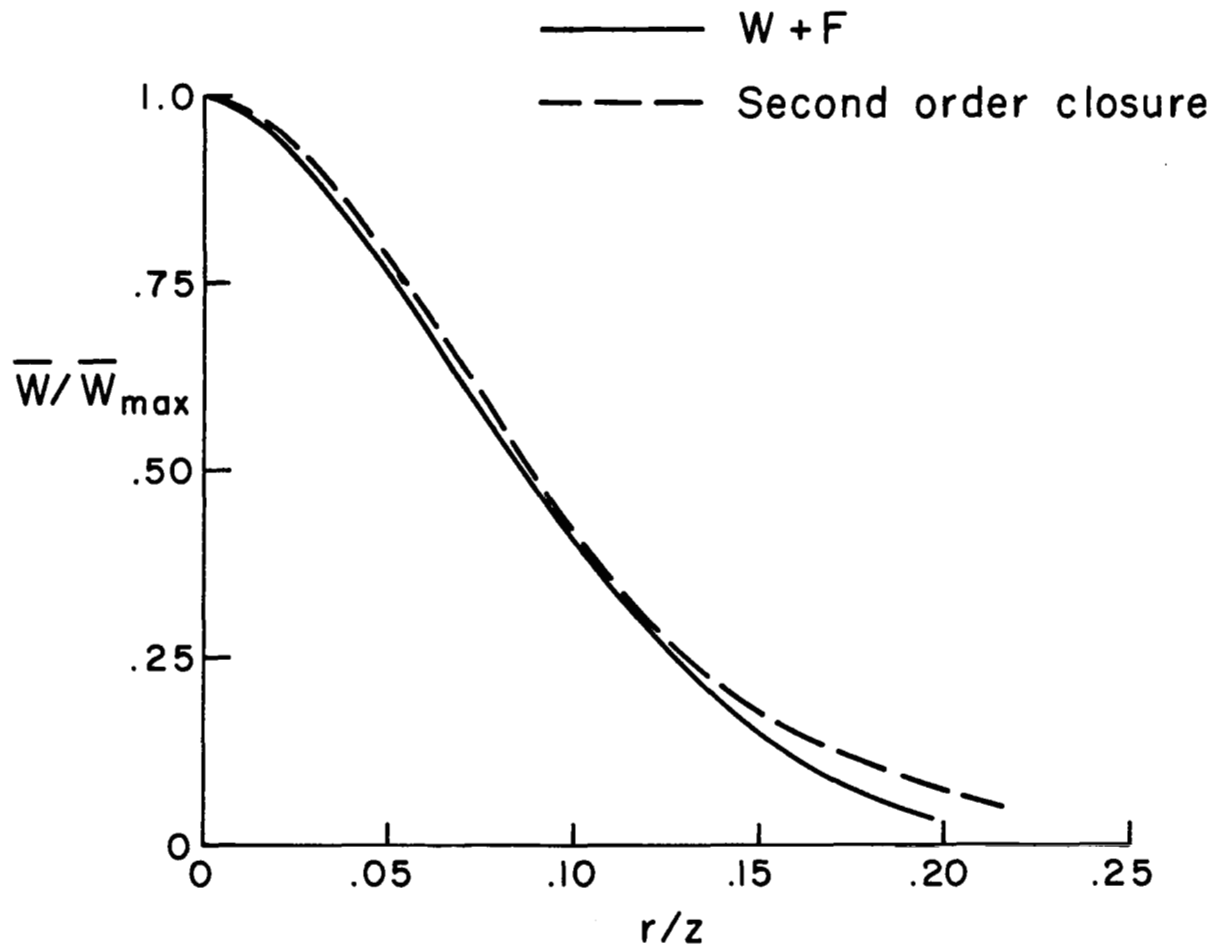
Figure 2. Mean axial velocity profile ——— W & F composite data (z/D = 40, 50, 60),   ---- Second-order closure composite data (z/D = 42, 57)

shown in Fig. 3. Again, the theoretical results are in good agreement with the data.

Figures 4-7 display the radial distribution of the various turbulent intensities at various stations downstream. In addition, Fig. 4 displays measurements of Corrsin and Uberoi[10] at z/D = 20 . Wygnanski and Fiedler attribute the 25% disagreement between their measurements and Corrsin and Uberois to: (i) the fact that at z/D = 20 the flow was not yet self-preserving,and (ii) the poorer response of the equipment used by Corrsin. The results of the present study are in significantly better agreement with those of Wygnanski and Fiedler in the midrange of r/z . For r/z > 0.15 , the major part of the disagreement is most likely due to the asymptotic condition on W as discussed above.

In general, model predictions at least for this simple flowfield are in general agreement with measured data. Additional comparisons may be found in Ref. 5.

<div align="center">IV.   COUPLING TURBULENT JET STRUCTURE
TO AN ACOUSTIC MODEL</div>

We have chosen to use the Ribner and equivalent Lighthill formulation which models the sound radiated from a turbulent flow. Other competing models exist and our choice has been made solely on the grounds that the formalism behind this model is generally understood in the acoustic community.

The acoustic power radiated in the ϕ direction per unit solid angle from an elemental volume of turbulence located at $\vec{y}$ is

$$P(\phi,y) = \frac{1}{16\pi^2 \rho_o a_o^5} \int \frac{\partial^4}{\partial \tau^4} R_x(\phi,\vec{y},\vec{\xi},\tau) \, d\vec{\xi} \tag{15}$$

where

$$R_x(\phi,\vec{y},\vec{\xi},\tau) = \overline{\rho}^2 \, [\overline{u_x^2 u_x'^2} + 4 U_x U_x' \, \overline{u_x u_x'} + \text{other terms}] \tag{16}$$

U_x is the time mean velocity component in the $\vec{x}$ direction and u_x is the fluctuating component. The primed variables denote the point $\vec{y} - \vec{\xi}/2$ at time t and the unprimed denotes the point $\vec{y} + \vec{\xi}/2$ at time $t + \tau$. The omitted terms are argued to be either zero upon time differentiation or small. At this point, Ribner introduced the assumptions of isotropy and homogeneity of turbulence within a correlation volume in order to make further progress. These assumptions are not necessary, however, since
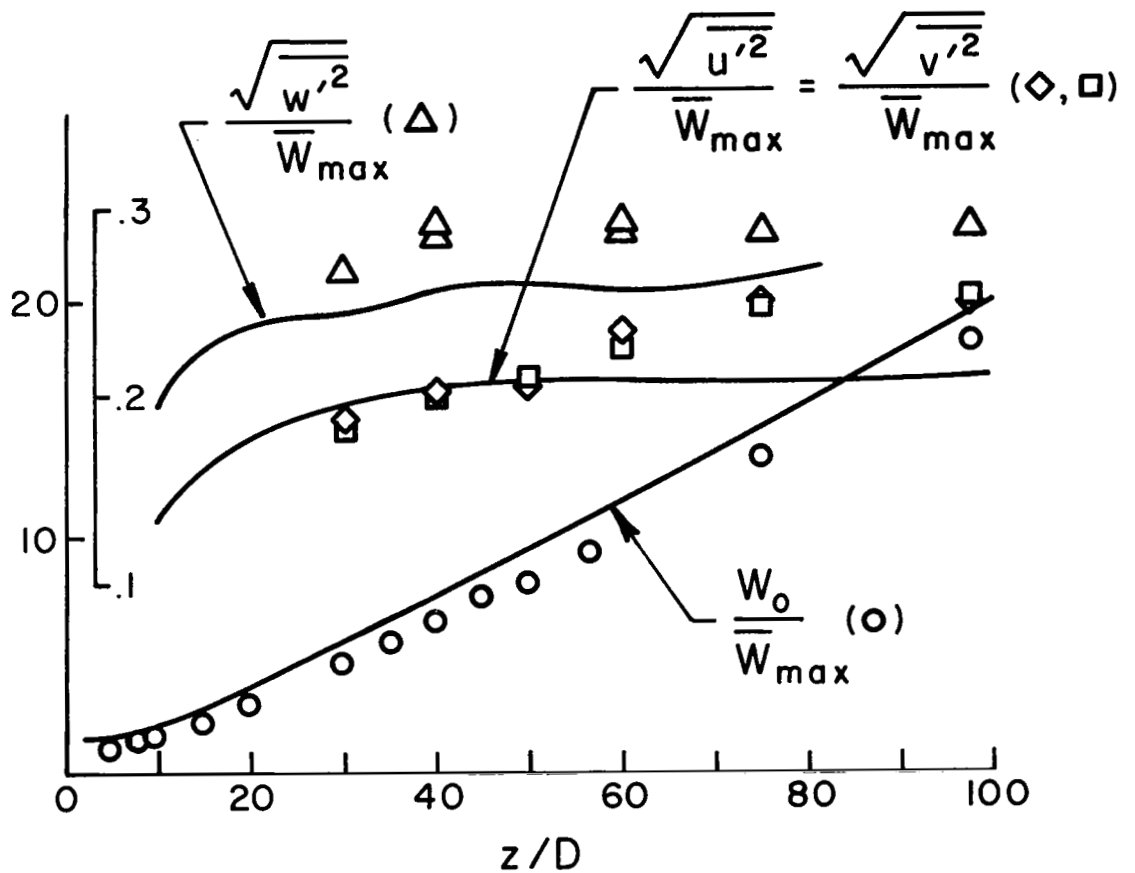
Figure 3. Variation of mean axial velocity and turbulent
intensities along the jet. Wygnanski & Fiedler
data: single data points, present study: solid
line

.3

.2

$\dfrac{\sqrt{\overline{w'^2}}}{\overline{W}_{max}}$

.1

0

0   .05   .10   .15   .20   .25

r/z

$\dfrac{z}{D} =$
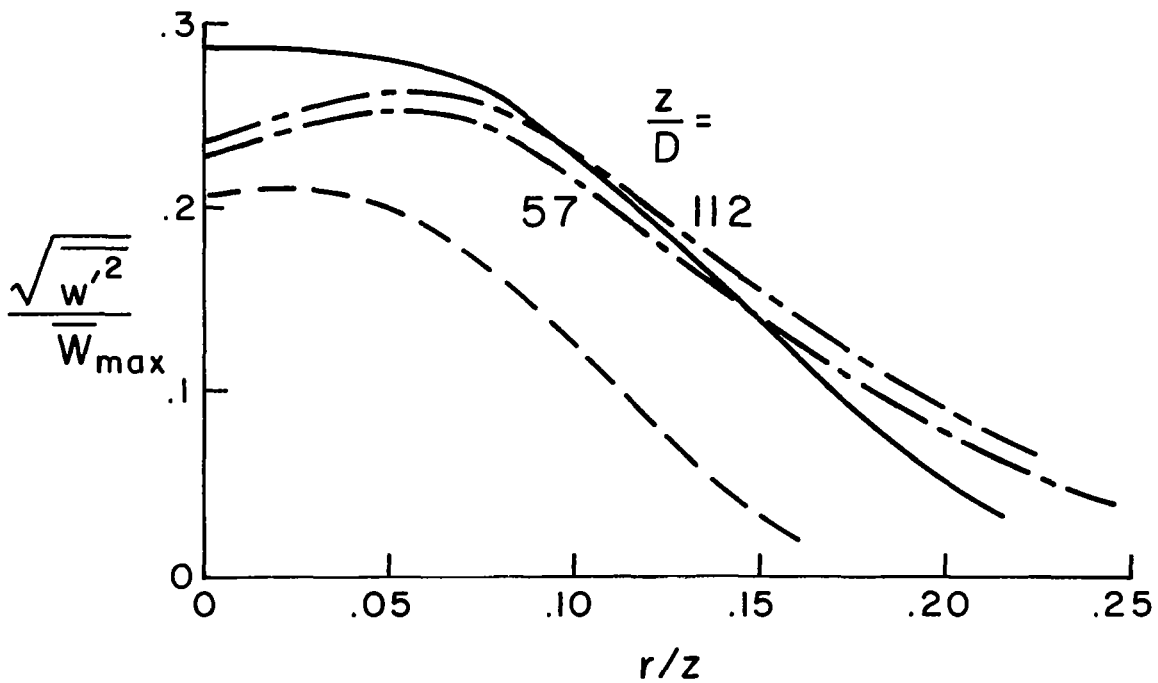
57   112

Figure 4.   Intensity of $\sqrt{\overline{w'^2}}$ fluctuation across the jet.
--- , Corrsin, z/D = 20 ; —— Wygnanski &
Fiedler composite data z/D = 50 , 60 , 75 ;
-·-·- ; present study z/D = 57 , 112
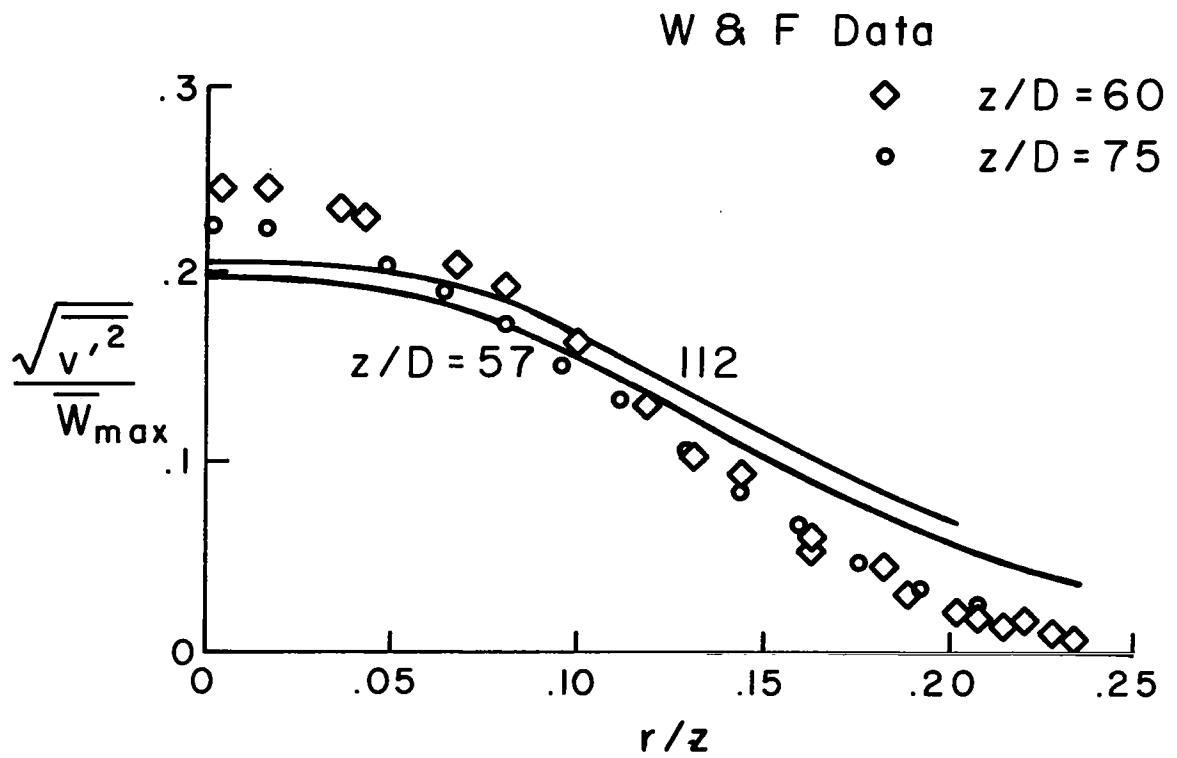
Figure 5. Intensity of $\sqrt{\overline{v'^2}}$ across the jet. Wygnanski & Fiedler data: single points. Present study: solid line
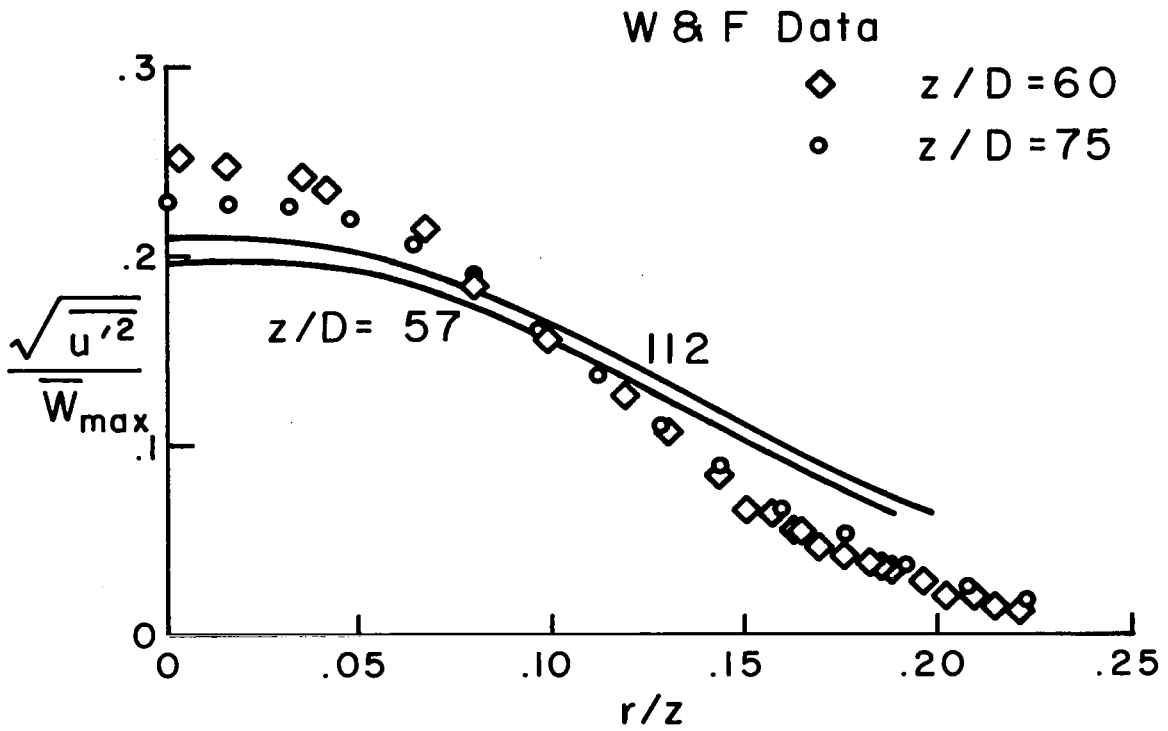
Figure 6. Intensity of $\sqrt{\overline{u'^2}}$ across the jet. Wygnanski & Fiedler data: single points. Present study: solid line
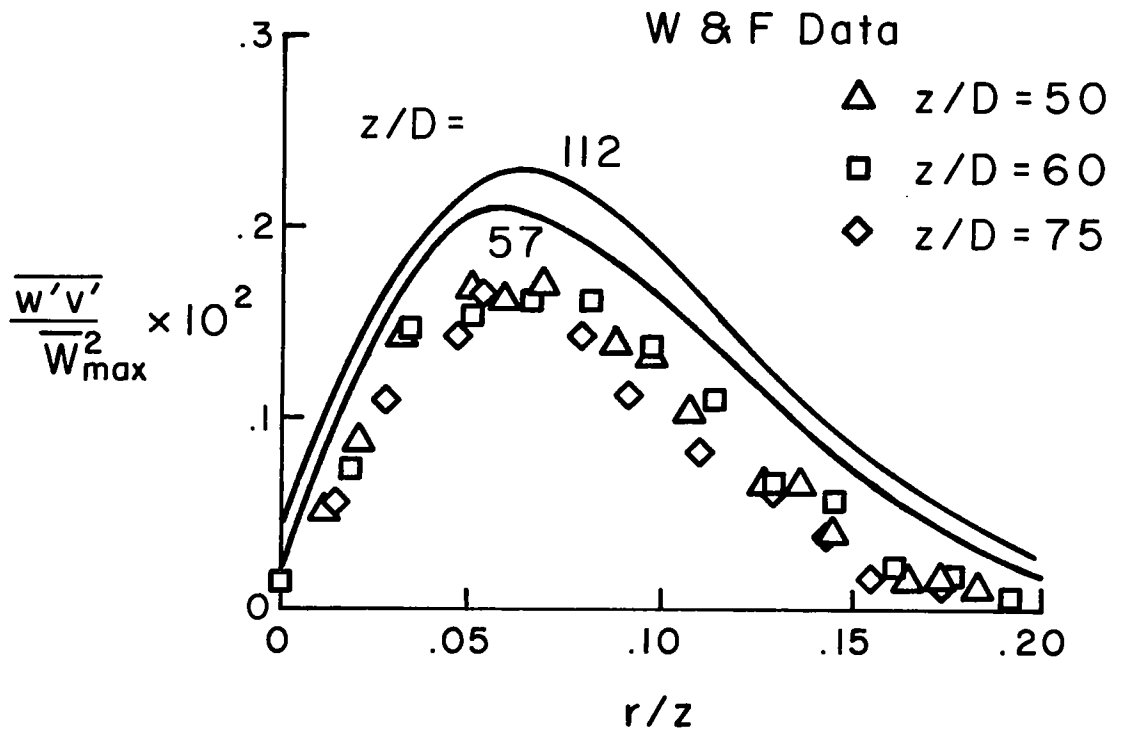
Figure 7. Intensity of $\overline{w'v'}$ across the jet. Wygnanski & Fiedler data: single points. Present study: solid line

second-order closure modeling predicts both anisotropy and inhomogeneity. At this point, however, we have chosen not to alter the basic Ribner analysis, so that the acoustic model will remain simple. It is suggested, however, that future efforts should utilize the full power of second-order closure. Requiring that the joint probability density is Gaussian yields that

$$\overline{u_x^2 u_x'^2} = \overline{u_1^2}^2 + 2R_1^2 \tag{17}$$

where $R_1 = \overline{u_x u_x'} = \overline{u_1 u_1'}$. Utilizing results from the isotropic theory of turbulence, it was suggested that

$$R_1(\vec{\xi}, \tau) = \overline{u_1^2} \ [1 - \pi \xi^2 / \Lambda^2 + (\pi \xi_1^2 / \Lambda^2)] \ \exp(-\pi \xi^2 / L^2 - \omega_f \tau) \tag{18}$$

where Λ is the integral scale length of the turbulence and ω_f is the inverse turbulent correlation time scale. Substituting R_1 into (17), and (17) into (15) yields

$$P(\phi, y) = \frac{\Lambda^3 \omega_f^4}{\pi^2 \rho_0 a_0^5} \left[\frac{2}{9}^{-3/2} q^4 - \frac{\Lambda g^2}{96} W \frac{\partial W}{\partial r} (\cos^2 \phi + \cos^4 \phi) \right] \cdot C \tag{19}$$

after carrying out the time differentiation and the integration over ξ and setting $\tau = 0$. Also, we have approximated

$$U_x U_x' = W^2(\vec{y}) + W \left. \frac{\partial W}{\partial r} \right|_y \sqrt{\xi_2^2 + \xi_3^2} \tag{20}$$

The convective factor C is given by

$$C = \left[(1 - \frac{W}{a_0} \cos\phi)^2 + \frac{\omega_f^2 \Lambda^2}{\pi a_0^2} \right]^{-5/2} \tag{21}$$

and has been added by Ribner after the fact to account for the eddy motion down the jet. The equation is yet to be integrated over y. This is accomplished numerically in our turbulent code. What remains to be done is to argue the functional form of ω_f. Second-order closure in its present form makes no direct prediction of ω_f but we argue that the turbulent correlation time scale should be proportional to L/q where L is a characteristic turbulent scale. We, therefore, assume

$$\omega_f = L/q \tag{22}$$

Now L is taken to be proportional to our turbulent macroscale parameter Λ so that $L = k\Lambda$.

Our strategy now is to determine k from data and then use Eq. (19) to make predictions of sound power radiated for more complicated flowfields. We have chosen to use Lush[11] data to make this calibration. Shown in Fig. 8, is a comparison of directivity as a function of emission angle for three jet velocities. It is suggested that $k = 0.5$ gives a best fit to the data. One does expect, as a consequence of the incompressible turbulence model and assumptions implicit in the acoustic model, that discrepancies will occur as jet Mach number approaches one from below. We have, therefore, biased our selection of k to give better agreement at the lower jet velocities. Equation (19) with the second-order closure model will now be used to make predictions of directivity and total sound power radiated from more complicated jet flowfields.

V. NOISE ESTIMATES FROM COLD JETS

In this section the noise radiated from several cold jets are estimated using the models described in Sections II and III.

Recently Lu, Ramsay and Miller[12] have made measurements of the noise radiated from a swirled and nonswirled model jet. We have attempted to numerically simulate their experiment and predict the total sound power radiated. In Fig. 9 is shown the measured swirl angle as a function of radius as well as the measured velocity profile at 2 jet diameters downstream. The dashed curves are the predicted distributions. Unfortunately, Lu et al. have not presented any measurements made further downstream. To make this comparison we have run TDV in a pipe, so that the initial conditions at $z/D_j = 0$ are those appropriate to a fully developed pipe flow. Then this mean velocity axial distribution was altered by

$$\overline{W} = \cos\alpha \ \overline{W}_{pipe}(r)$$

$$\overline{V} = \sin\alpha \ \overline{W}_{pipe}(r) \tag{23}$$

where α is the swirl angle measured at $z = 0$. The predicted profiles are shown in Fig. 10. We also present the results of the calculation where the mean axial flow was not swirled in Fig. 11. One obvious difference is the rate of decay of the maximum axial velocity as a function of downstream distance. This variation is shown plotted in Fig. 12. In general, it is also shown that the turbulent kinetic energy at equal downstream stations is higher in the jet which is swirled. This, of course, explains the more rapid aging of the swirled vs. the nonswirled case. We have estimated the thrust loss in the swirled case to be about 3%.

18
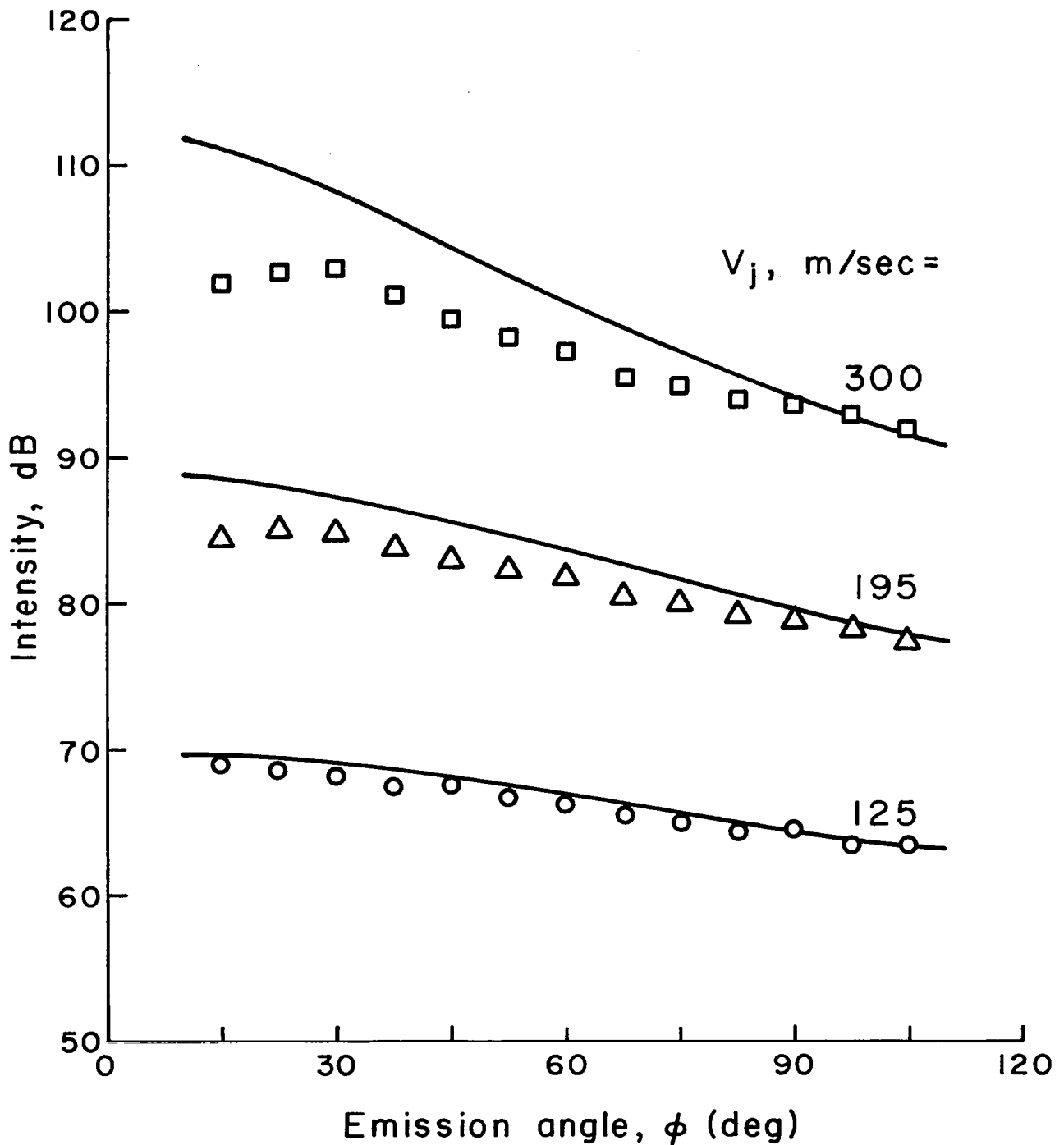
Figure 8. Directivity of sound intensity (dB, re 10^{-12} W/m^2) (k = 0.5) vs. Lush data for three values of jet velocity. Lush data: single points. Simulation: solid line. (ϕ is measured from the downstream jet axis.)
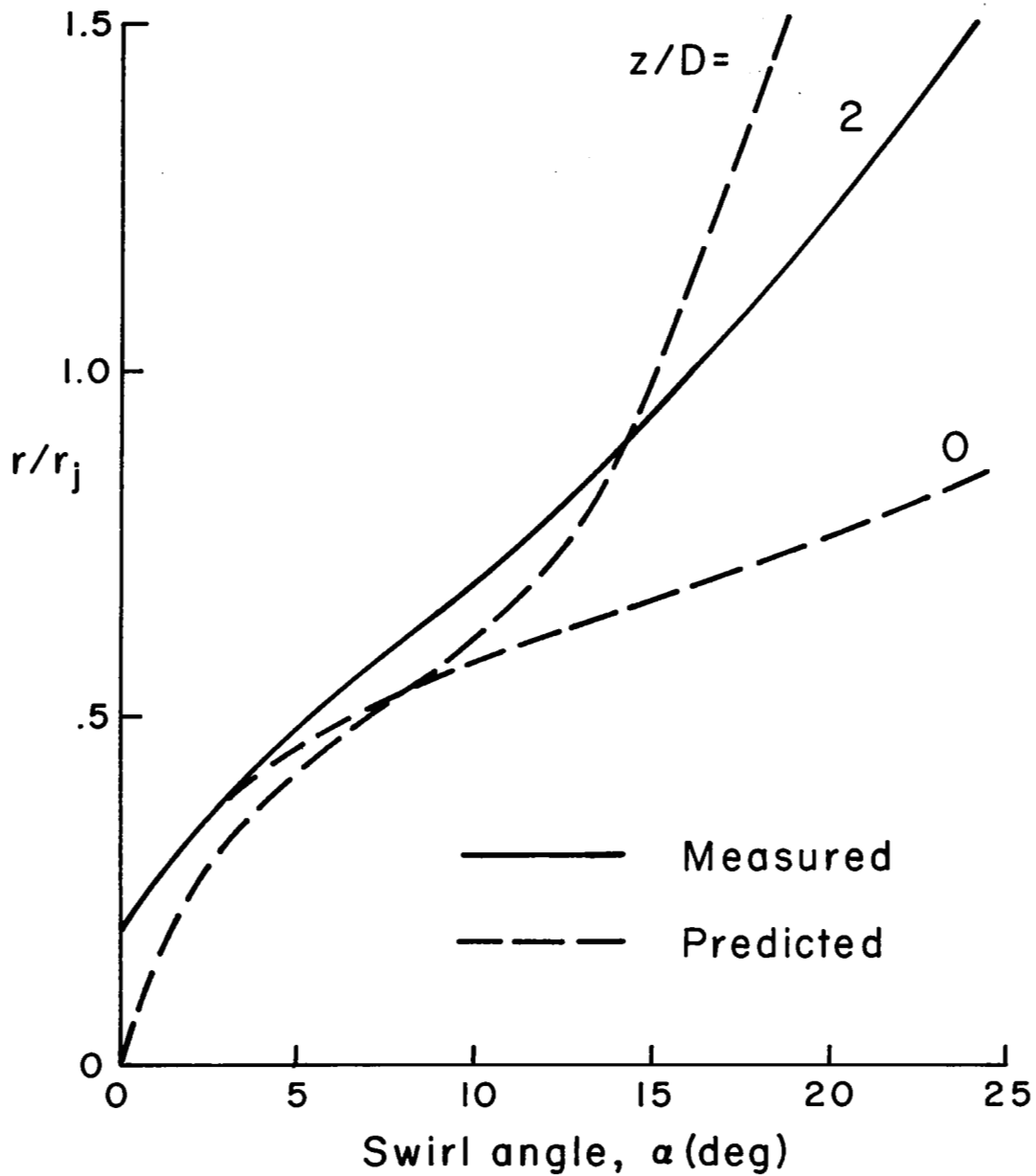
Figure 9a.   Measured and Predicted Swirl Angle
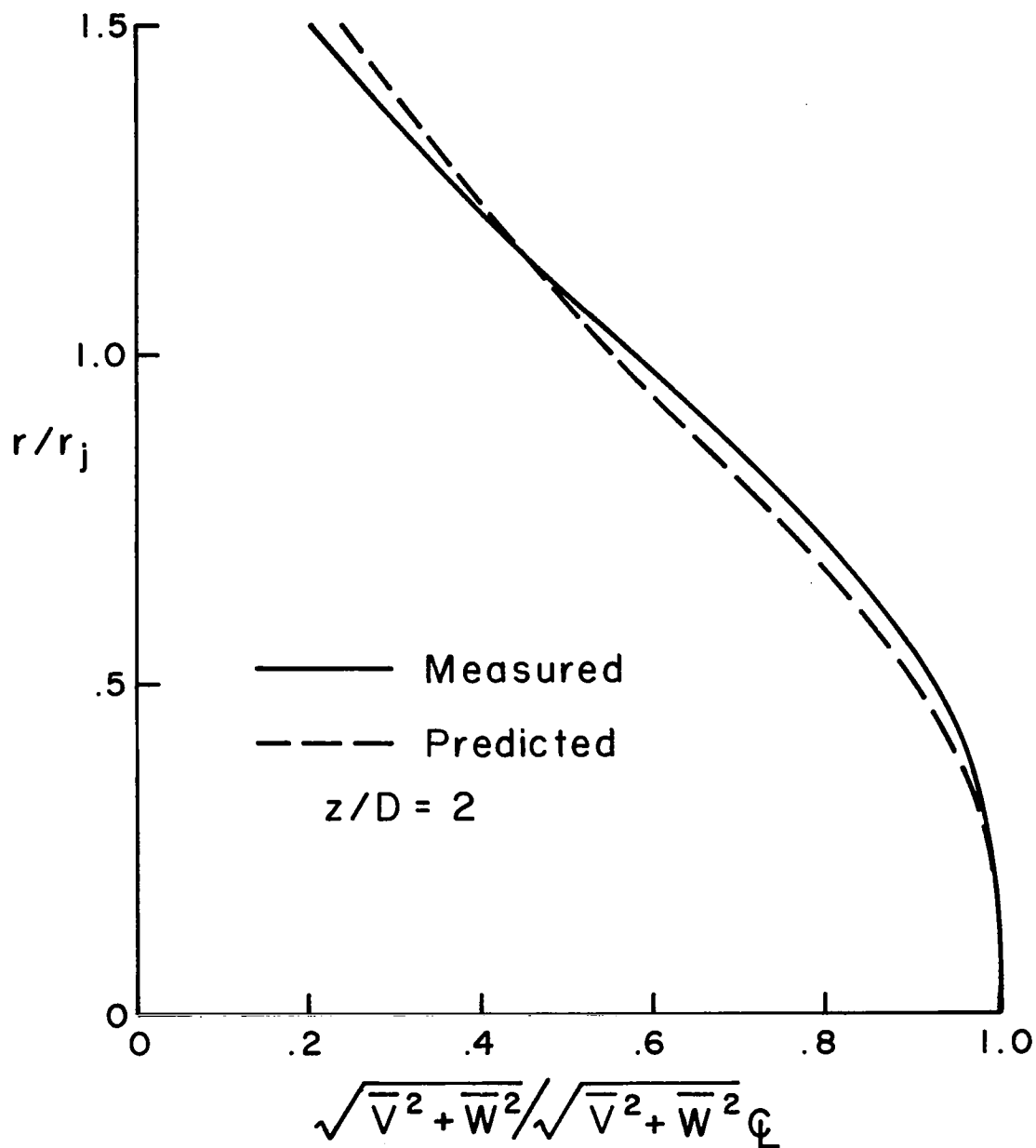
Figure 9b. Measured and predicted total velocity
distribution
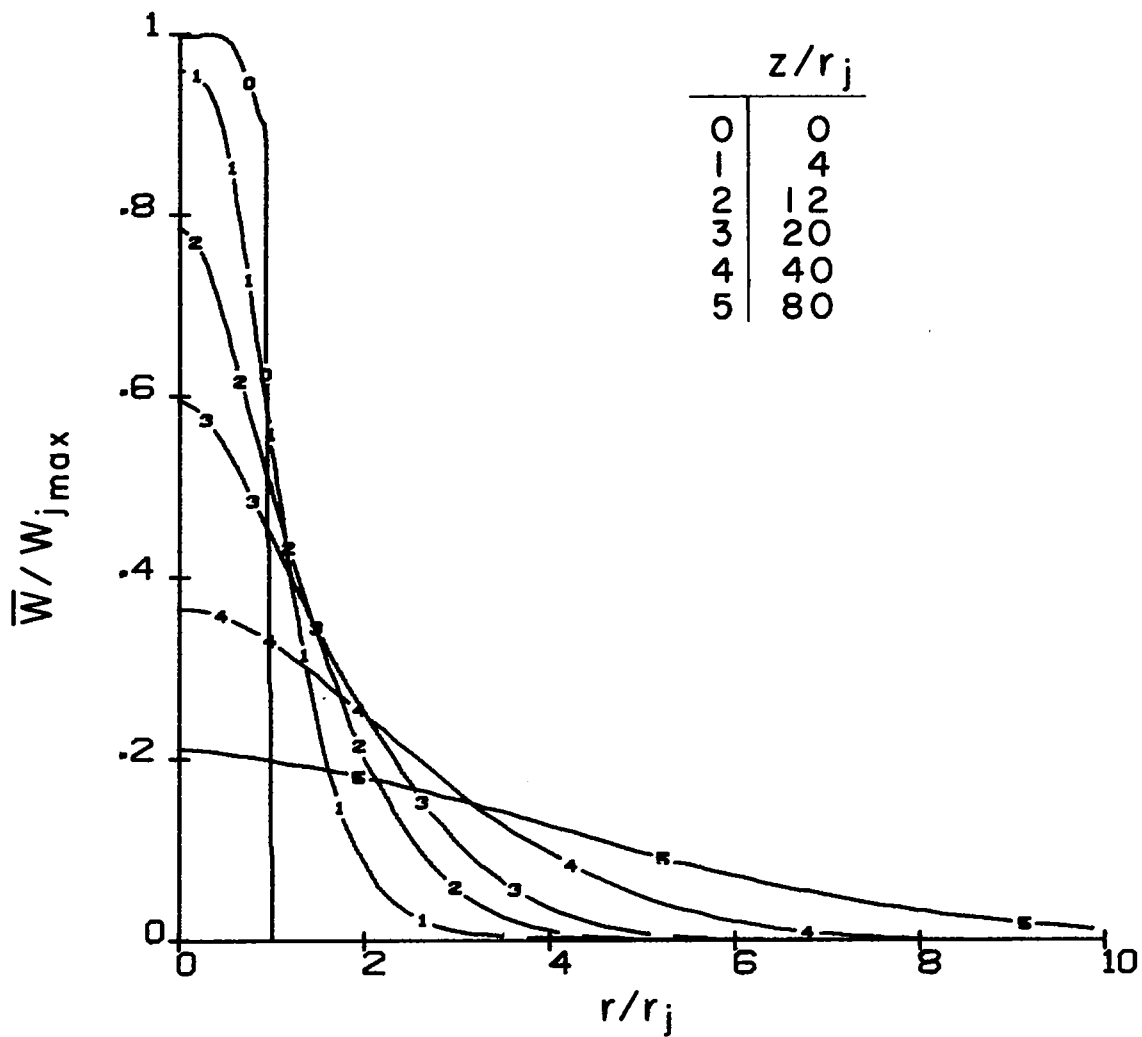
Figure 10a.   Predicted axial velocity profiles in the
Lu, et al   model swirled jet
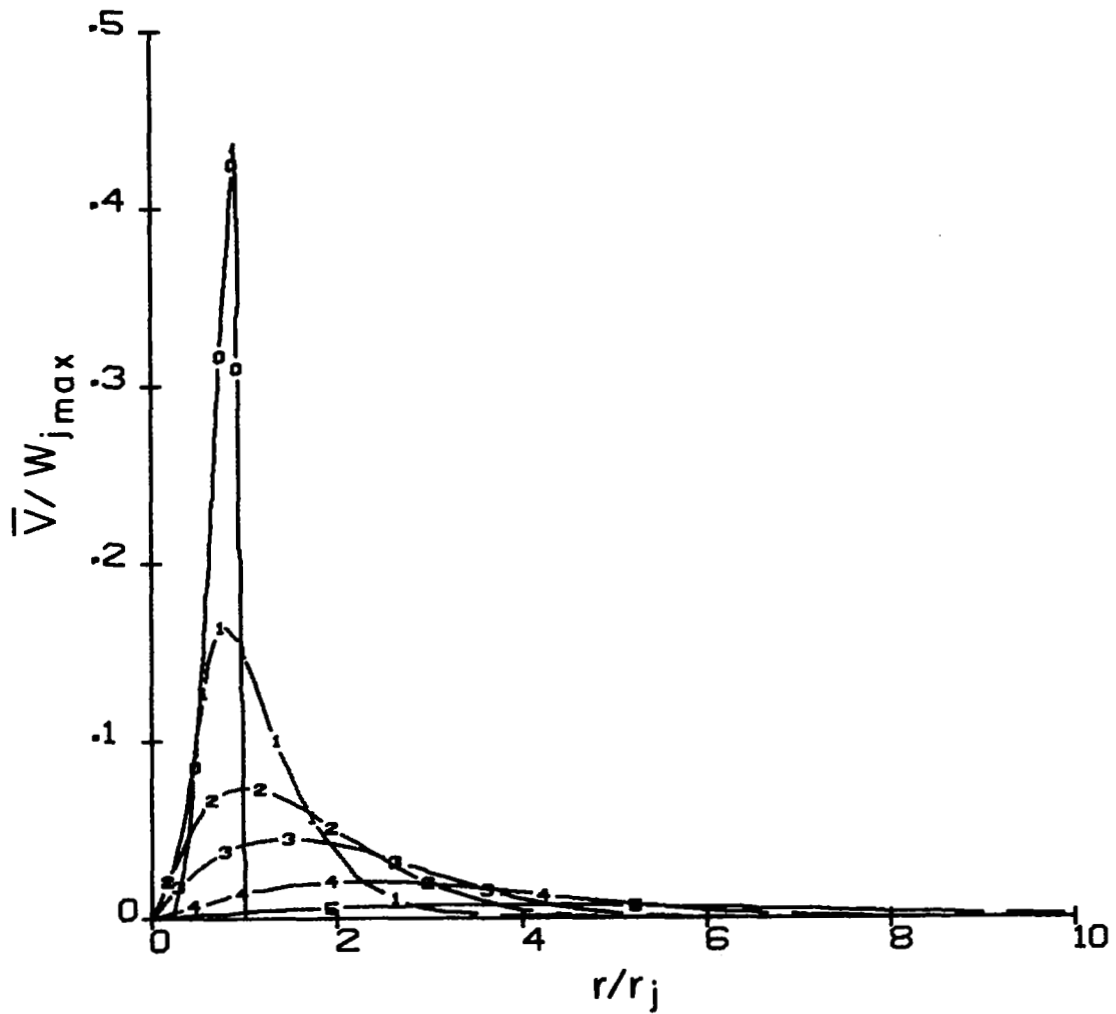
Figure 10b. Predicted swirl velocity profiles in the
             Lu, et al model swirled jet. Curve labels
             same as Fig. 10a
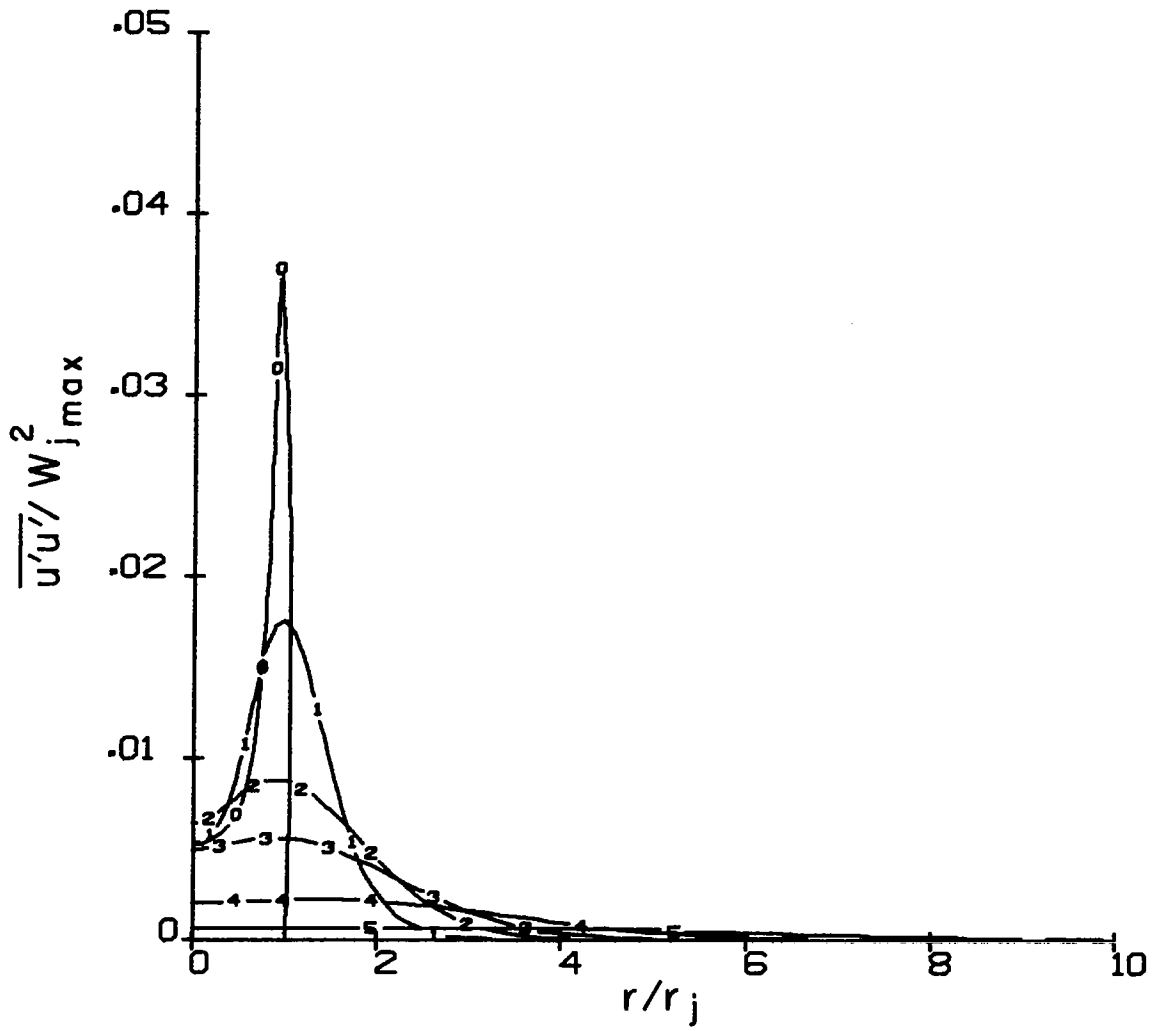
Figure 10c. Predicted $\overline{u'u'}$ correlation in the Lu, et al model swirled jet. Curve labels same as Fig. 10a
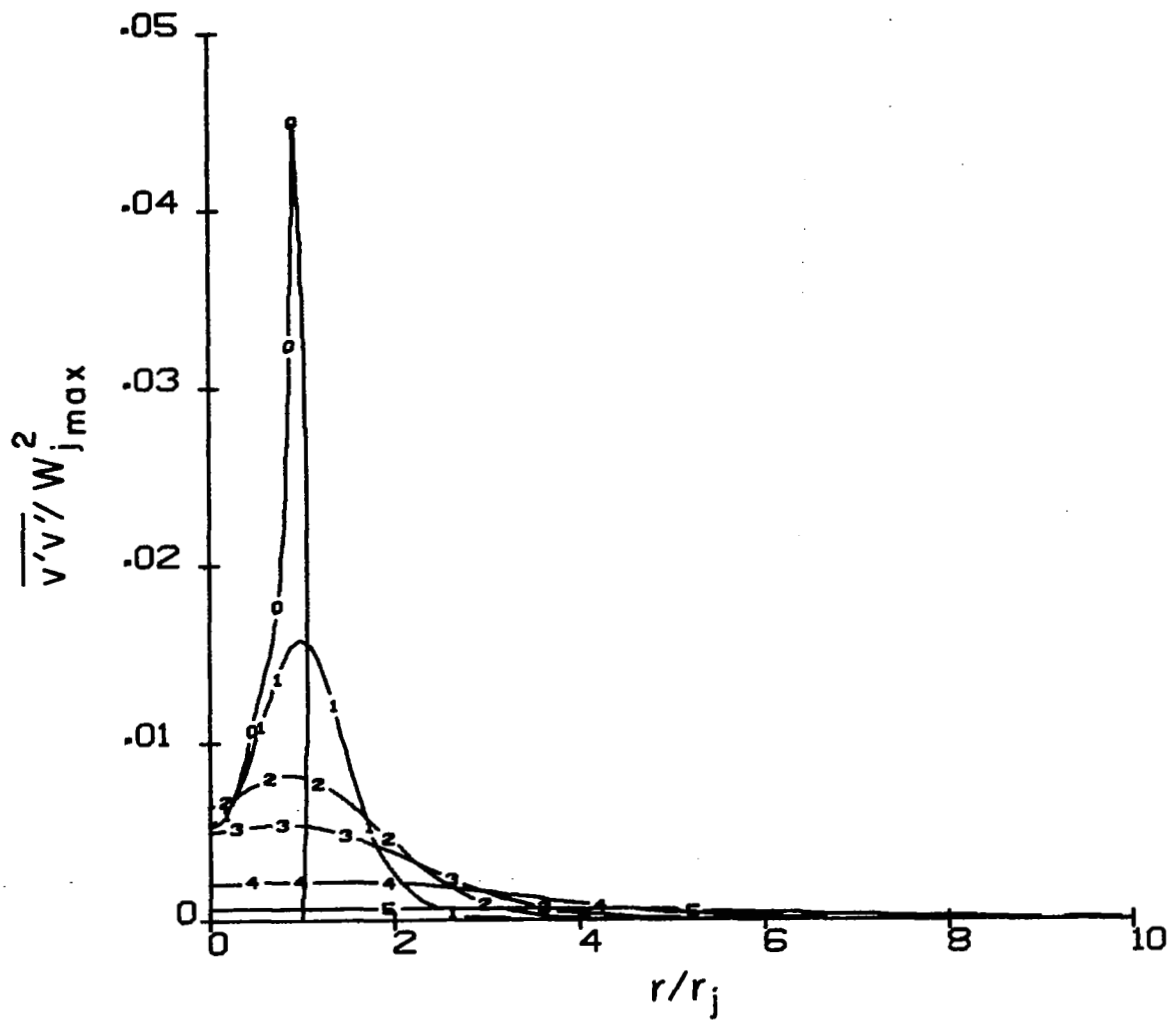
Figure 10d. Predicted $\overline{v'v'}$ correlation in Lu, et al model swirled jet. Curve labels same as Fig. 10a
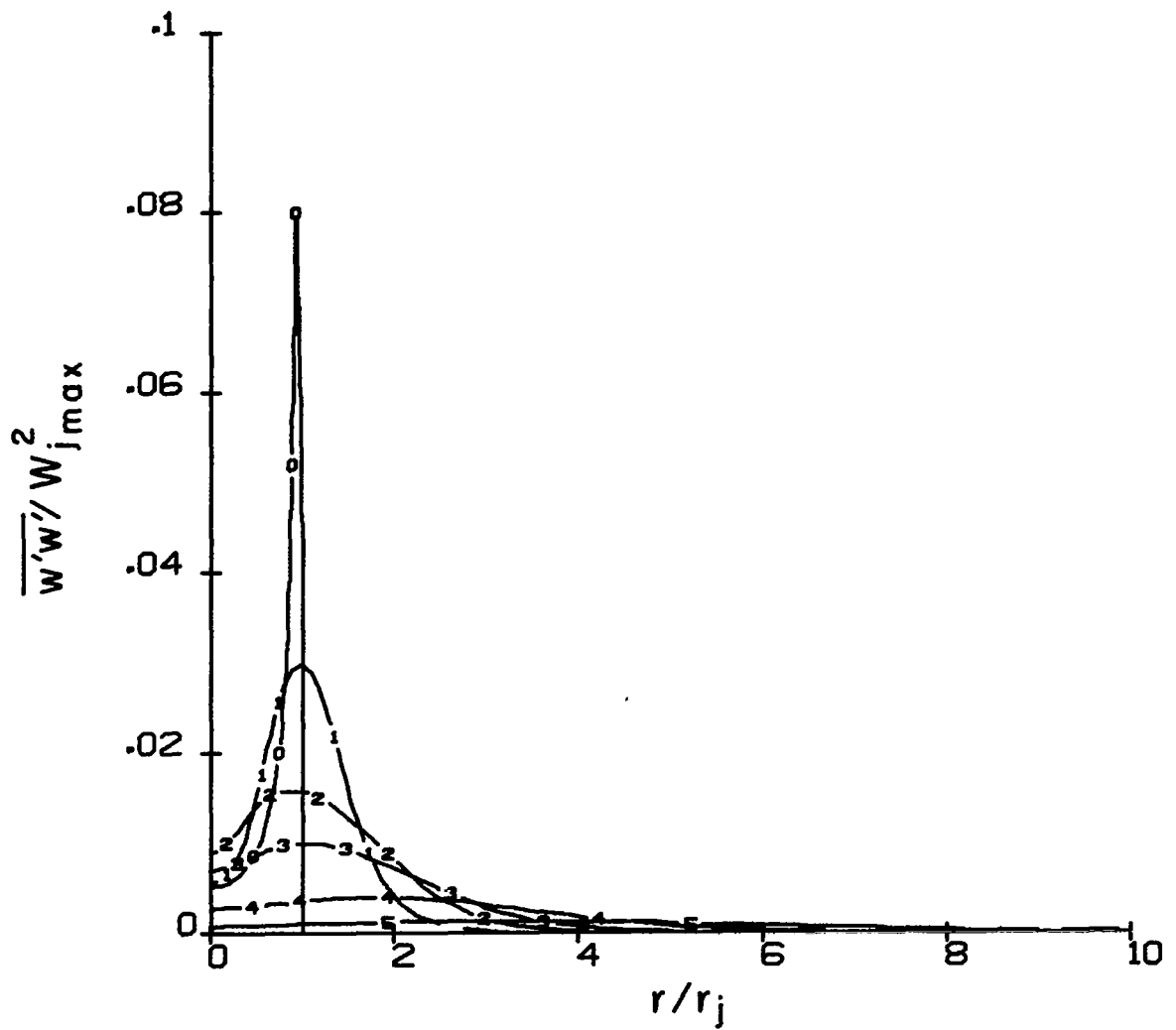
Figure 10e.   Predicted $\overline{w'w'}$ correlation in the Lu, et al model swirled jet.   Curve labels same as in Fig. 10a
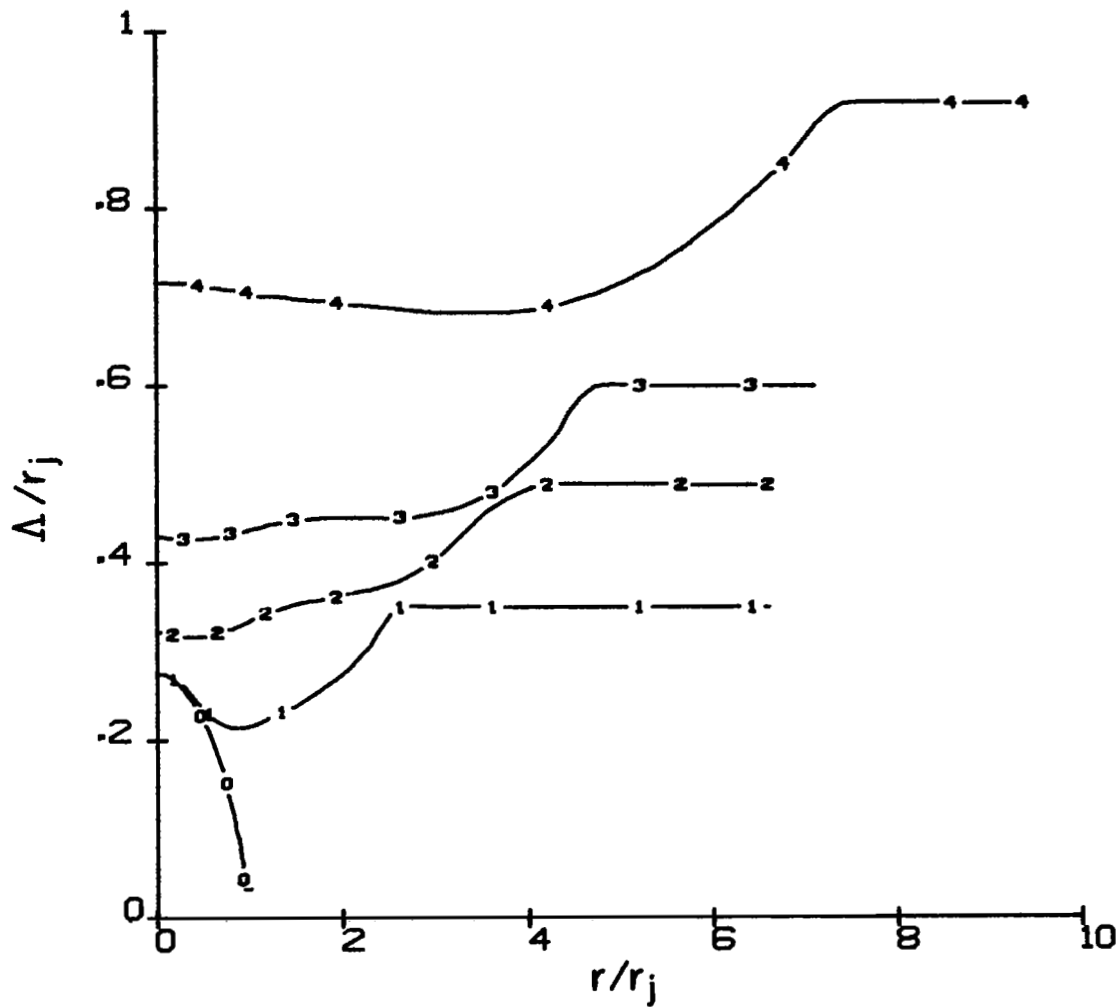
Figure 10f.   Predicted turbulent integral scale parameter Λ
in the Lu, et al model swirled jet.   Curve labels
same as in Fig. 10a
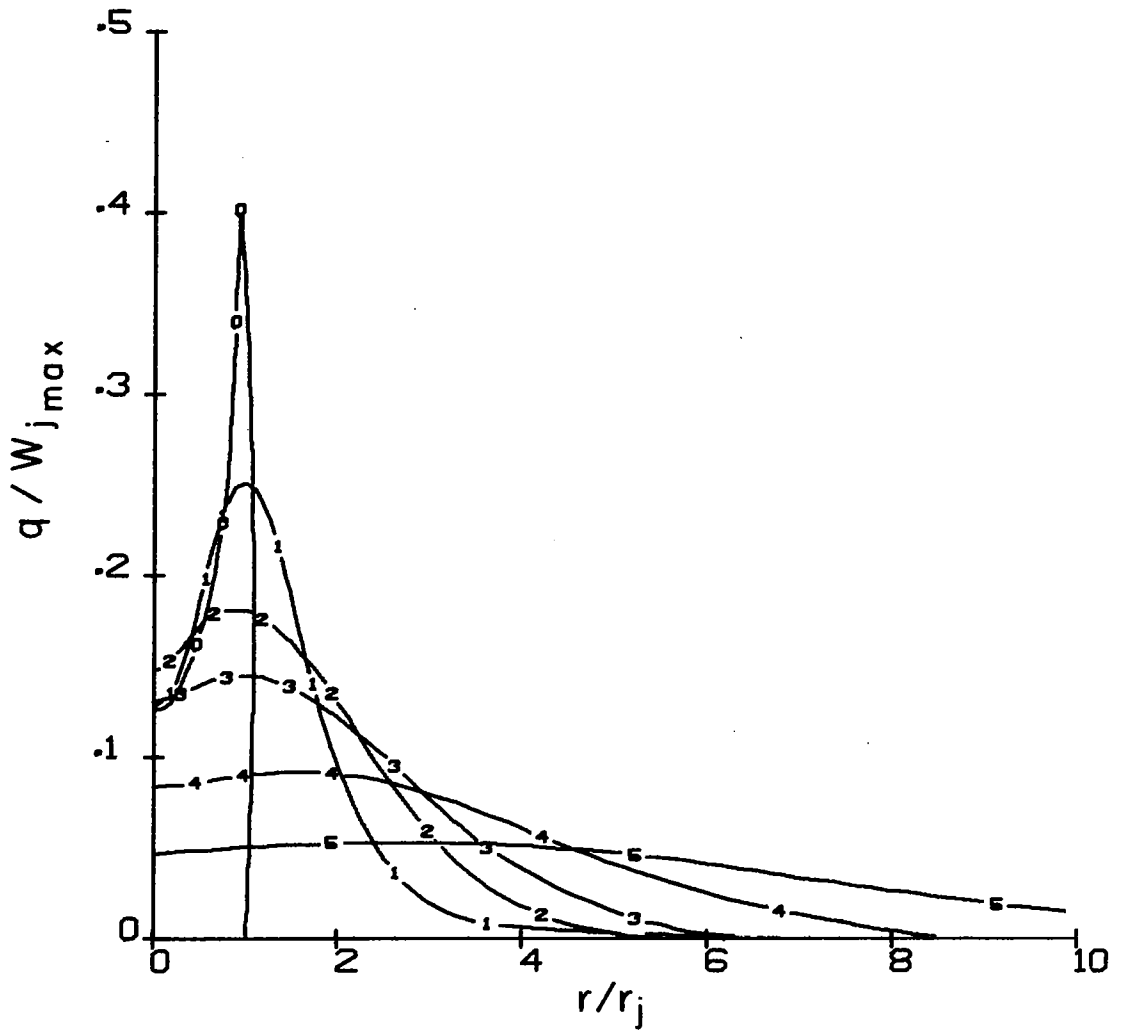
Figure 10g. Predicted turbulent intensity in the Lu, et al model swirled jet. Curve labels same as in Fig. 10a
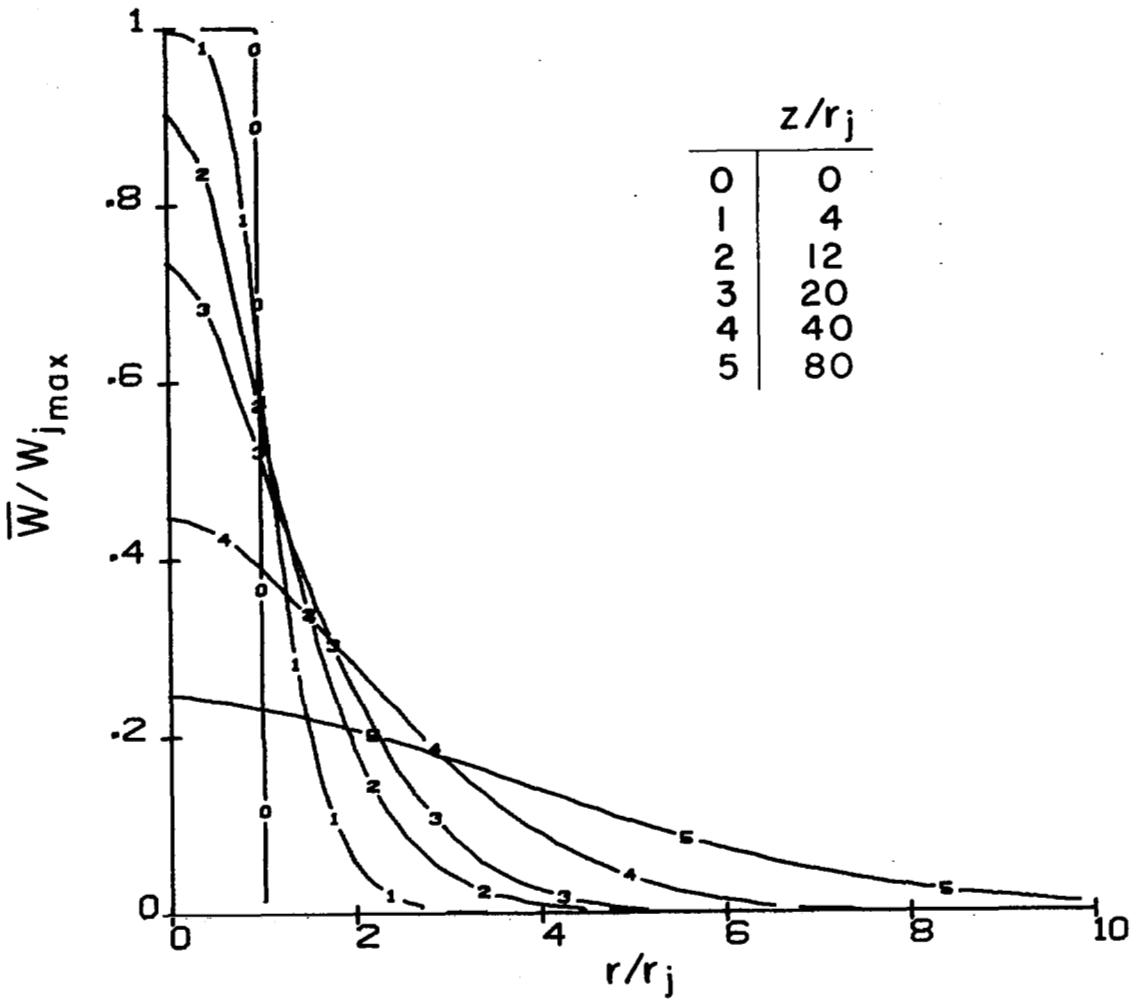
Figure 11a. Predicted axial velocity profiles in Lu, et al
model swirled jet (no swirl)
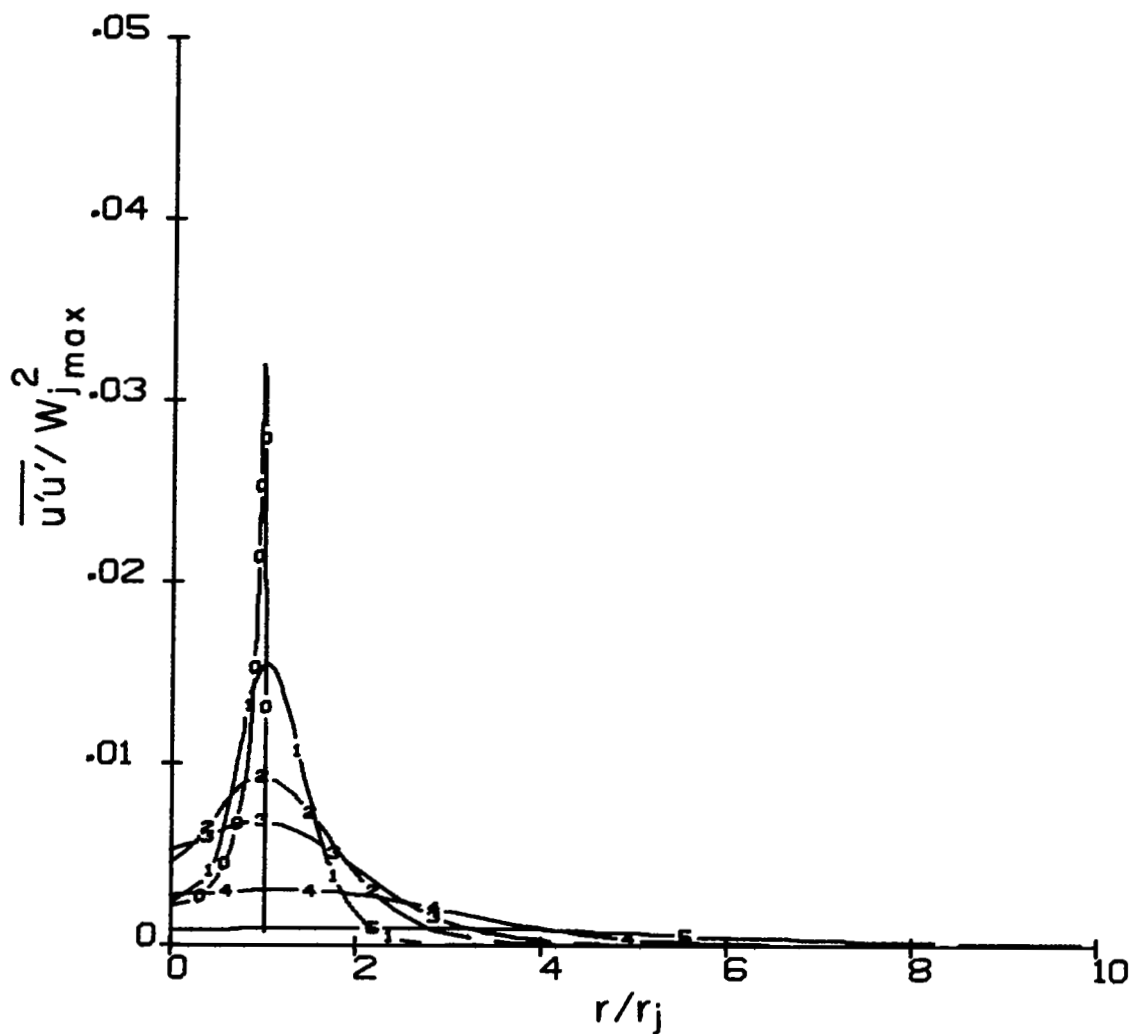
Figure 11b. Predicted $\overline{u'u'}$ correlation in the Lu, et al model swirled jet (no swirl). Curve labels same as in Fig. 11a
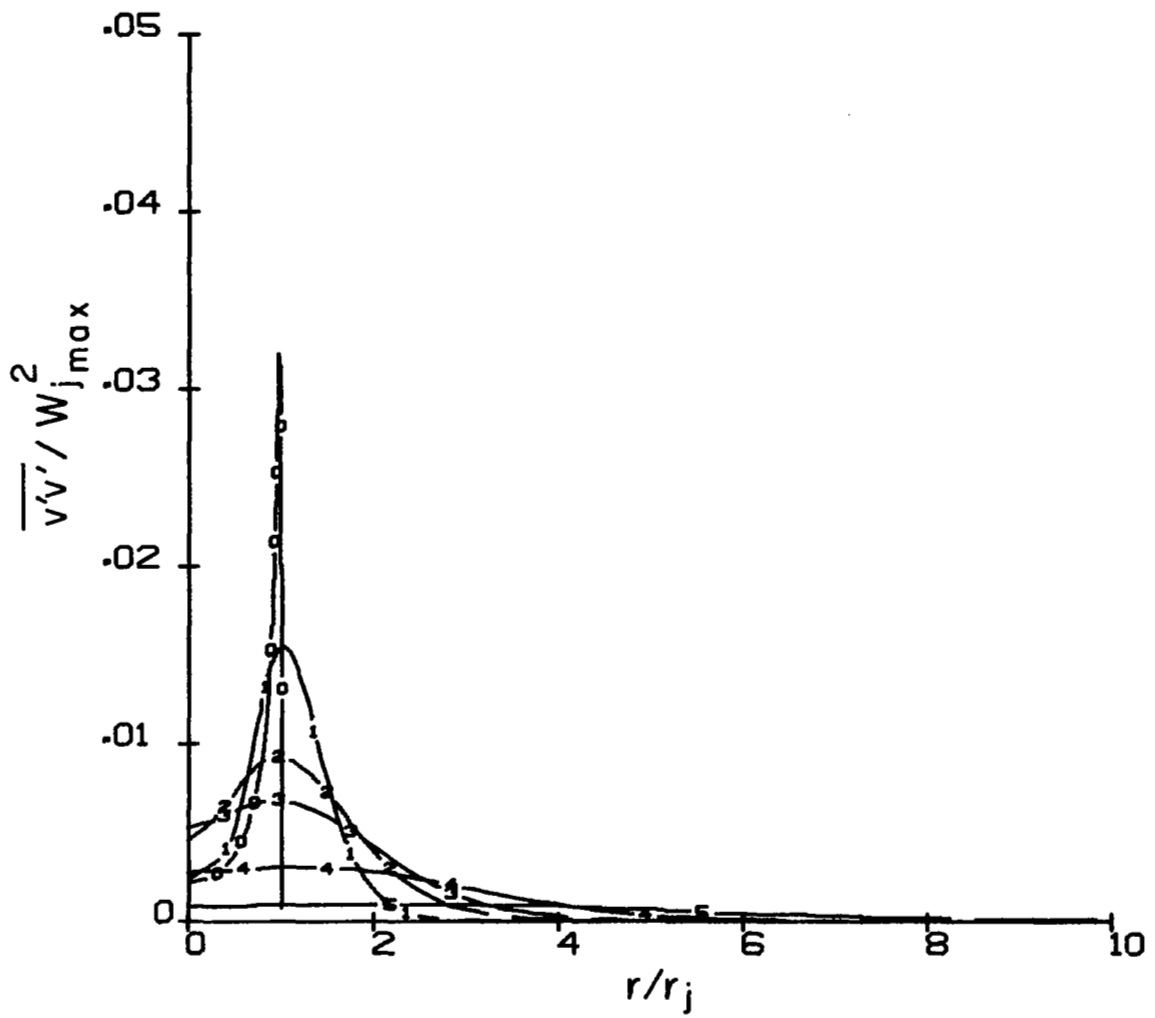
Figure 11c. Predicted $\overline{v'v'}$ correlation in the Lu, et al model swirled jet (no swirl). Curve labels same as in Fig. 11a
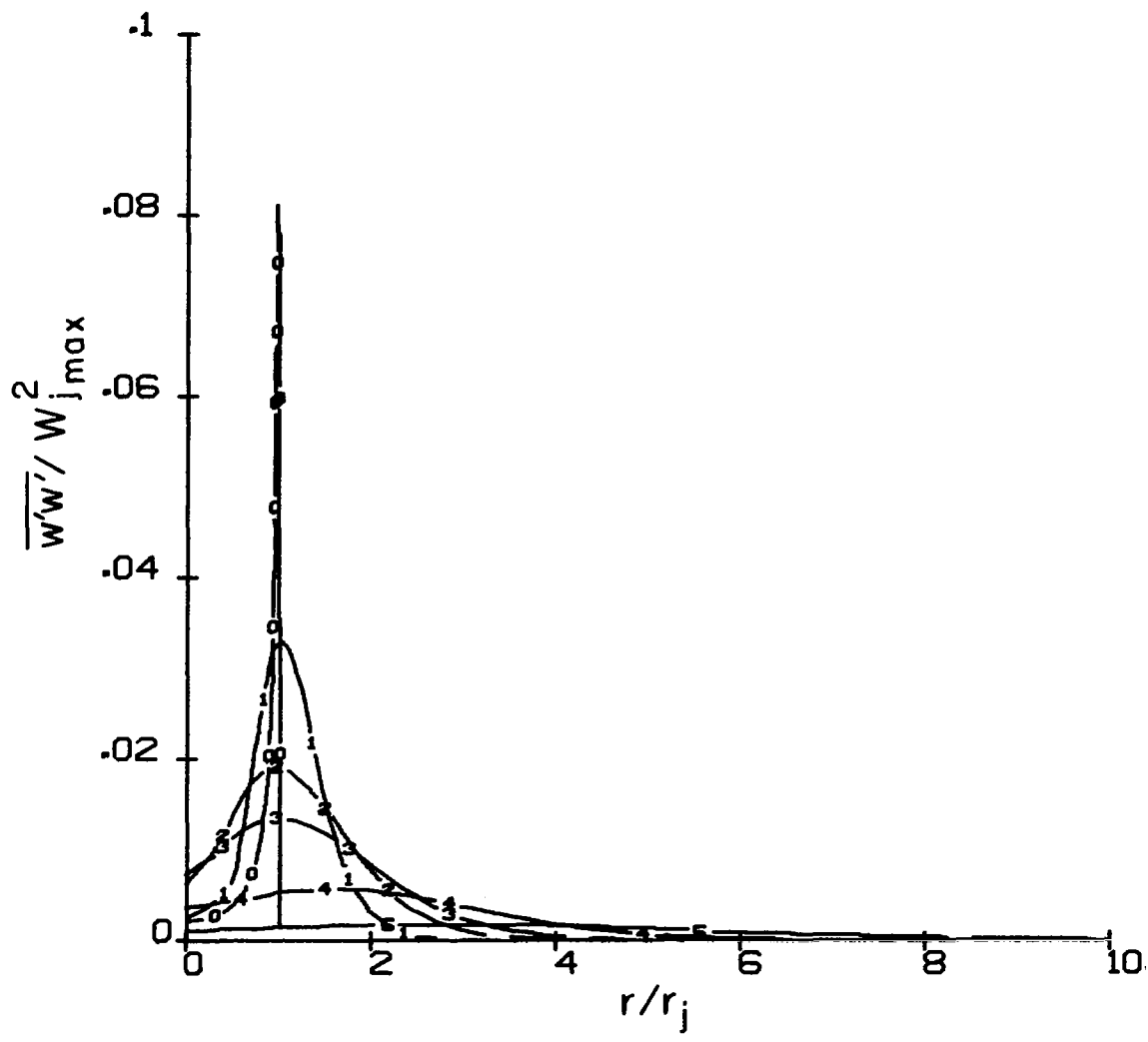
Figure 11d.   Predicted $\overline{w'w'}$ correlation in th e Lu, et al model
swirled jet (no swirl).   Curve labels same as in
Fig. 11a
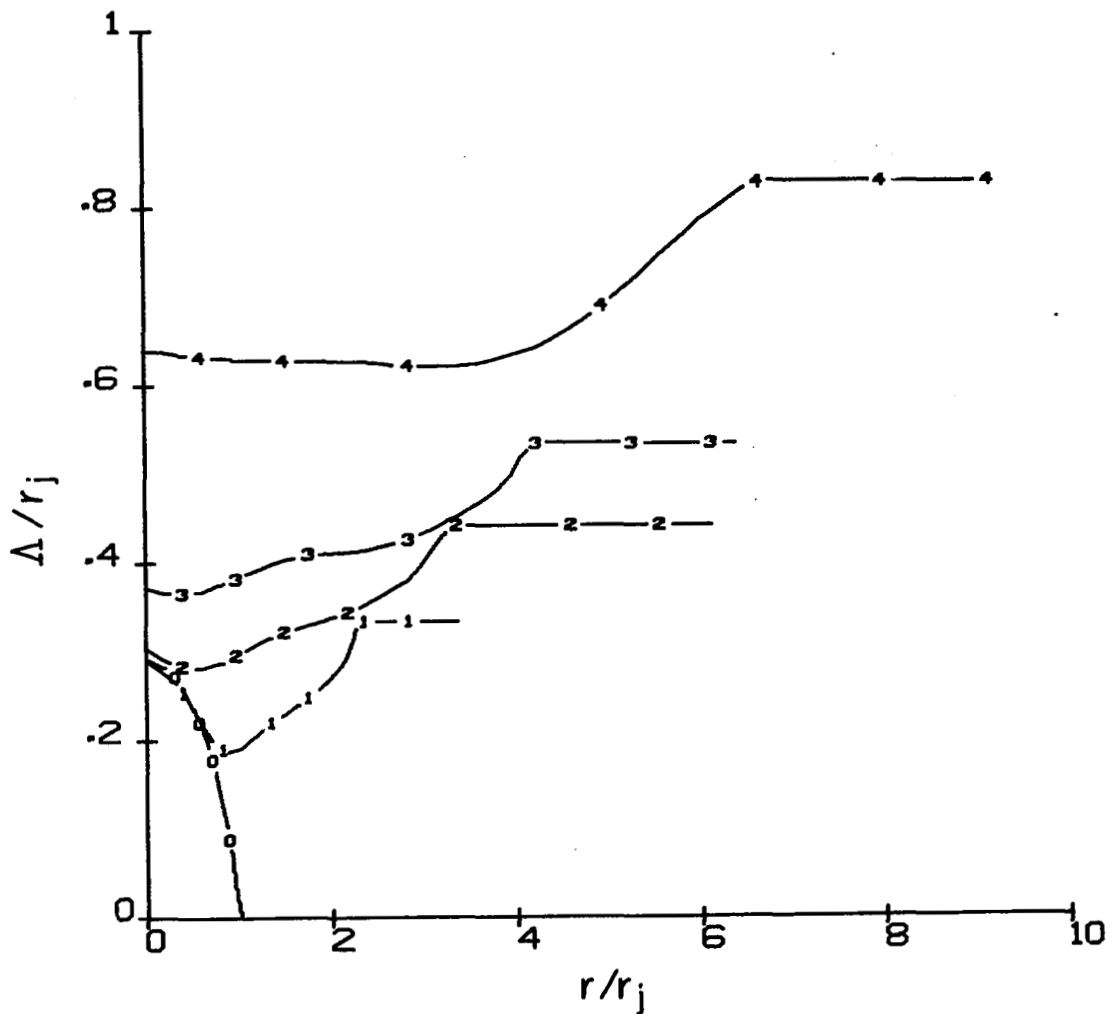
Figure 11e. Predicted turbulent integral scale parameter Λ in the Lu, et al model swirled jet (no swirl). Curve labels same as in Fig. 11a
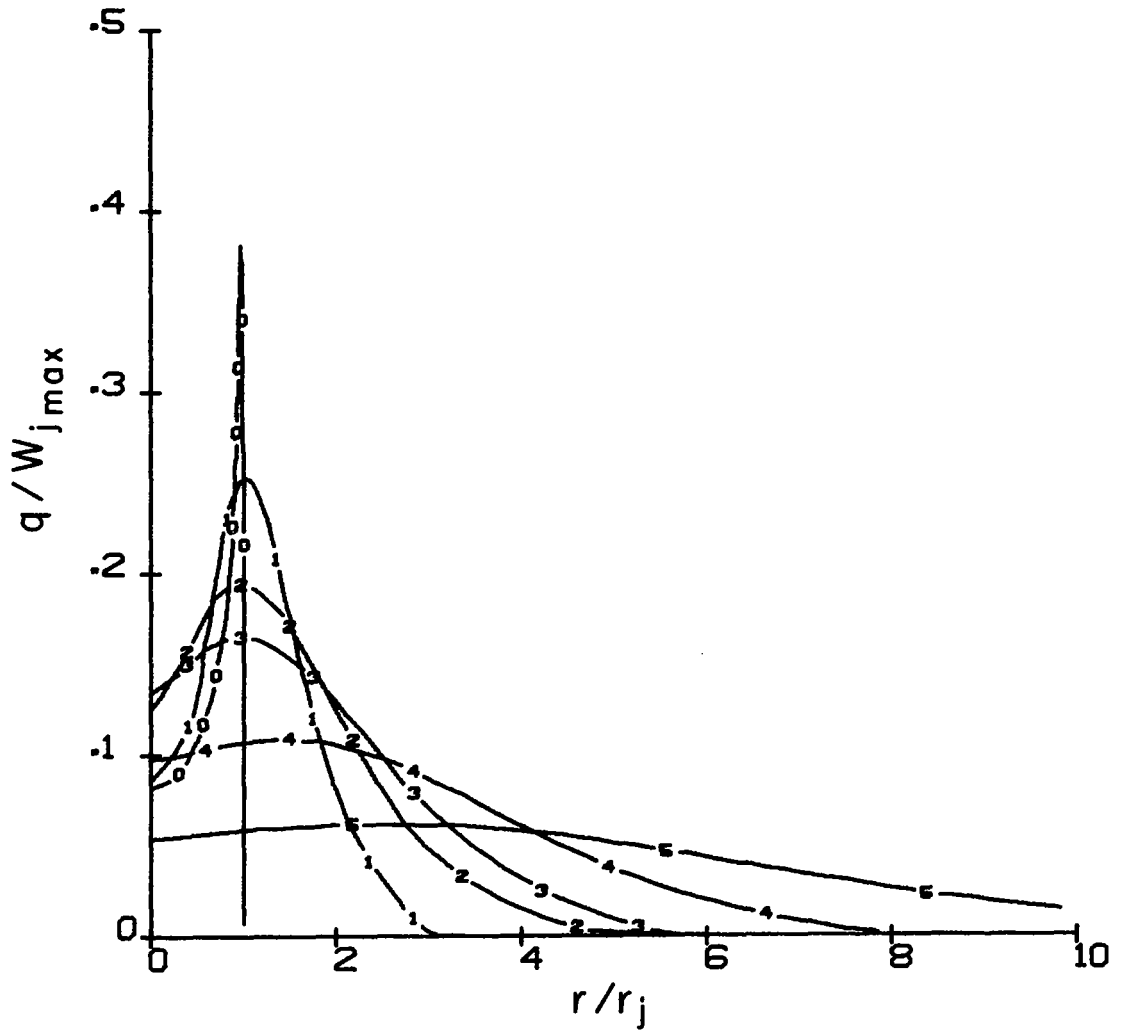
Figure 11f. Predicted turbulent intensity in the Lu, et al model swirled jet (no swirl). Curve labels same as in Fig. 11a
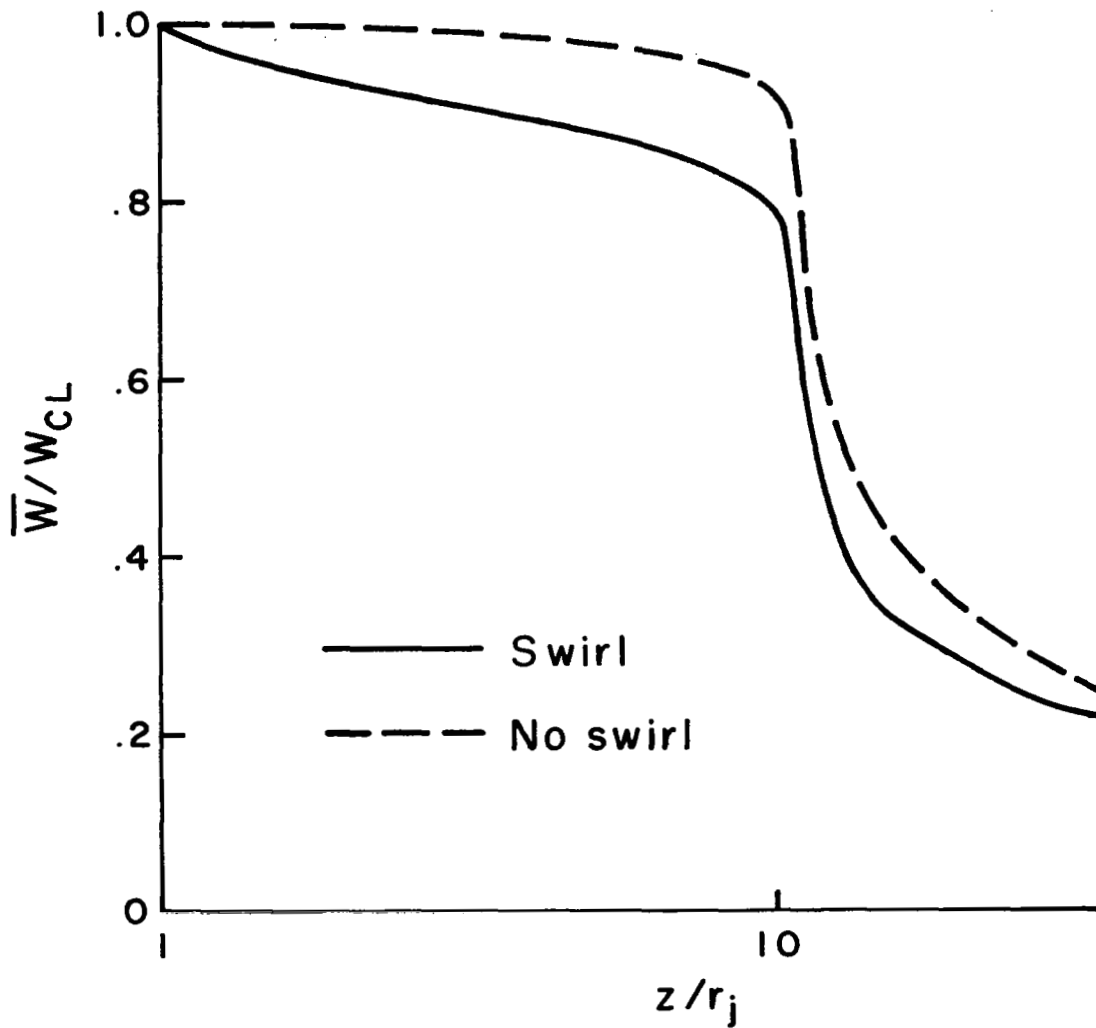
Figure 12.   Predicted decay of centerline axial velocity

In Fig. 13, we have shown the computed directivity for the swirled and nonswirled jet for pressure ratio equal to 1.2 (thrust estimated to be 33 pounds) and 1.8 (thrust estimated to be 100 pounds). In both cases, it is shown that the swirled jet is approximately one dB (sound intensity) noisier. At a given pressure ratio the thrust between swirled and nonswirled is approximately the same. Lu et al. have not given directivity plots for this case but have presented spectra 70° from the downstream axis. Here we estimate from their data a 5 db increase in intensity when the jet is swirled. To explain this result we have examined the sensitivity of our directivity prediction to small changes in turbulent initial conditions. Shown in Fig. 14, is the computed directivity which results when the initial specification of the second-order velocity correlations are increased or decreased by 20%. It is not difficult to argue that the swirl vanes do in fact increase the initial turbulence level, although an estimation of the amount would be difficult. Also, it seems reasonable that swirl vanes will alter the initial integral scale. However, this effect was not investigated. Within the limitations which are detailed above, these results do indicate that the Lu et al. cold swirling jet does not offer any sound intensity reduction over the nonrotating counterparts.

We have also made a simulation of the jet flowfield of a high by-pass ratio jet engine (by-pass ratio 3 typical of a JT 15 D) where the primary exhaust is swirled. We have simply added a by-pass jet flow around the simulation of the Lu et al. model jet above. Here we have estimated initial conditions for the by-pass flow by computing the fully developed pipe flow in an annular pipe to approximate the exit conditions on the by-pass flow. In Figs. 15 and 16, is shown the initial, as well as downstream, predicted profile for a swirled and nonswirled primary flow. Note the initially high turbulence level in the region of mixing between the primary and by-pass flow and also the reduction of Λ in these regions. Again, we note that the effect of swirl is to increase the decay rate of the centerline axial velocity. Predicted directivity is shown in Fig. 17. Here thrust was held constant for both swirled and non-swirled cases at 113 pounds. Again, it is seen that swirl does not offer any reduction in sound power radiated over the nonswirled case.

As a final computation which demonstrates the general jet flow-fields which can be studied using second-order closure modeling, we have simulated a multitube suppressor. We have used nine Gaussian jets with the initial turbulence specified using super-equilibrium theory. These initial conditions were inputted into a code named "WAKE" which is a nonaxisymmetric version of TDV. WAKE is a fully elliptic computation in the cross plane and is parabolic in the streamwise direction. The computed decay of axial velocity is shown in isopleth form in Fig. 18. Isopleths of turbulent intensity are also shown in Fig. 19. We have computed the directivity of this jet and compared it with that predicted from
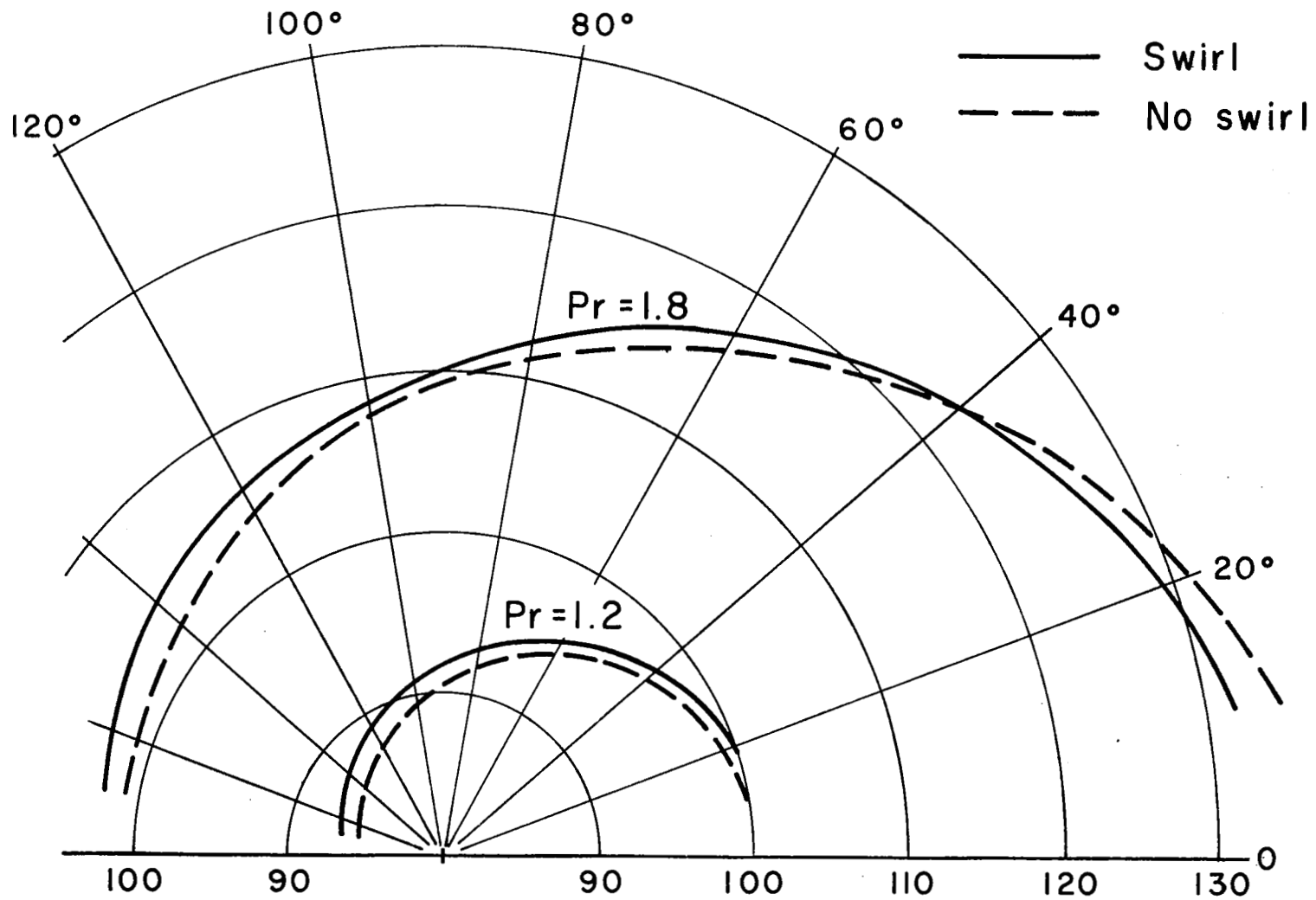
Figure 13. Intensity (dB re 10^{-12} W/m^2) measured from the downstream axis for the swirled and nonswirled jets for pressure ratios of 1.2 and 1.8 (from Lu, et al data simulation)
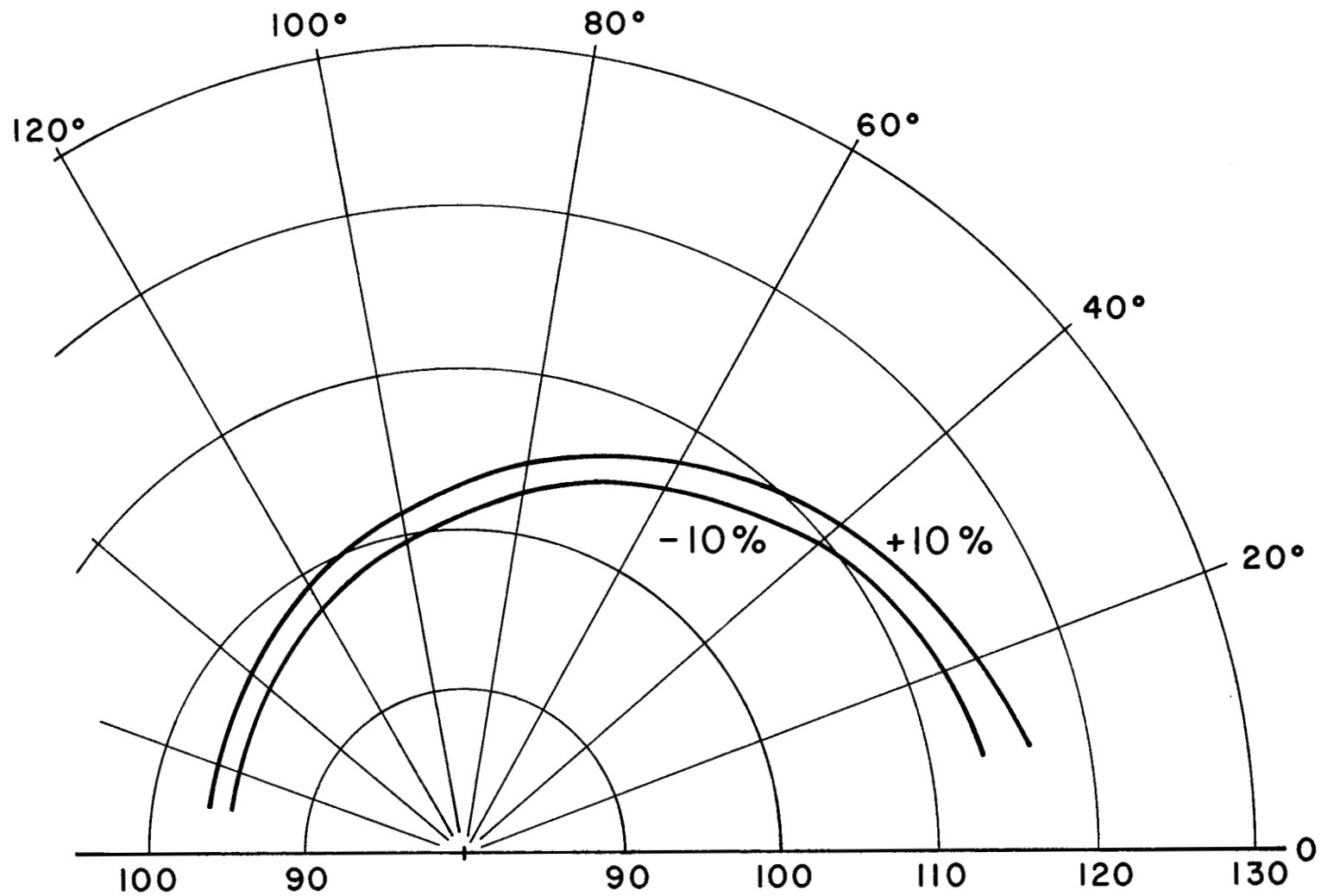
Figure 14. Change in intensity (dB re 10^{-12} W/m^2) which results from a ± 20% change in q^2 at z/r_j = 0
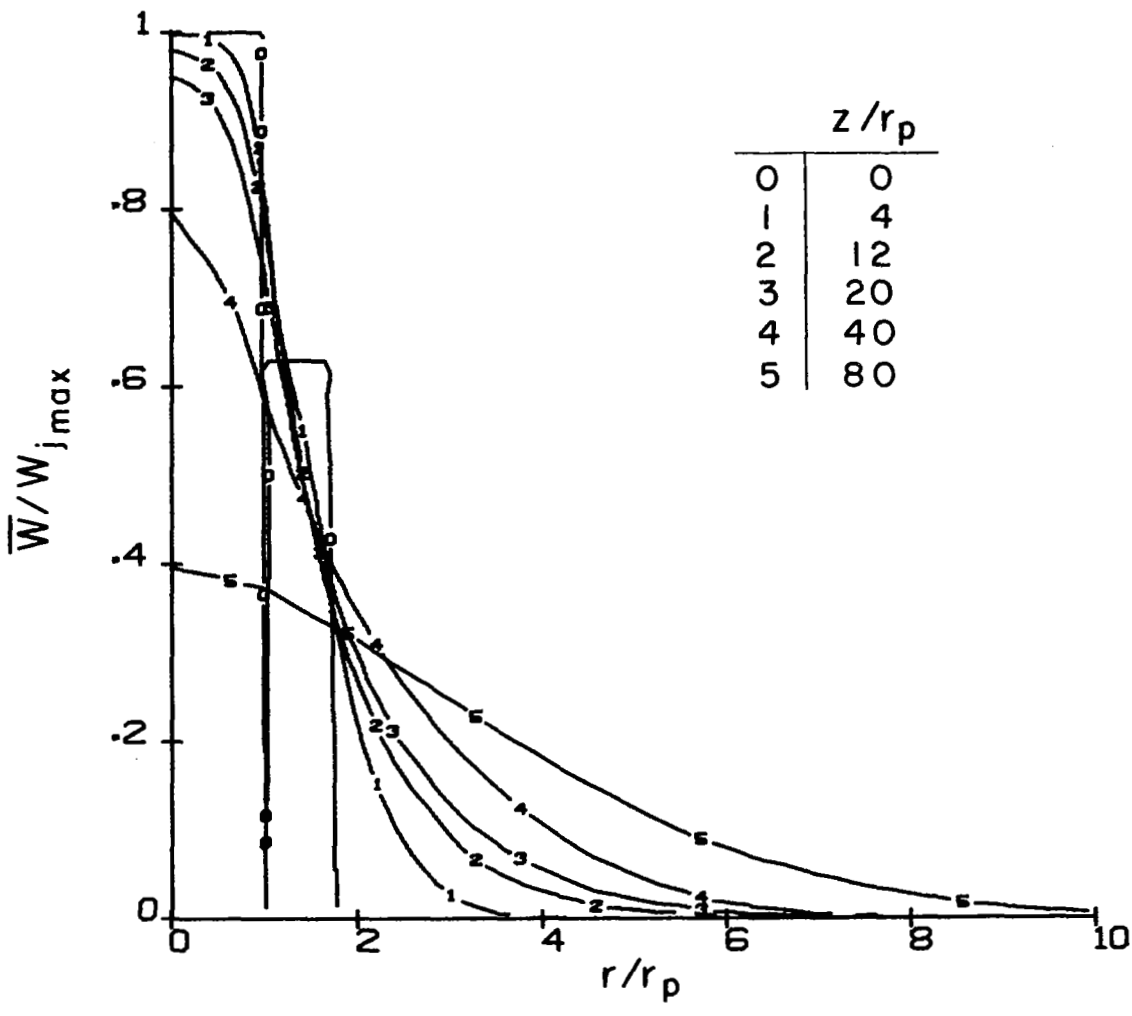
Figure 15a. Predicted axial velocity profiles (no swirl) for a high by pass ratio jet as a function of downstream distance (Lu, et al simulation)
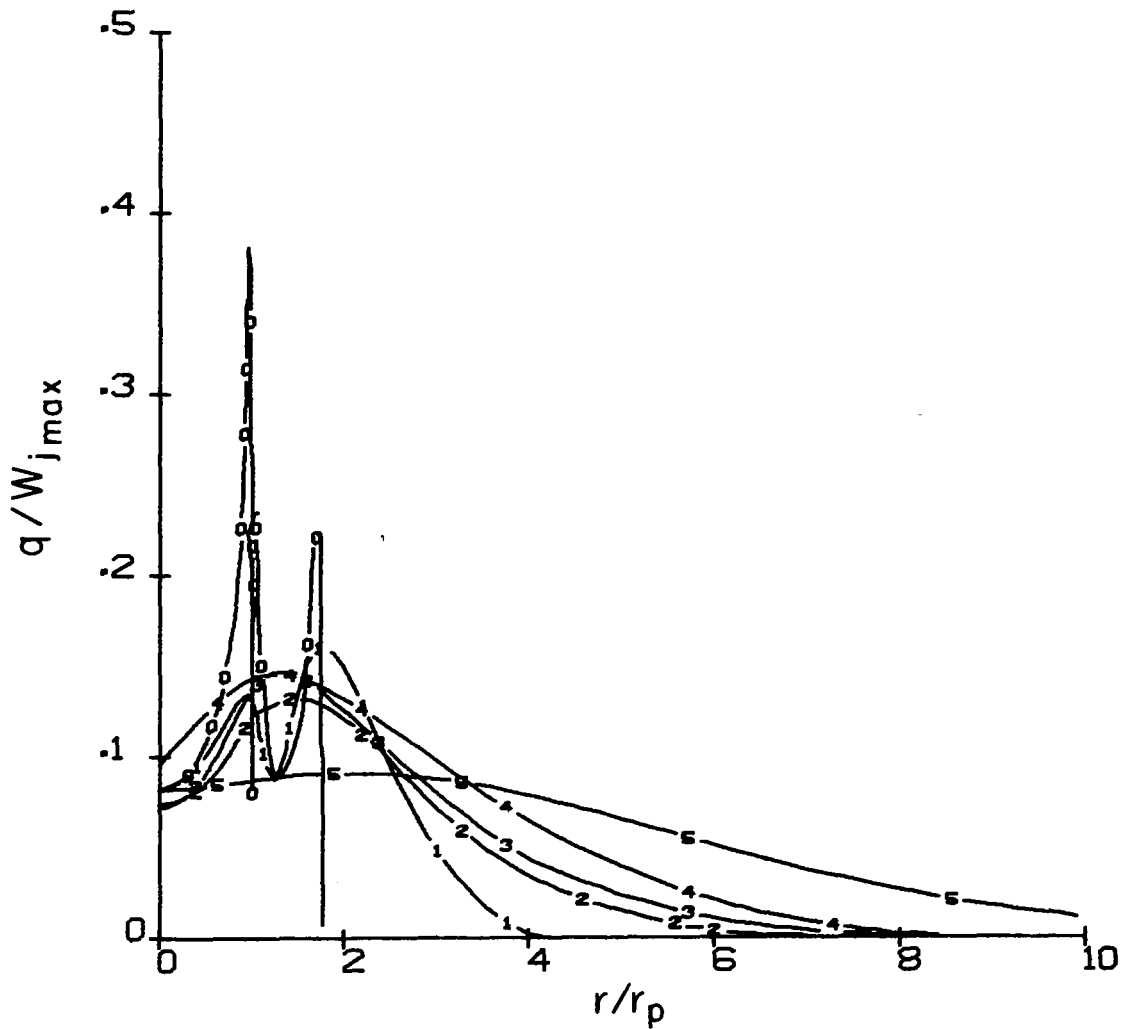
Figure 15b. Predicted turbulence profiles (no swirl) for a high by pass ratio jet as a function of downstream distance (Lu, et al simulation). See Fig. 15a for legend
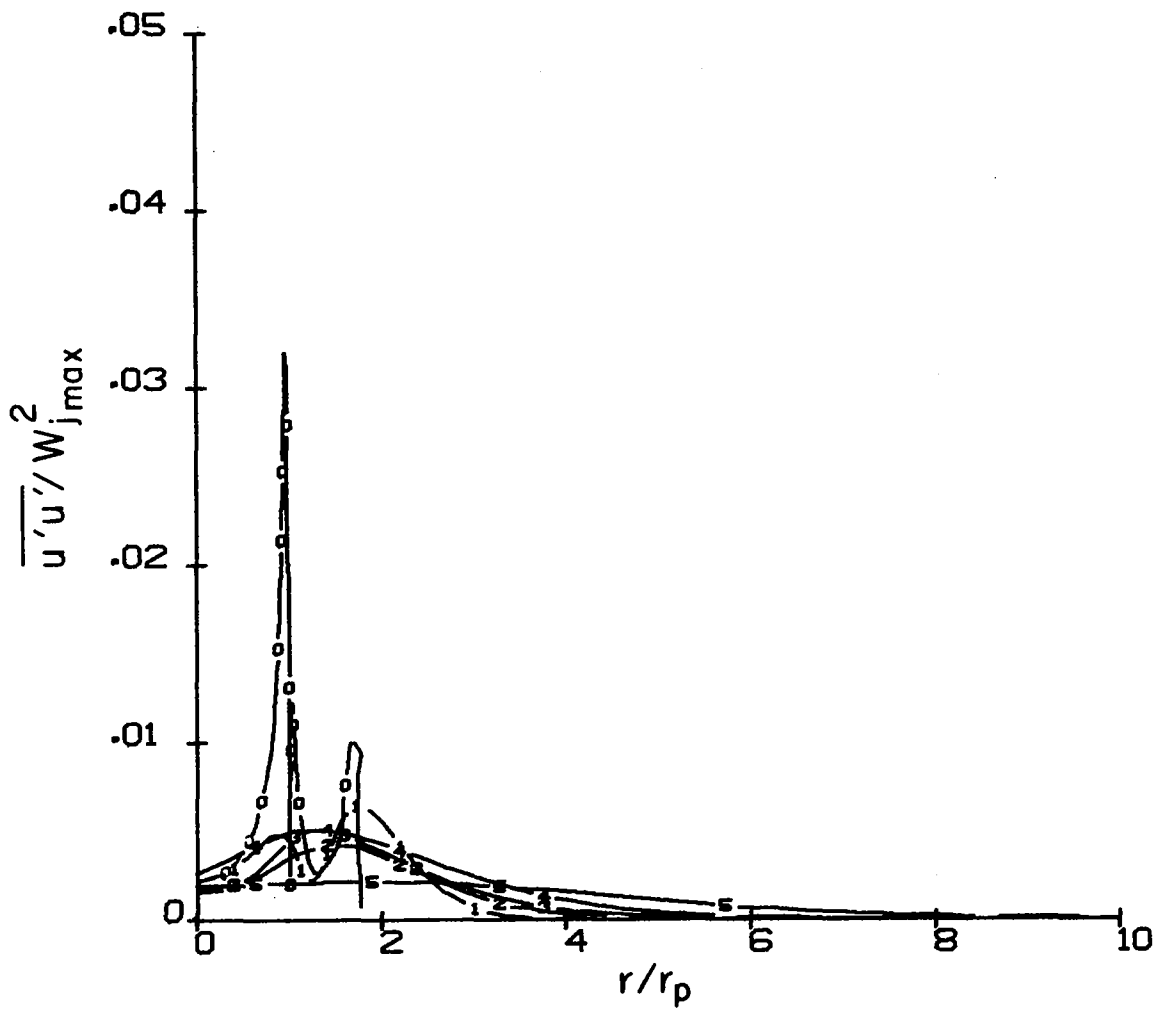
Figure 15c. Predicted $\overline{u'u'}$ profiles (no swirl) for a high by pass ratio jet as a function of downstream distance (Lu, et al simulation). See Fig. 15a for legend
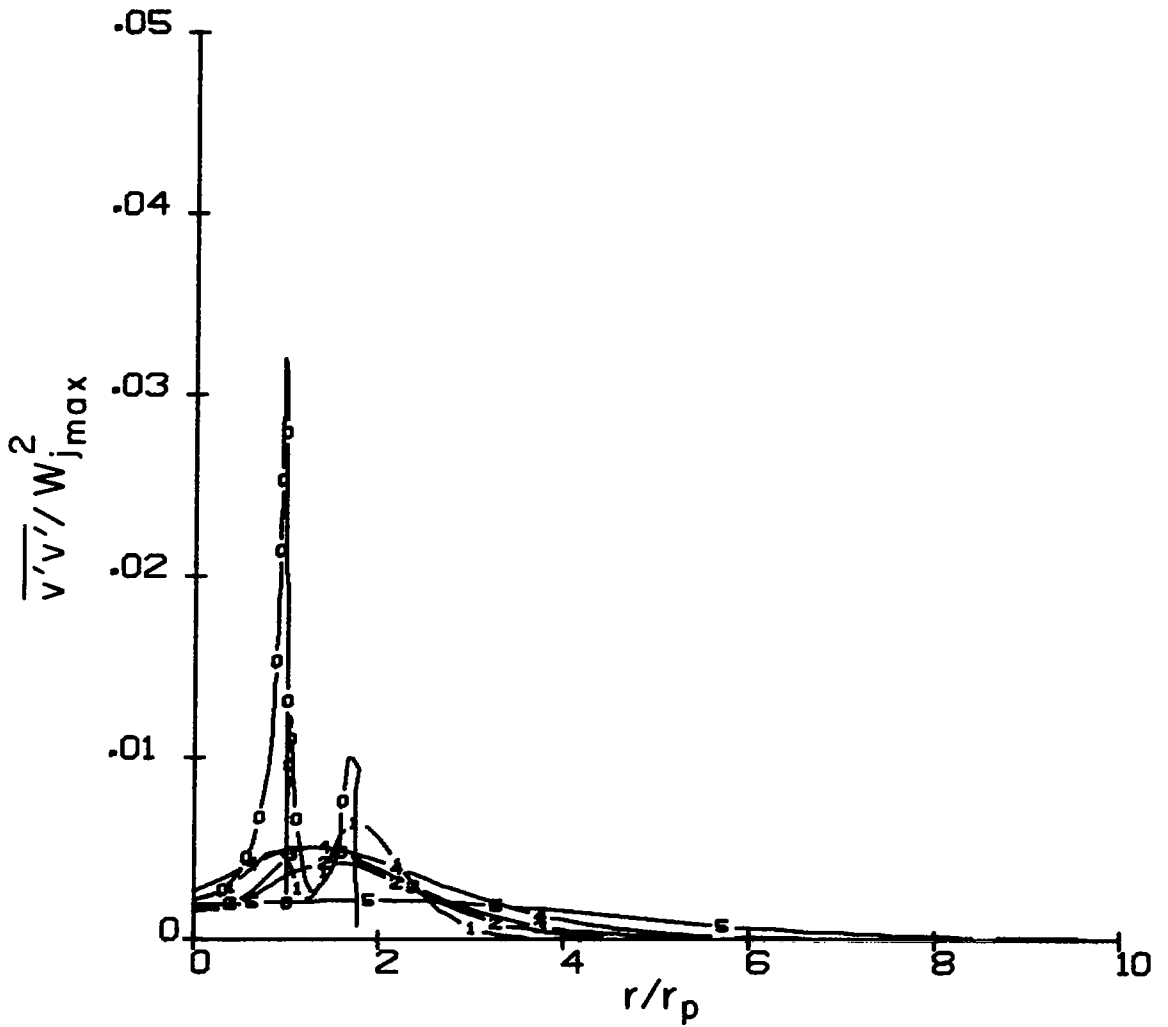
Figure 15d. Predicted $\overline{v'v'}$ profiles (no swirl) for a high
by pass ratio jet as a function of downstream
distance (Lu, et al simulation). See Fig. 15a
for legend

42
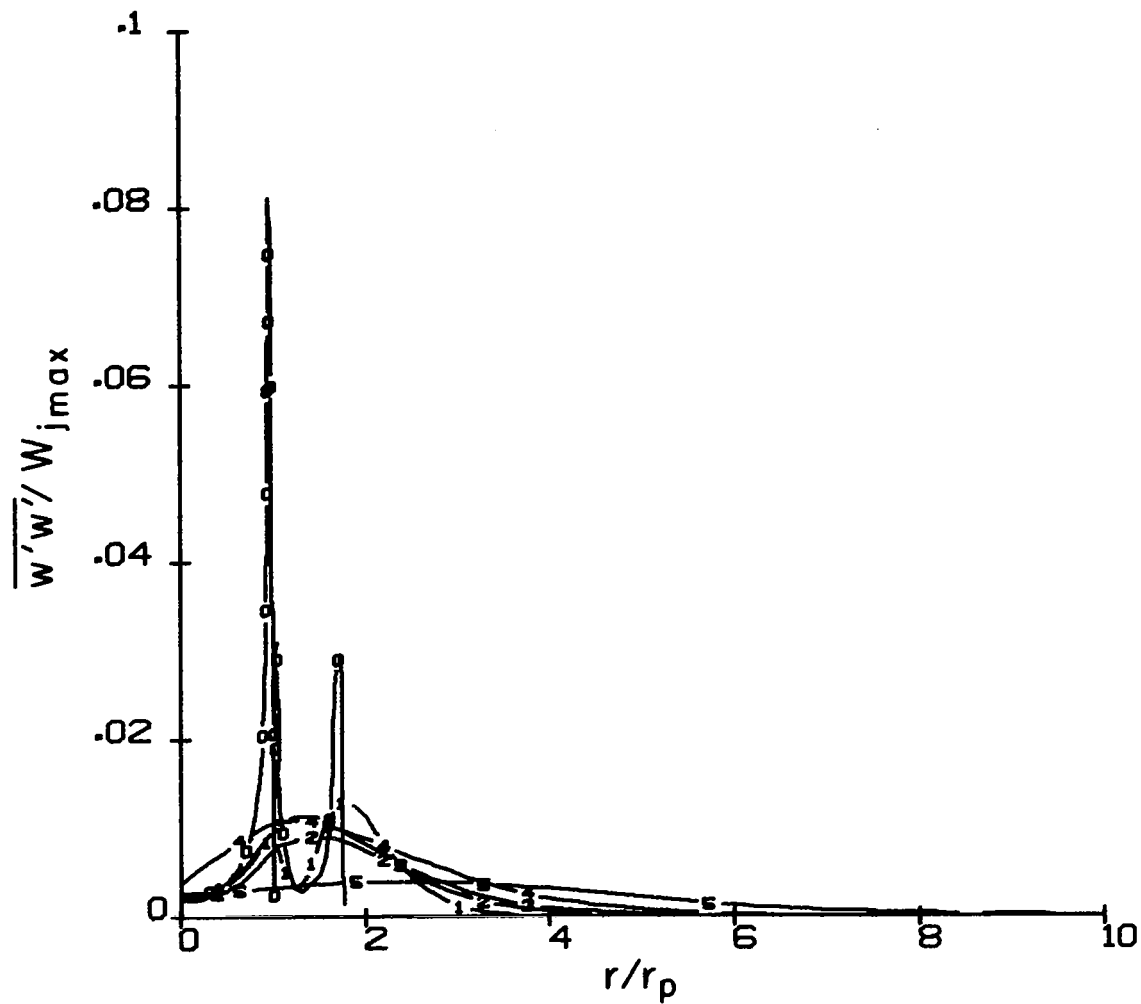
Figure 15e. Predicted $\overline{w'w'}$ profiles (no swirl) for a high by pass ratio jet as a function of downstream distance (Lu, et al simulation). See Fig. 15a for legend
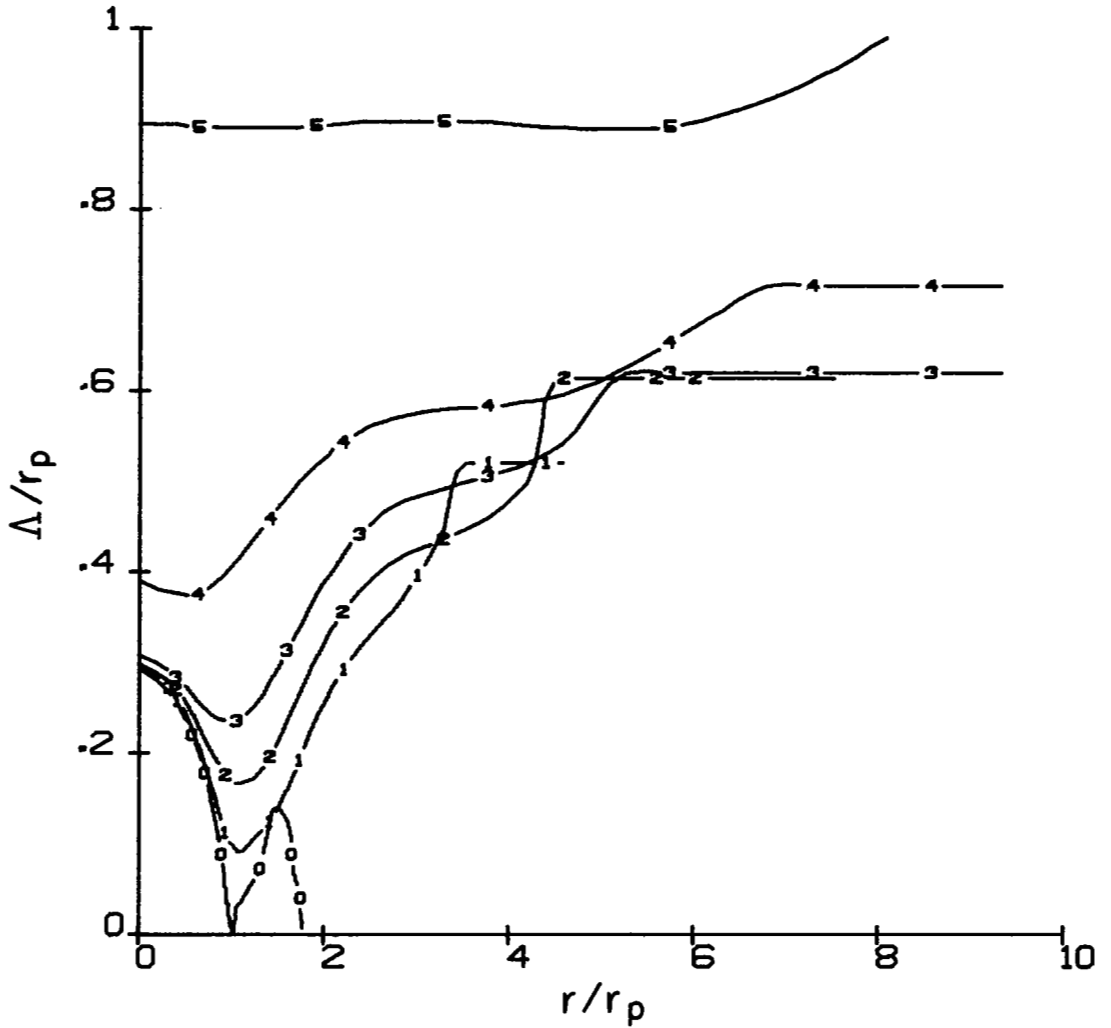
Figure 15f. Predicted integral scale parameter profiles for a high by pass ratio jet as a function of downstream distance (Lu, et al simulation). See Fig. 15a for legend
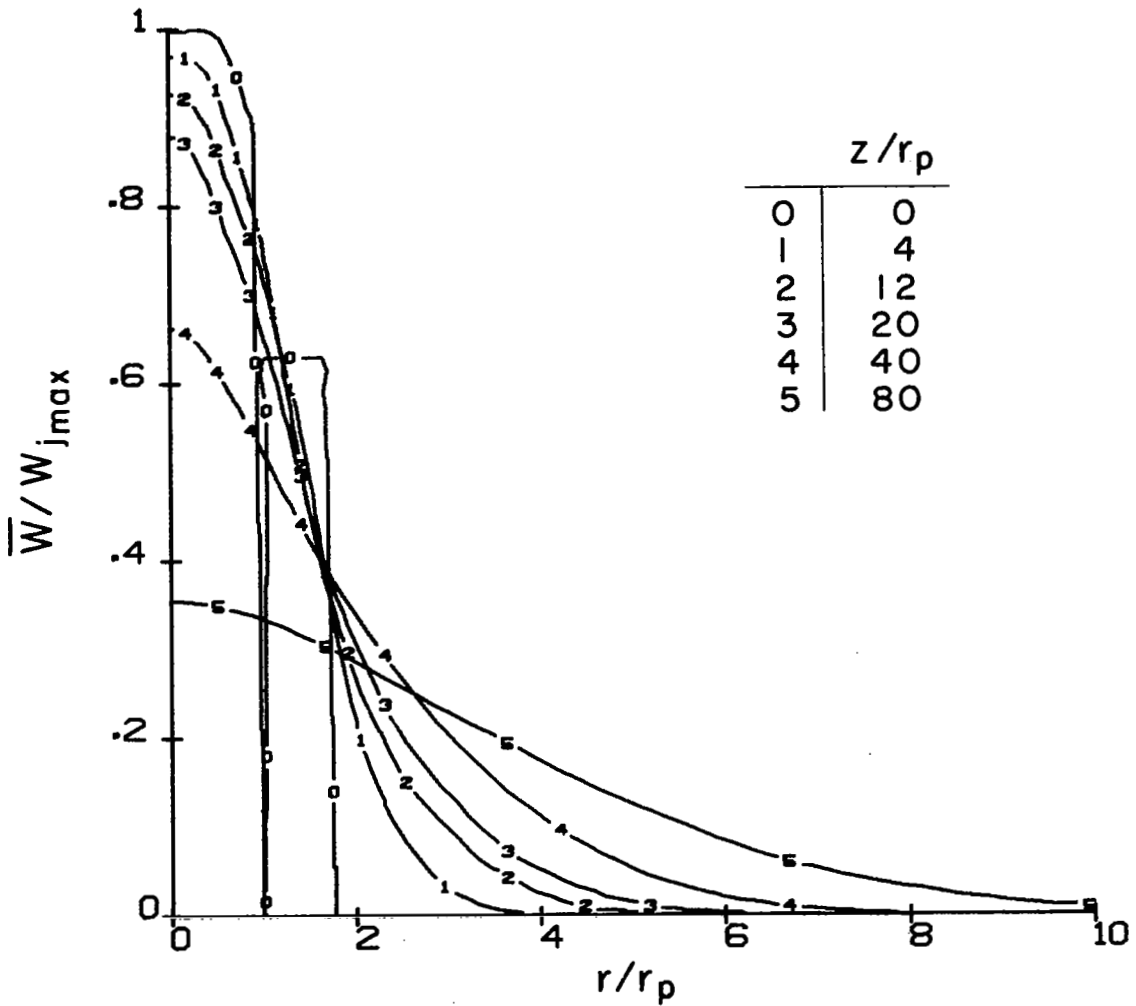
Figure 16a. Predicted axial velocity profiles (swirl V_{max}/W_{max} = 0.45) for a high by pass ratio jet as a function of downstream distance (Lu, et all simulation)
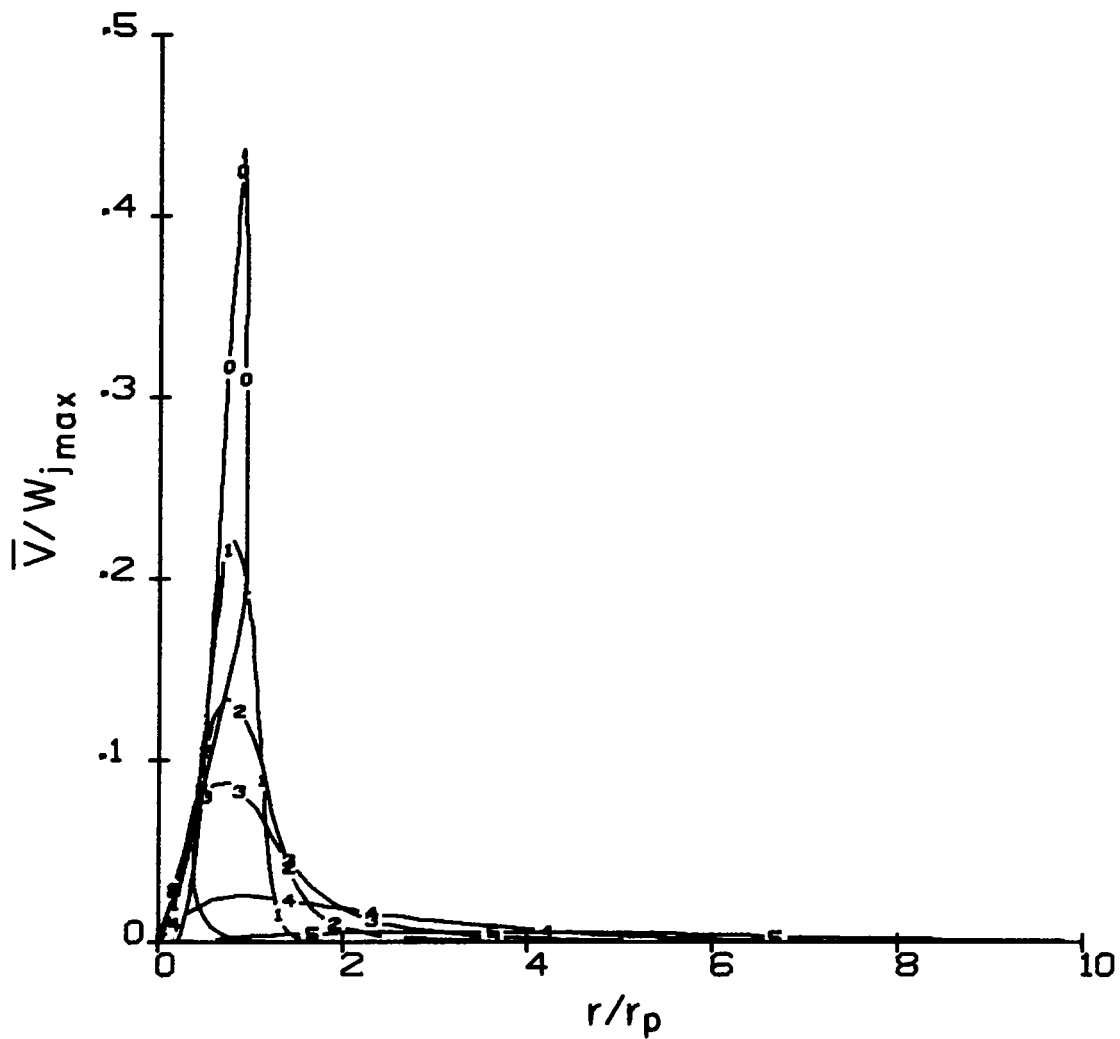
Figure 16b.   Predicted swirl velocity profiles for a high by
              pass ratio jet as a function of downstream distance
              (Lu, et all simulation).   See Fig. 16a for legend
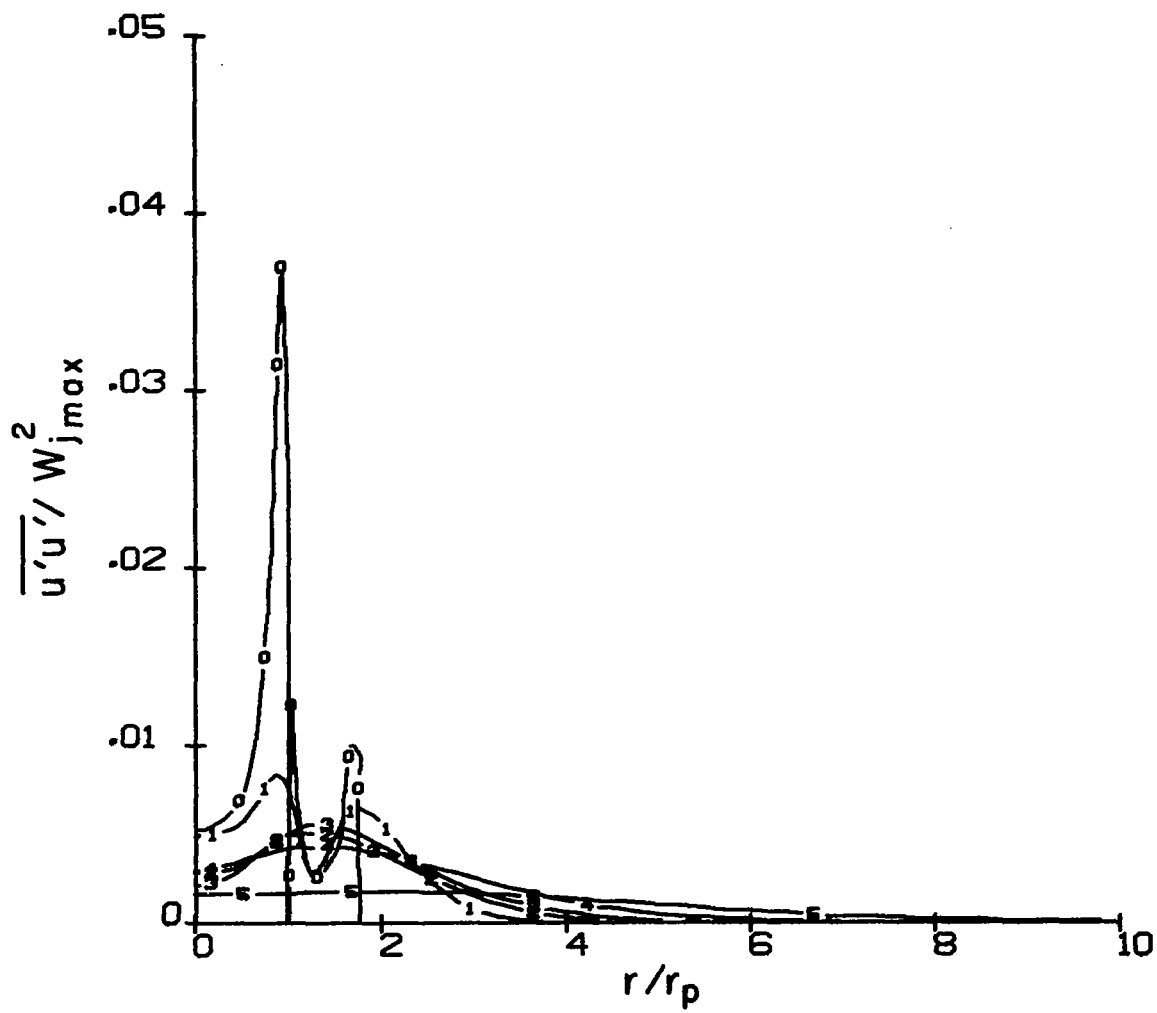
Figure 16c.   Predicted $\overline{u'u'}$ profiles (swirl) for a high by
               pass ratio jet as a function of downstream
               distance (Lu, et al simulation). See Fig. 16a
               for legend

47
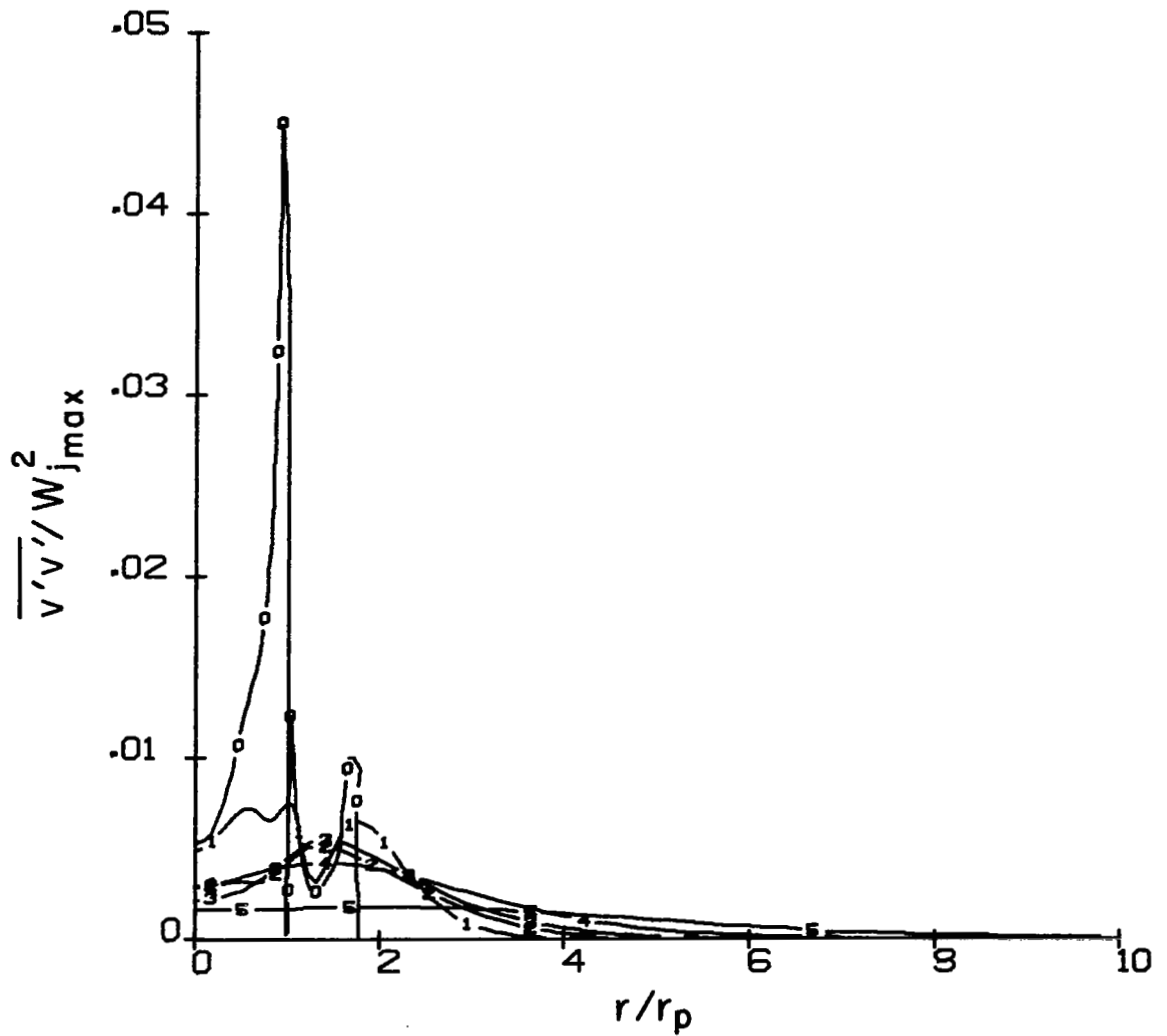
Figure 16d.   Predicted $\overline{v'v'}$ profiles (swirl) for a high by pass ratio jet as a function of downstream distance (Lu, et al simulation).   See Fig. 16a for legend
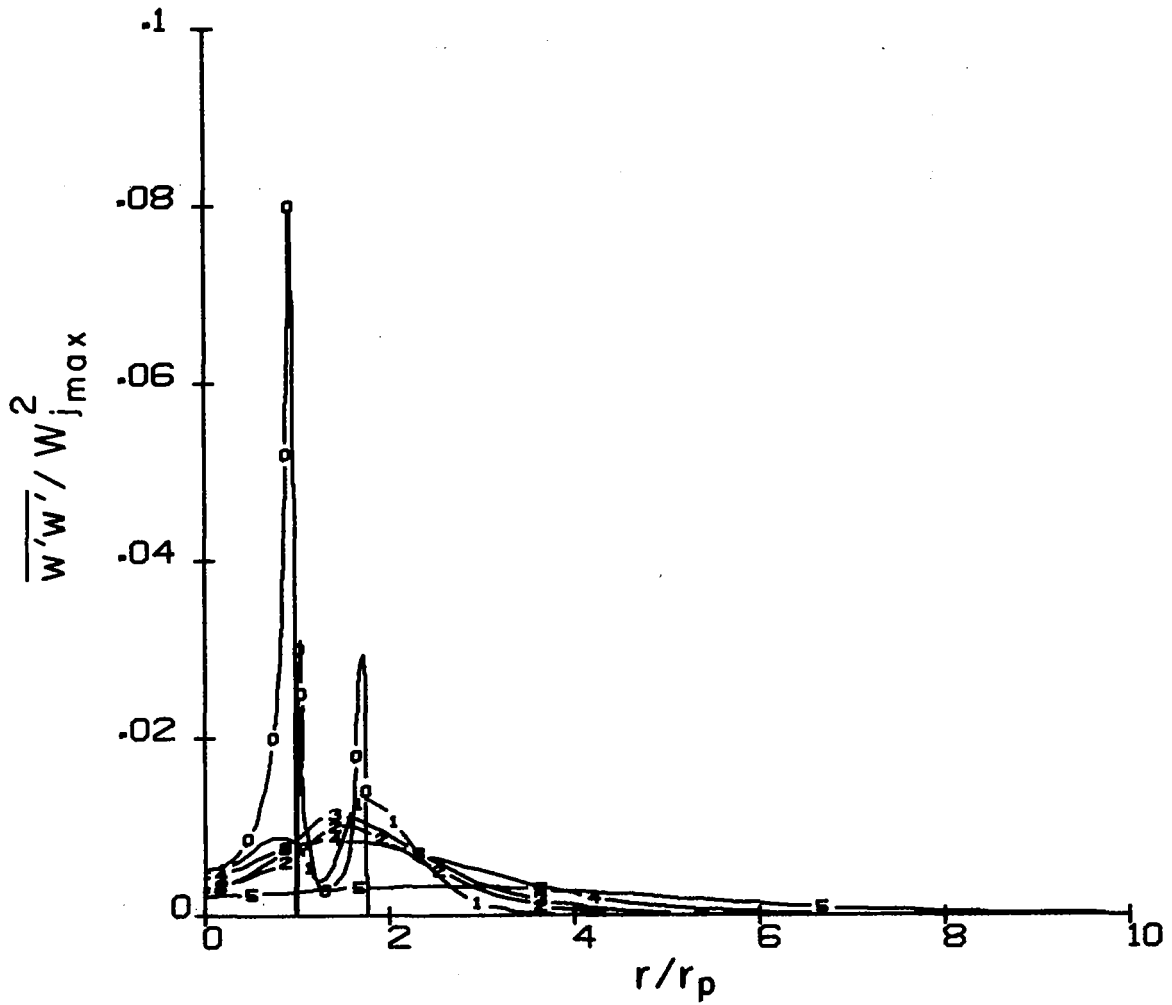
Figure 16e. Predicted $\overline{w'w'}$ profiles (swirl) for a high by pass ratio jet as a function of downstream distance (Lu, et al simulation). See Fig. 16a for legend
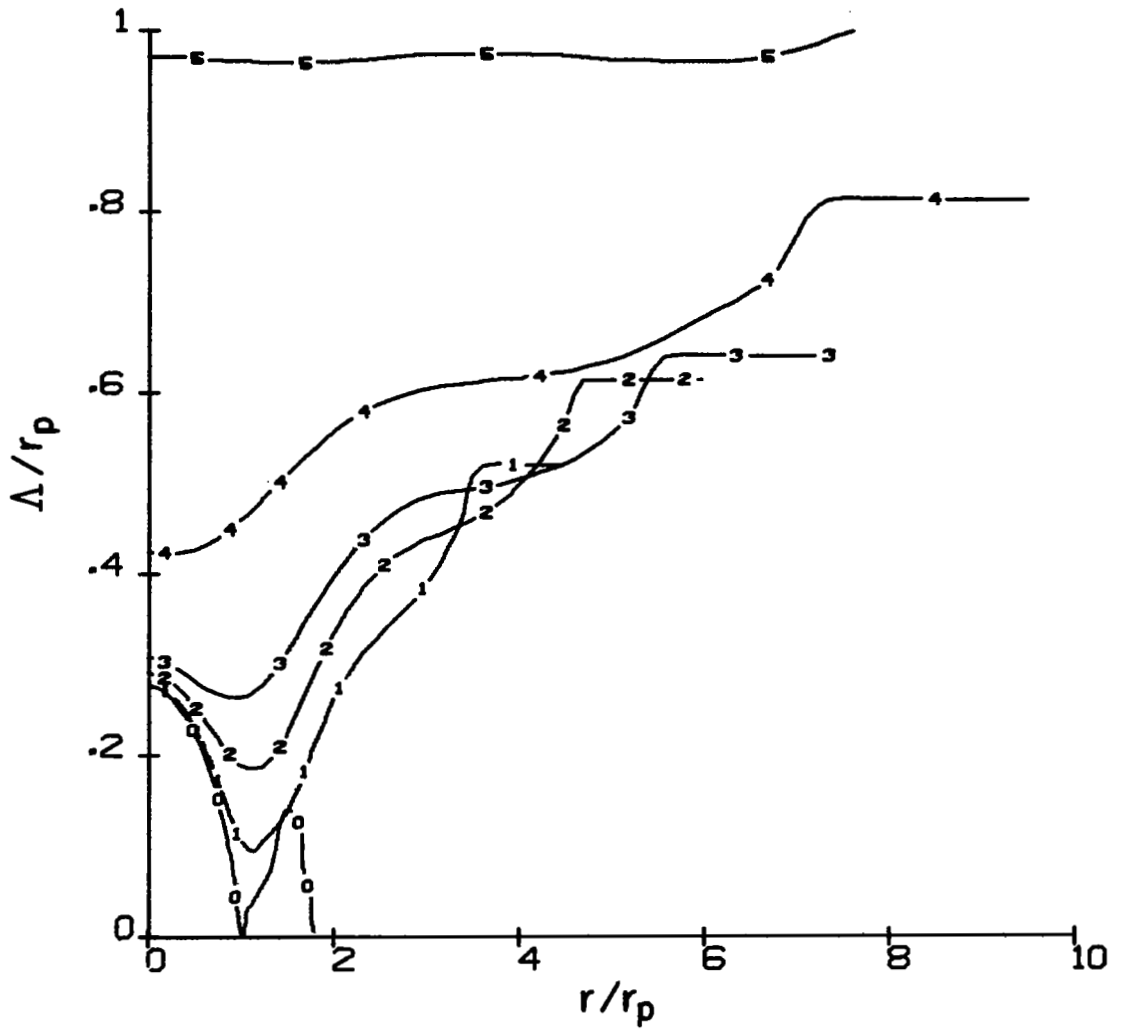
Figure 16f.   Predicted integral scale parameter (swirl) pro-
              files for a high by pass ratio jet as a function
              of downstream distance (Lu, et al simulation).
              See Fig. 16a for legend
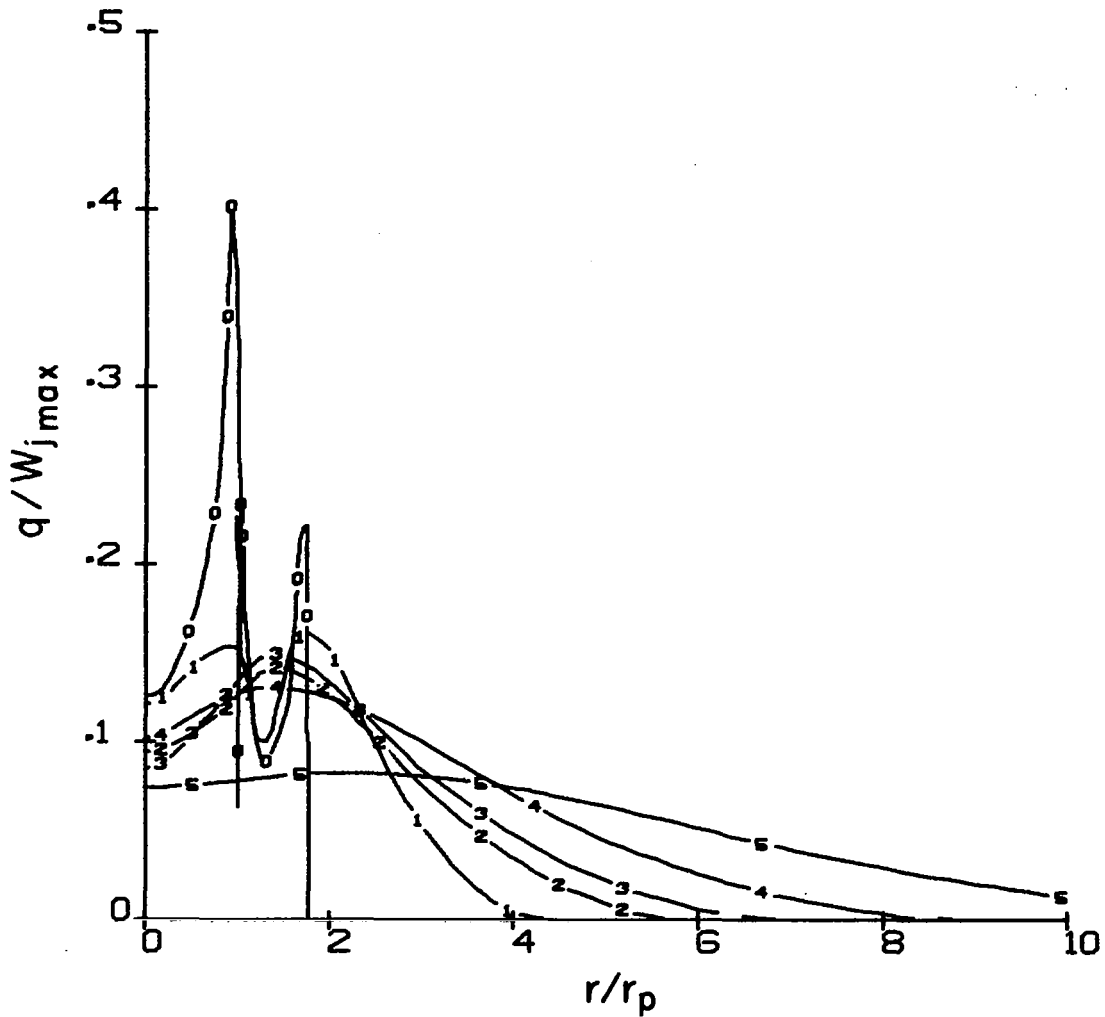
Figure 16g. Predicted turbulence profiles (swirl) for a high
by pass ratio jet as a function of downstream
distance (Lu, et al simulation). See Fig. 16a
for legend
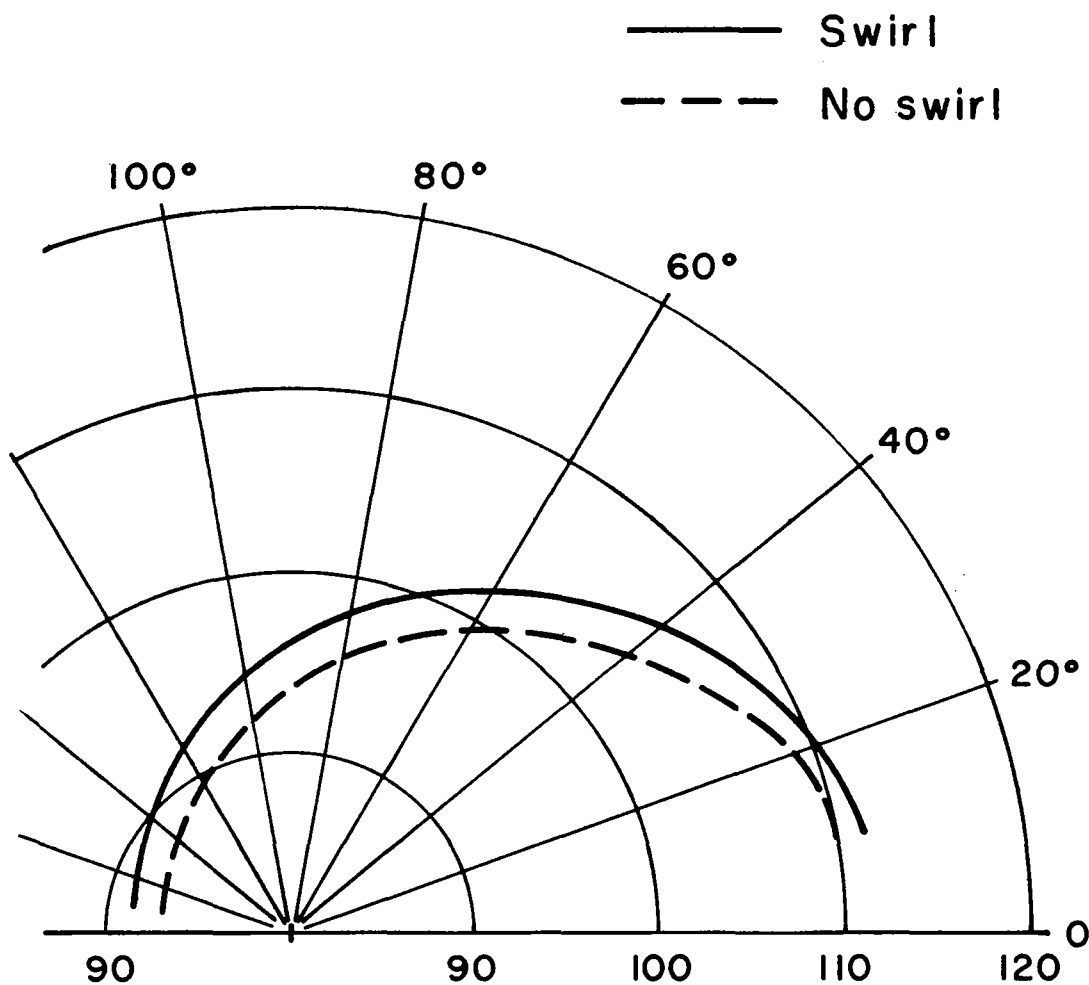
Figure 17. Predicted directivity for high by pass swirled and nonswirled jets, intensity (dB re 10^{-12} W/m^2)

$$\Delta W_{max}/W_o = 1$$

$$x/D = 0$$
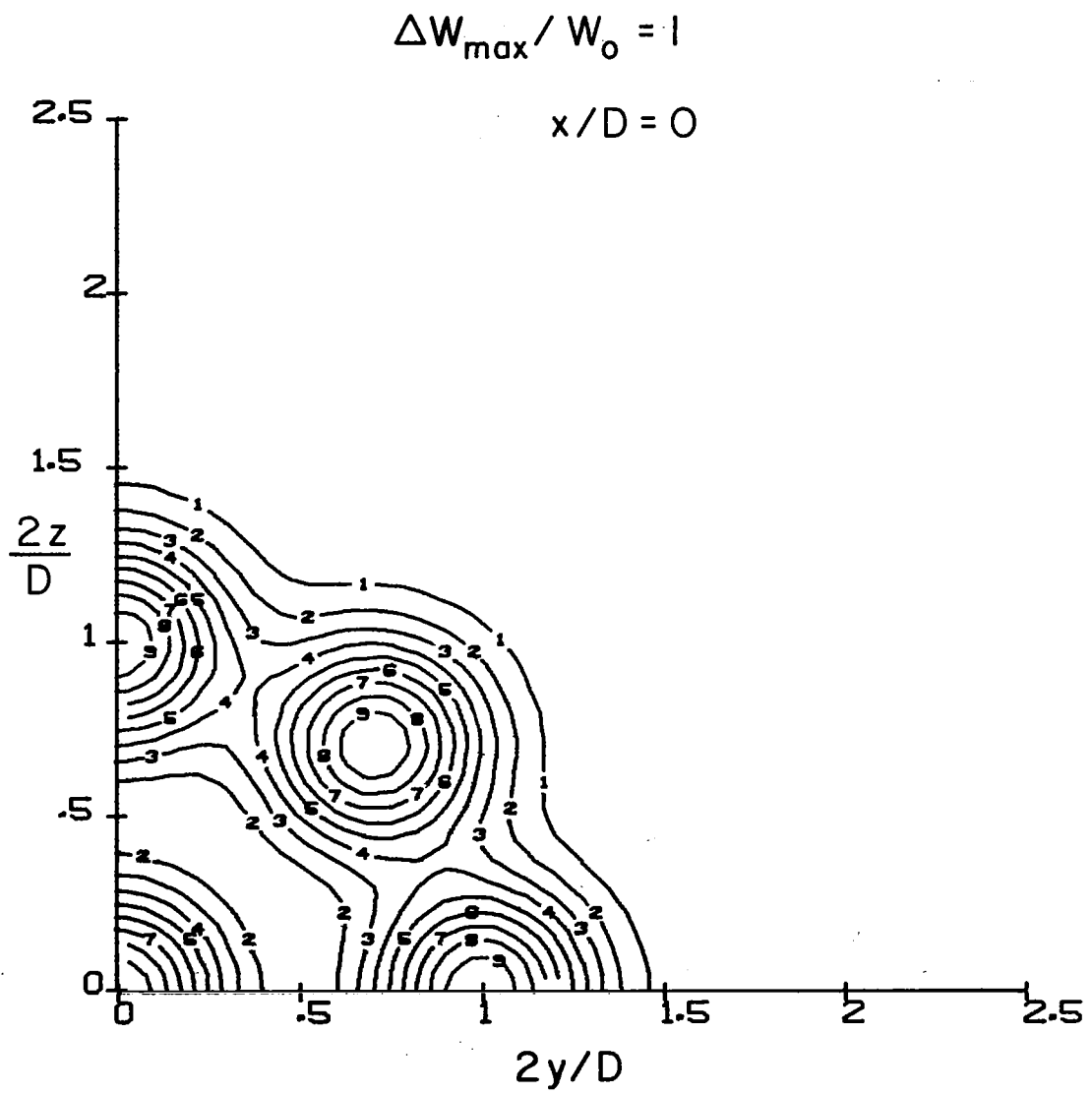
Figure 18a. The curves are numbered such that the maximum value is scaled to be 10 with 5 denoting 50%, etc.
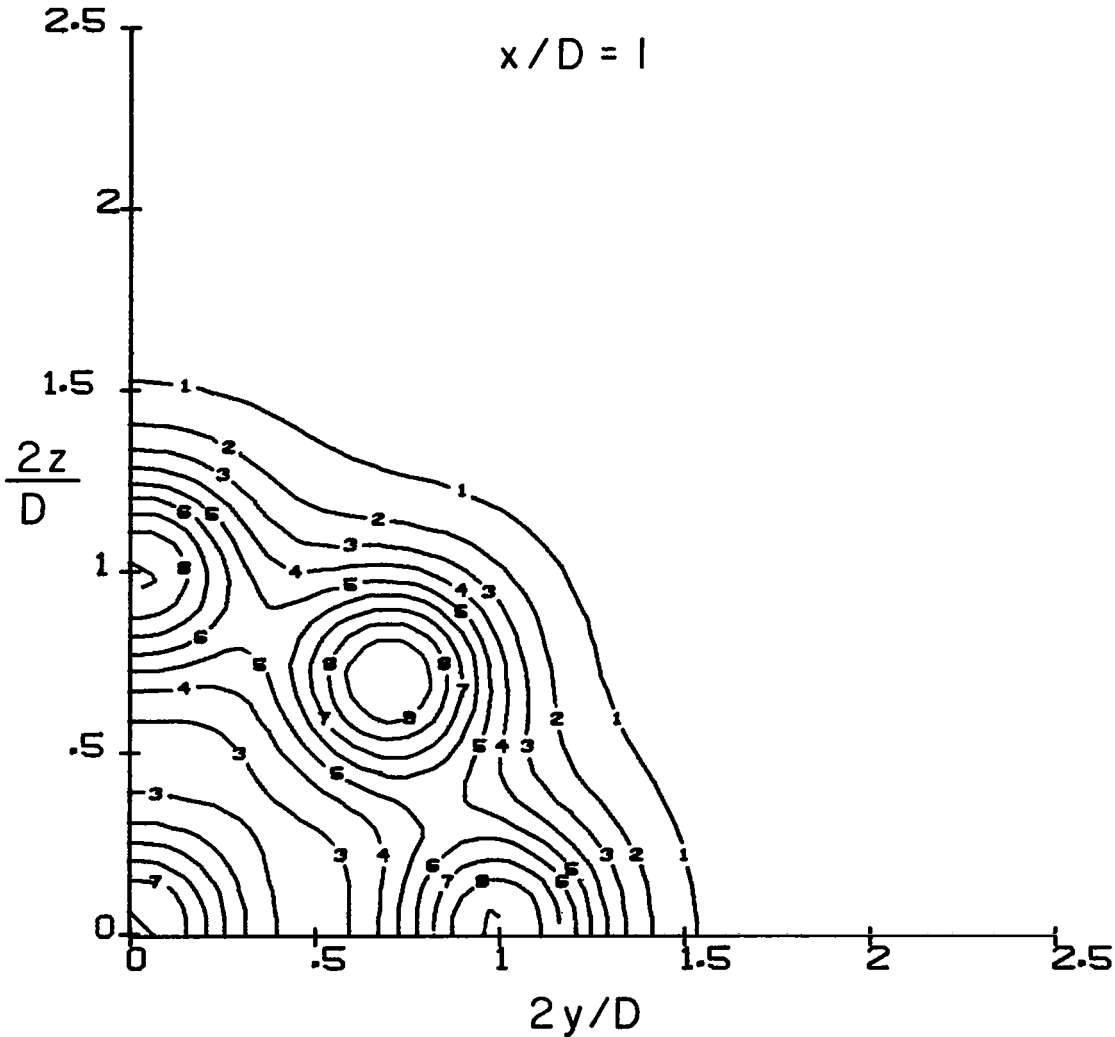
Figure 18b.   Isopleths of axial velocity at downstream position
x/D = 1

$\Delta W_{max} / W_o = .59$
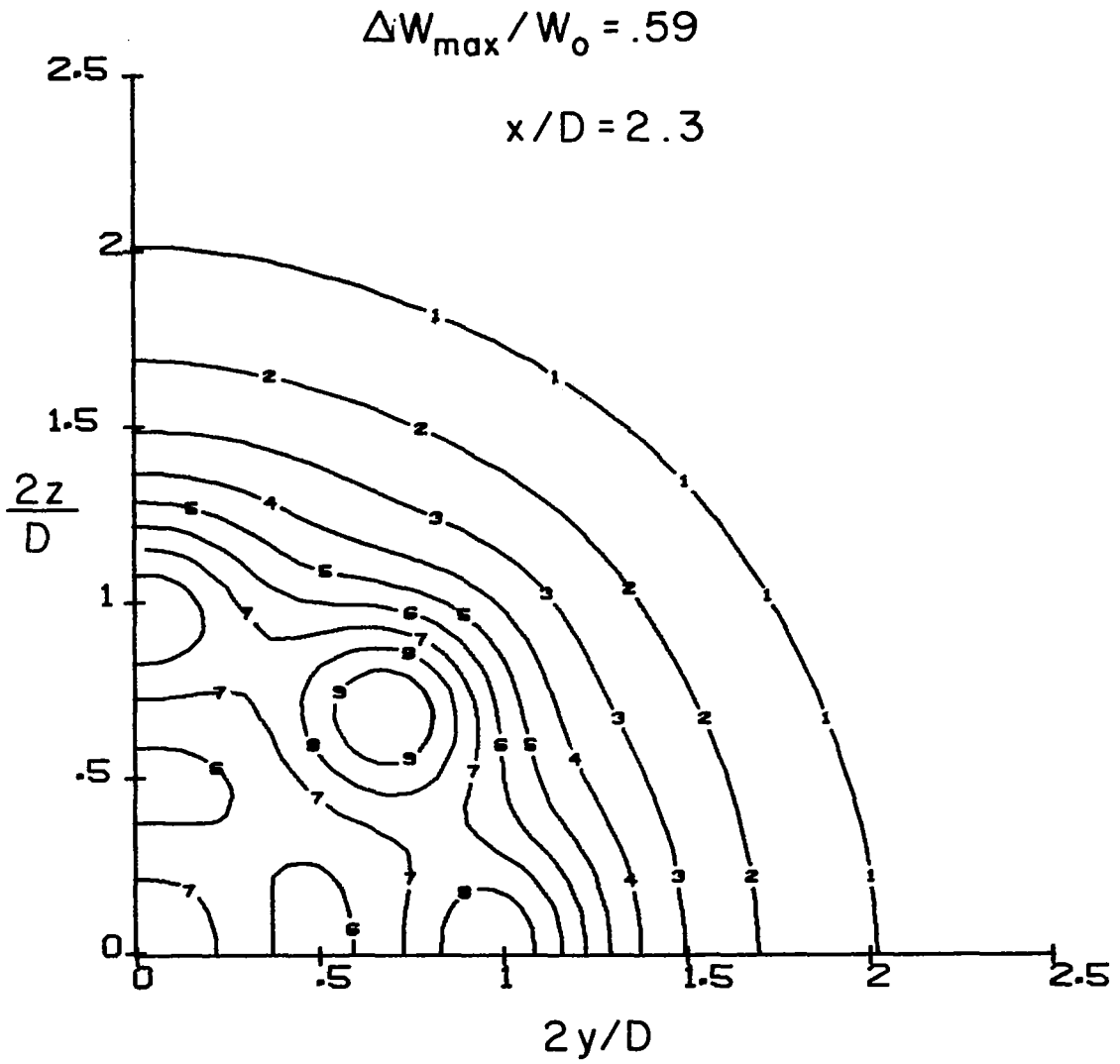
$x/D = 2.3$

Figure 18c. Isopleths of axial velocity at downstream position
x/D = 2.3
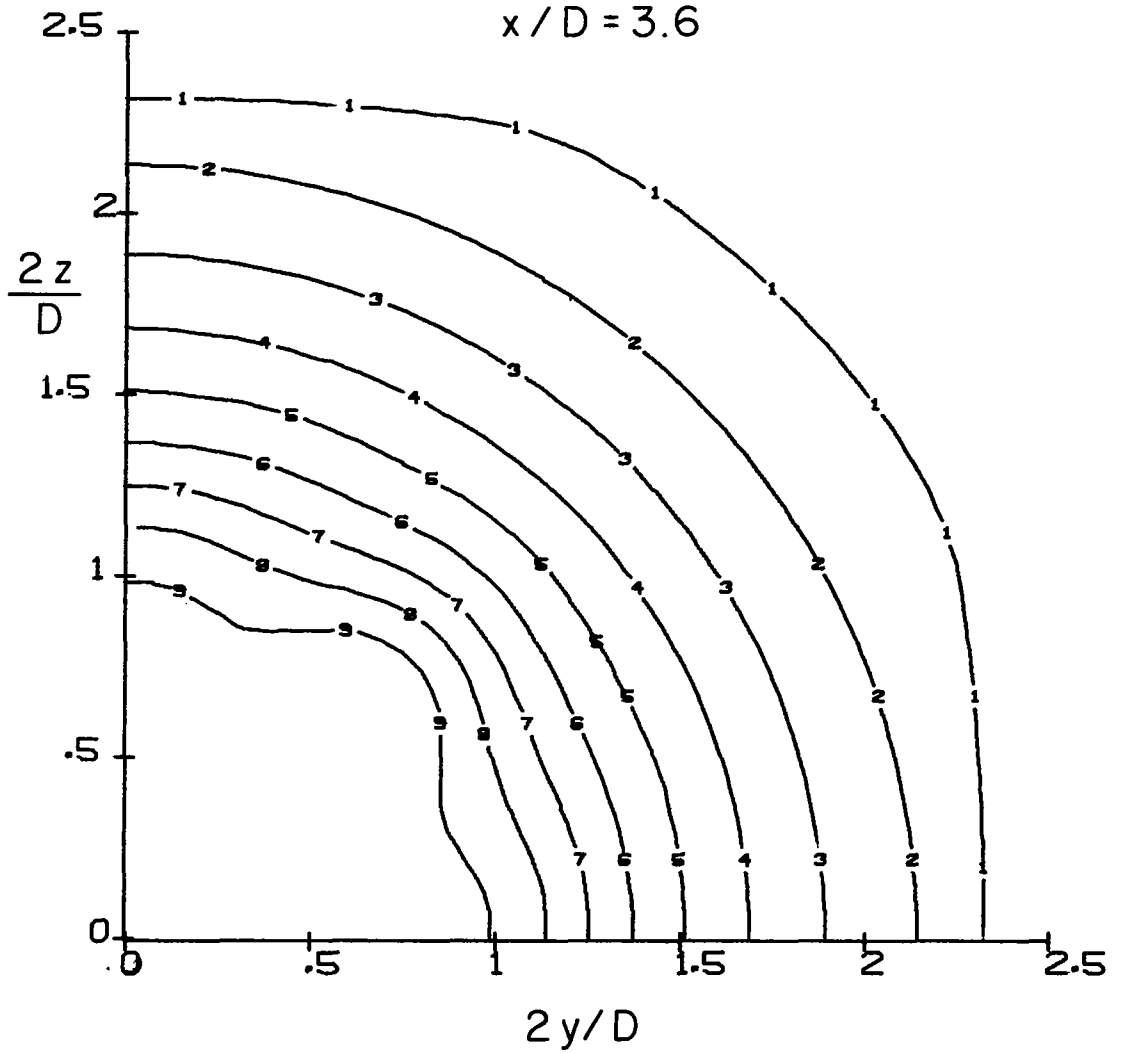
Figure 18d. Isopleths of axial velocity at downstream position
x/D = 3.6
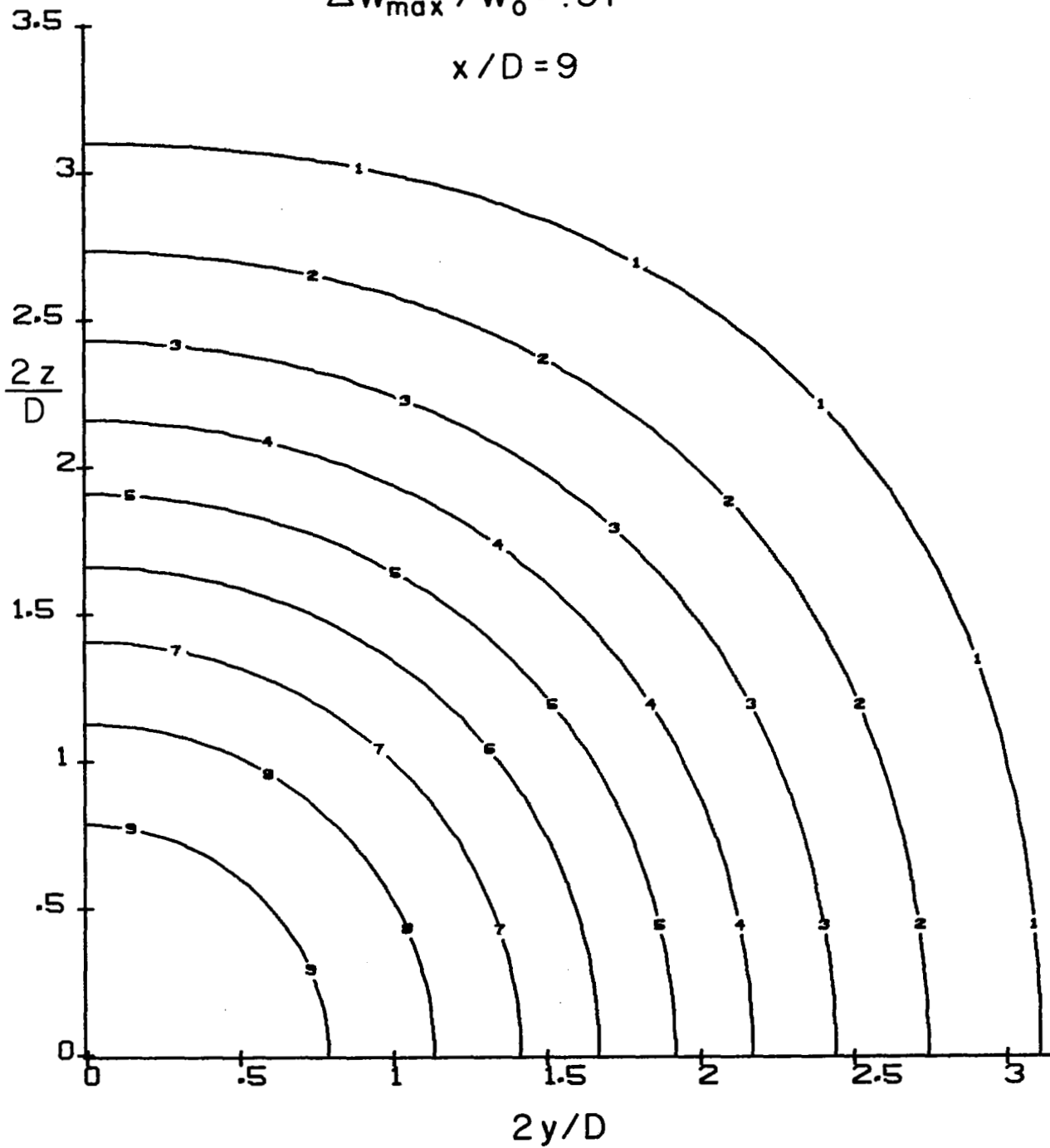
Figure 18e. Isopleths of axial velocity at downstream position x/D = 9
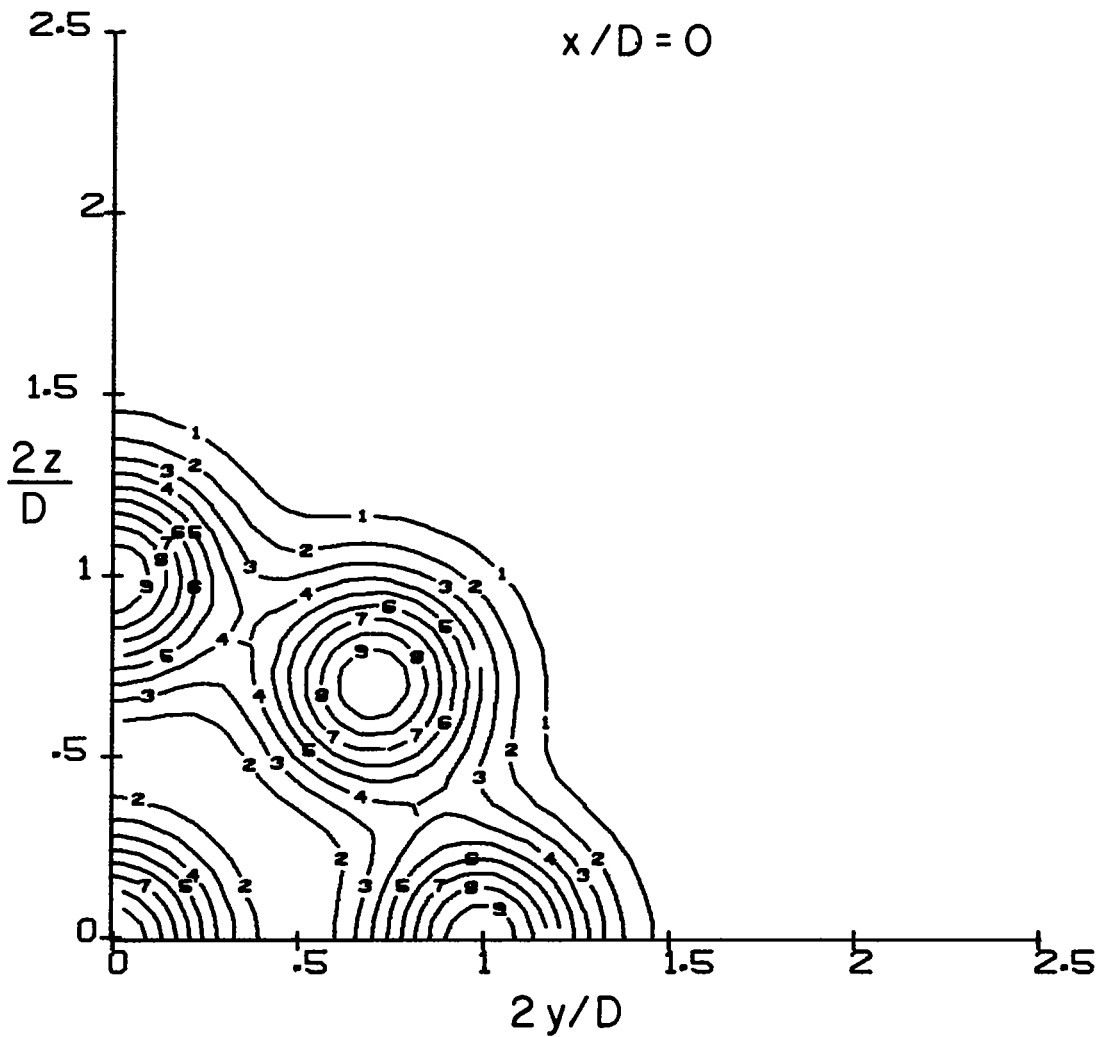
Figure 19a. Isopleths of turbulent intensity at downstream position x/D = 0. The numbers on the curves indicate the value of the turbulent intensity such that the maximum value = 10

$$q_{max}^2 / W_o^2 = .0334$$

$$x/D = 1$$
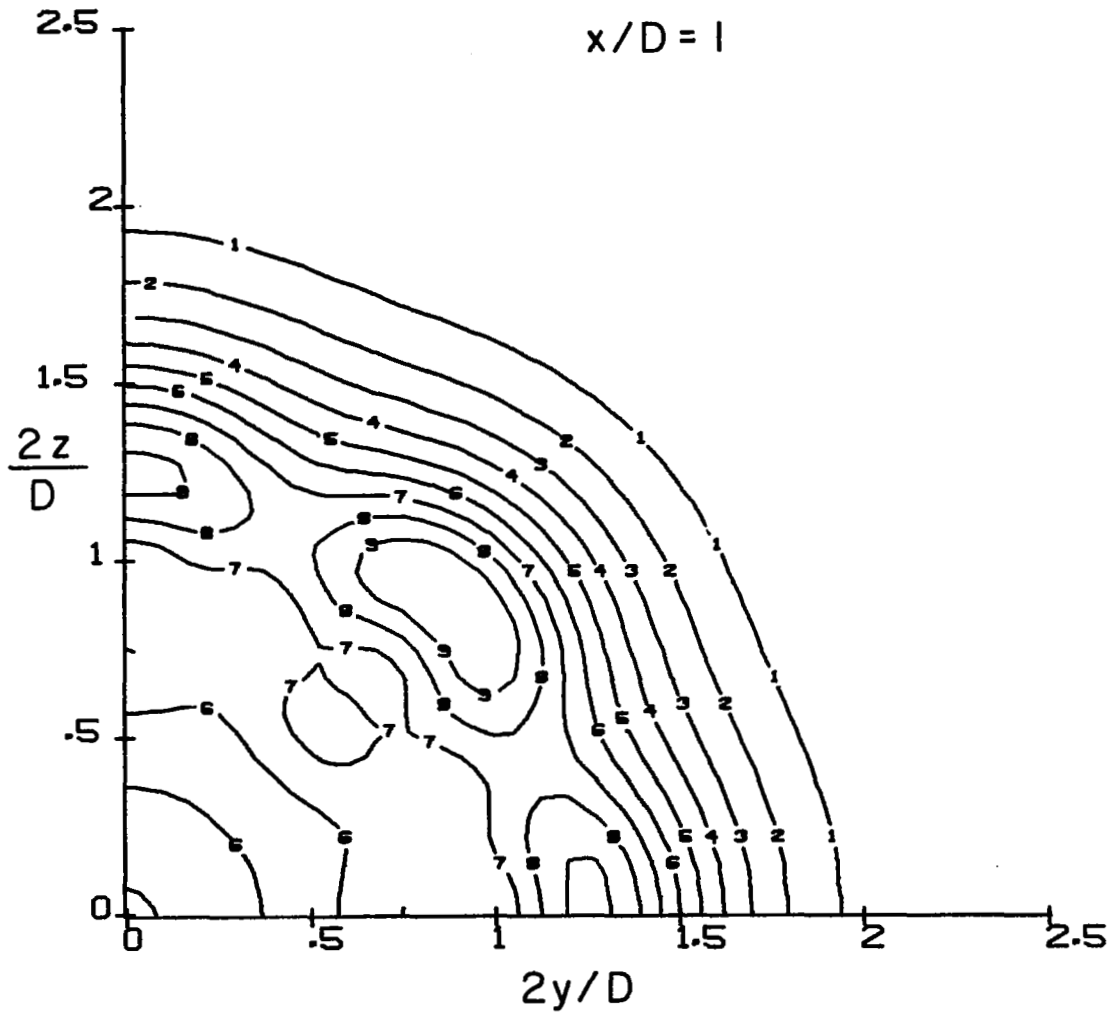
Figure 19b.   Isopleths of turbulent intensity at downstream
              position   x/D = 1

$$q^2_{max} / W^2_o = .045$$
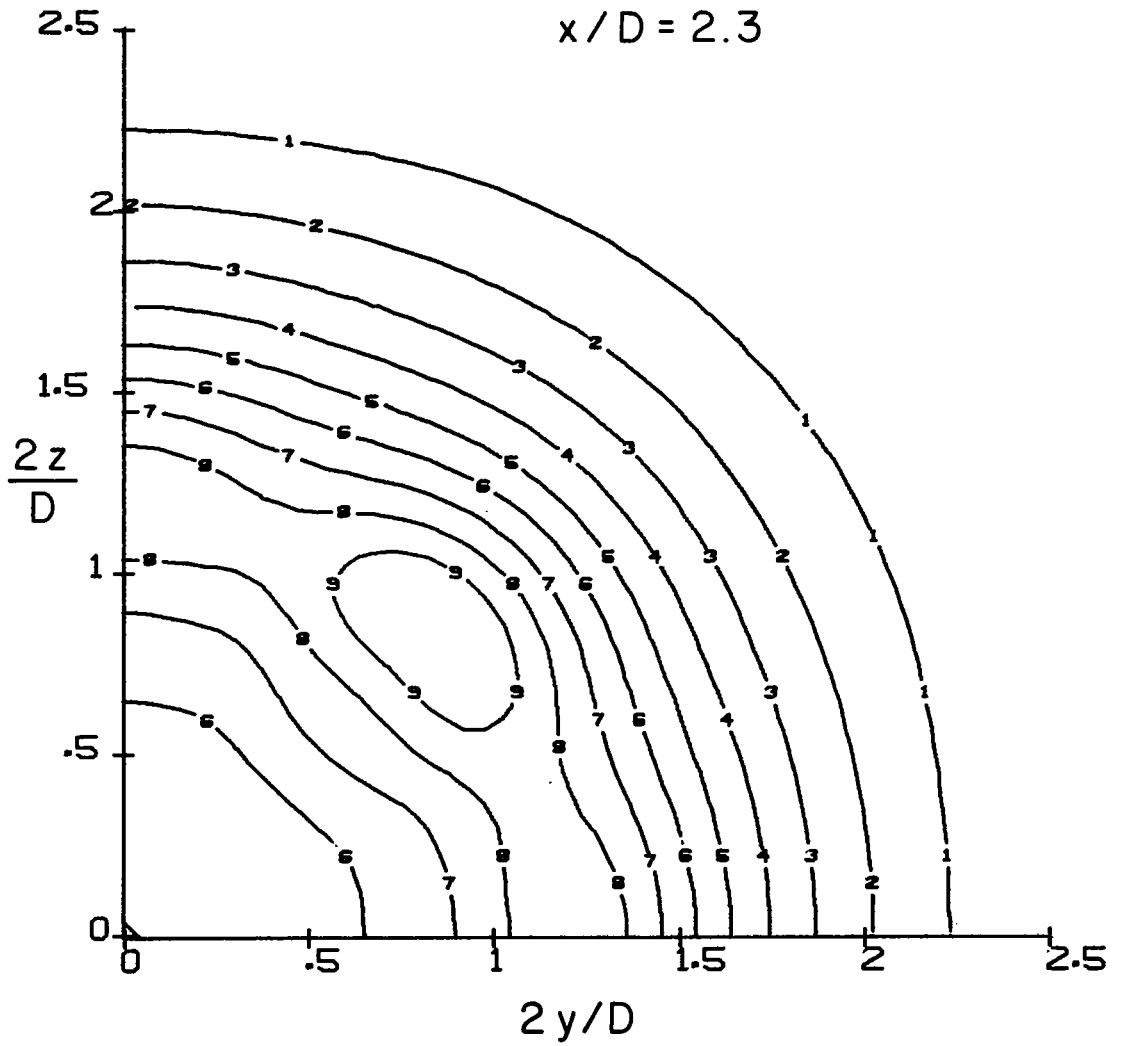
$$x / D = 2.3$$

Figure 19c. Isopleths of turbulent intensity at downstream
position x/D = 2.3

60

$$q_{max}^2 / W_o^2 = .0293$$
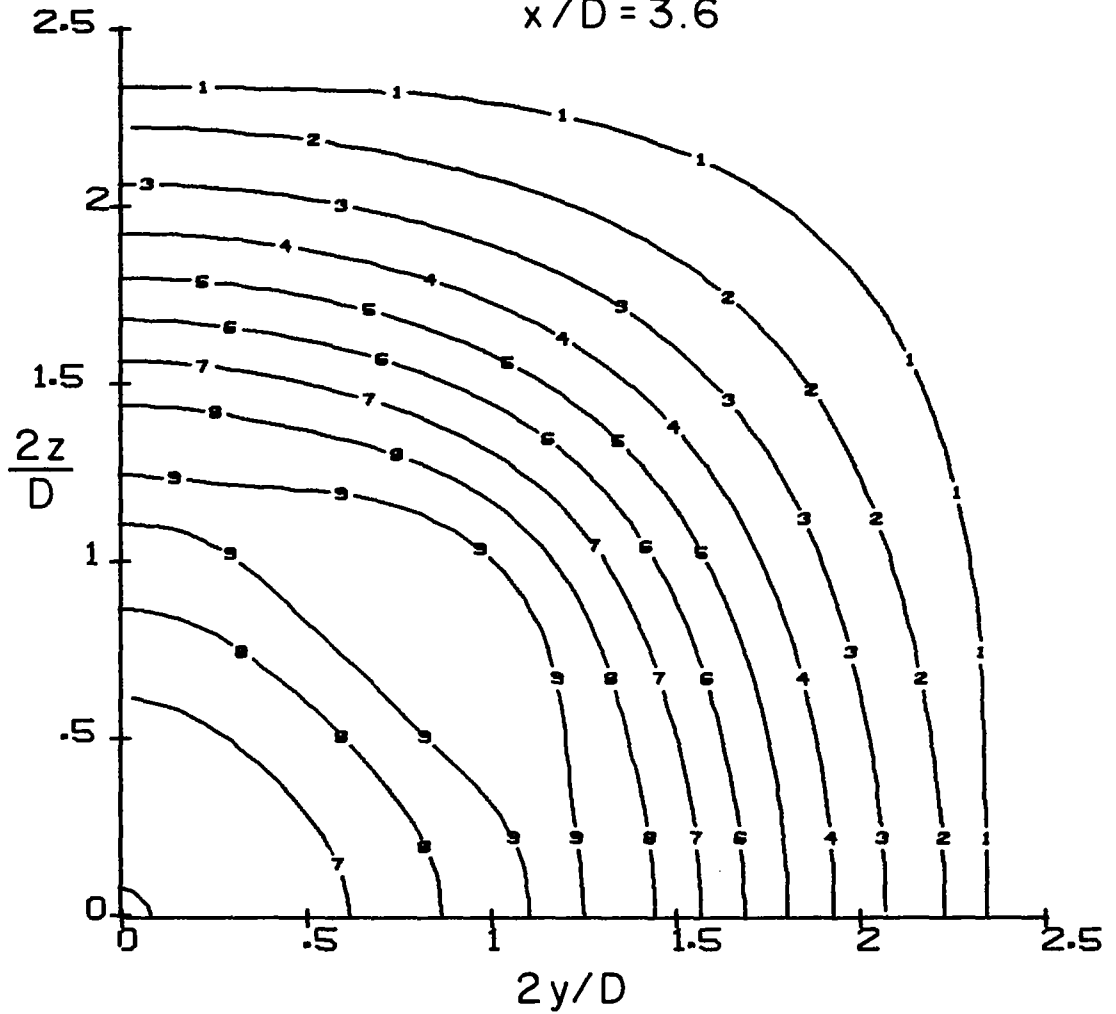
$$x/D = 3.6$$

Figure 19d. Isopleths of turbulent intensity at downstream
position $x/D = 3.6$

$$\frac{q^2_{max}}{W^2_o} = .00837$$

$$x/D = 9$$
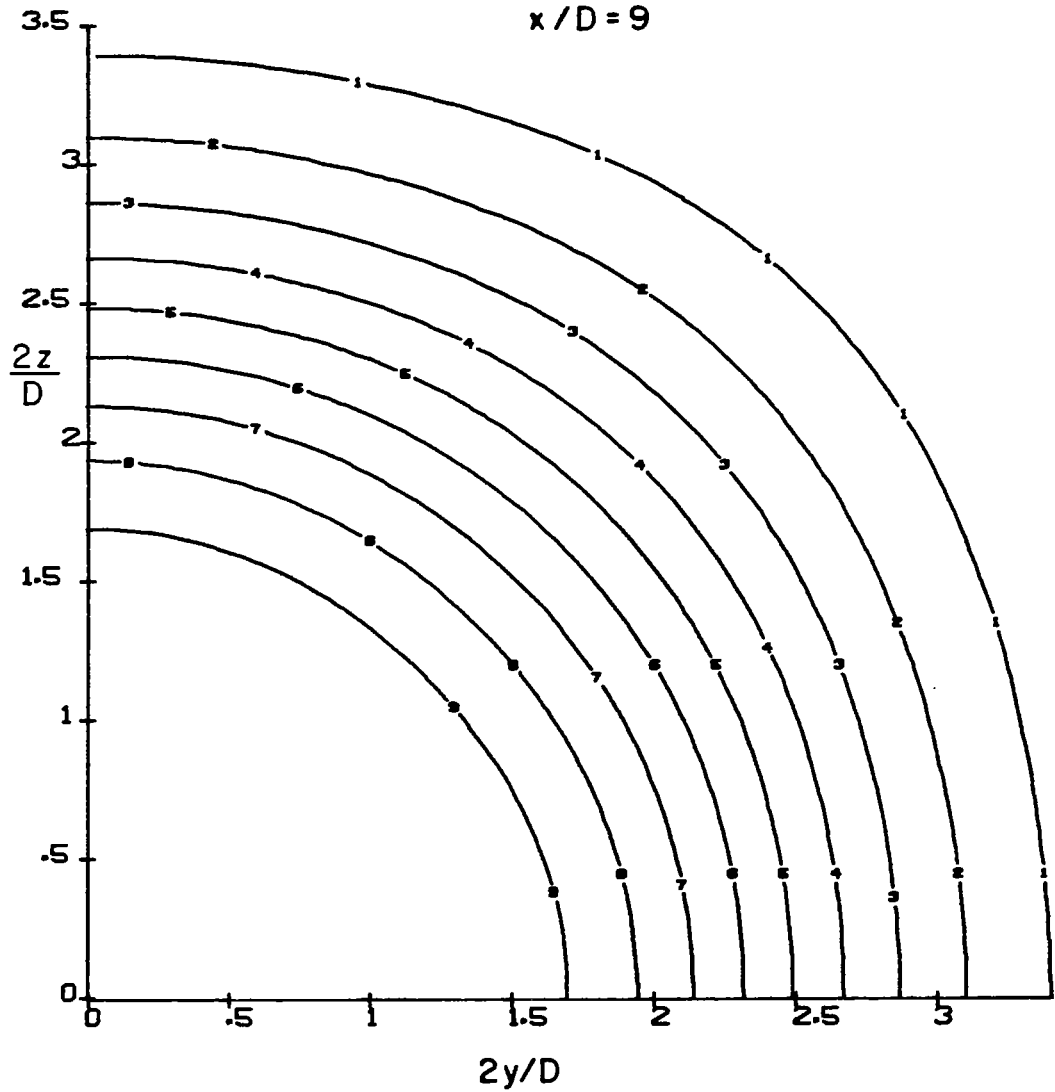
Figure 19e.   Isopleths of turbulent intensity at downstream
position   z/D = 9

an equal thrust, equal diameter axisymmetric Gaussian jet, using TDV. The reduction of intensity Δdb is shown in Fig. 20.

VI.   THE EFFECT OF HEAT AND SWIRL ON TURBULENT JET STRUCTURE

It is apparent that model predictions show that swirl does substantially alter the structure of a cold jet but that substantial reduction in the sound power radiated has not been computed to occur. It is clear that this result is opposite of that obtained by Schwartz[13] experimentally where swirl was imparted to hot jets. Here, he has shown that by swirling the exhaust from turbo-fan and turbo-jet engines, substantial reductions in total sound power radiated can be achieved with little loss of thrust.

In this section we propose a possible explanation of this discrepancy based on the neglect of mean density gradients. Our approach is to again examine the superequilibrium limit of our turbulent model including the effects of radial variation of density.

Consider the flow geometry shown in Fig. 21. To reduce the algebraic manipulations, we will neglect streamwise dependence on all variables and seek only a radial balance between terms. Furthermore, we will suppress the turbulence produced by the axial velocity and only examine the production of turbulence by swirl and radial density gradients. This assumption again reduces the algebraic complexity but still retains the swirl and radial density gradient production terms in the rate equations for the correlations. When the Mach number is moderate and the superequilibrium limit of the modeled rate equations are taken, the rate equations become
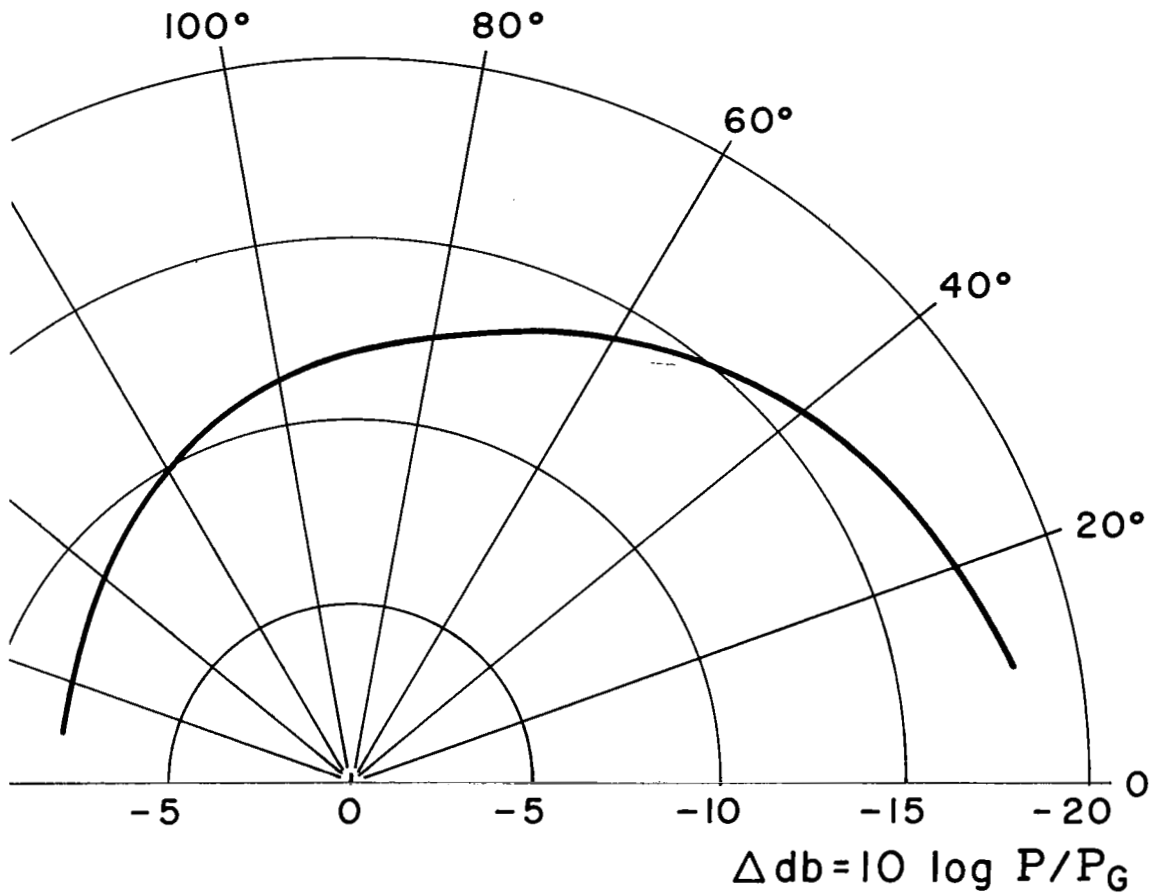
Figure 20. Comparison of the directivity of the multitube
suppressor to the axisymmetric jet. I = intensity
of the multitube, I_G = intensity of the axi-
symmetric Gaussian
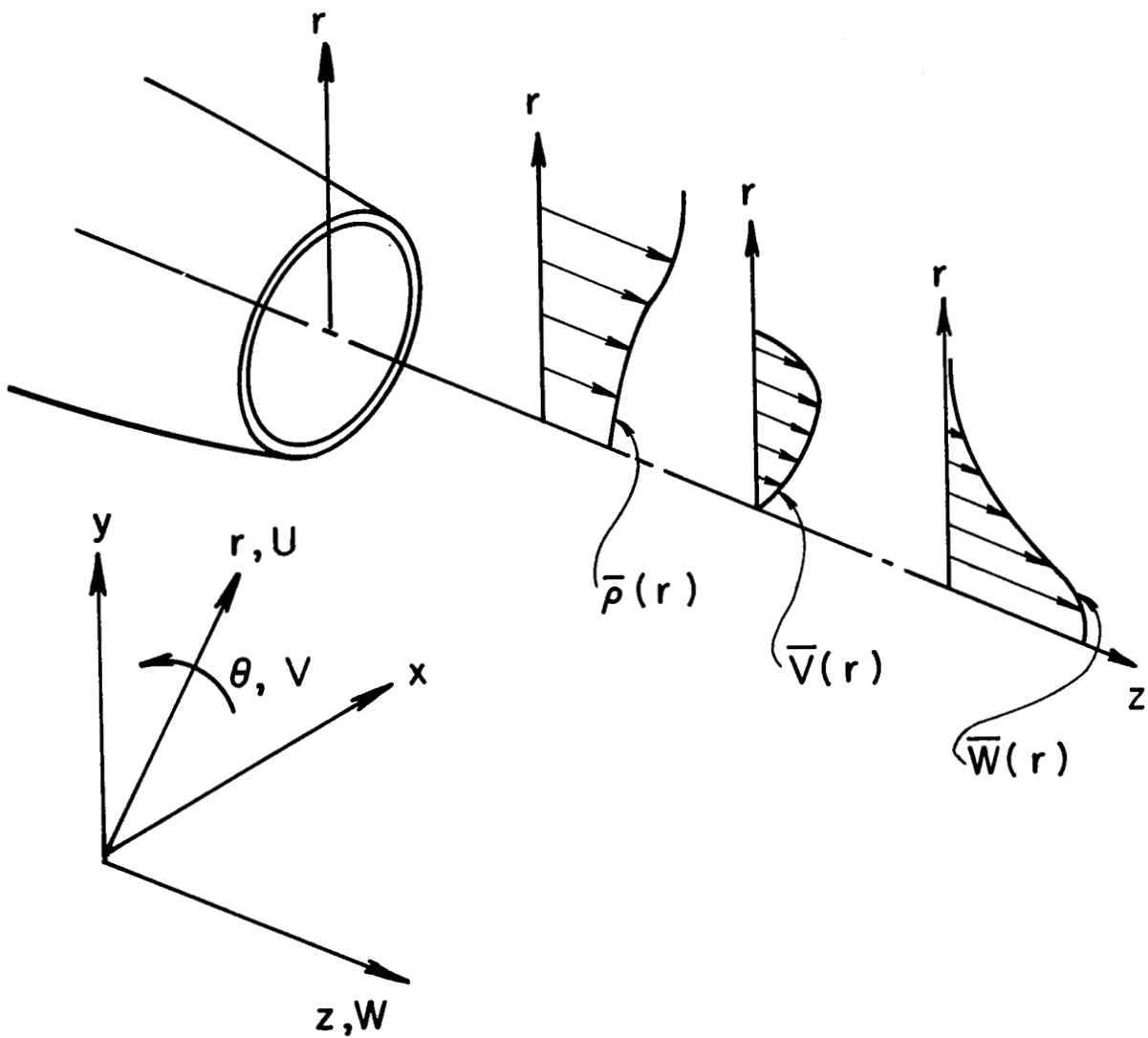
Figure 21. Radial density, axial and swirl velocity distributions in a jet exhaust.

$$q \frac{\overline{u'u'}}{\Lambda} = \frac{q^3}{4\Lambda} + 4 \frac{\overline{V}}{r} \overline{u'v'} + 2 \frac{\overline{\rho'u'}}{\overline{\rho}} \frac{\overline{V}^2}{r}$$

$$q \frac{\overline{v'v'}}{\Lambda} = \frac{q^3}{4\Lambda} - 2 \frac{(r\overline{V})_r}{r} \overline{u'v'}$$

$$q \frac{\overline{w'w'}}{\Lambda} = \frac{q^3}{4\Lambda}$$

$$q \frac{\overline{u'v'}}{\Lambda} = - \frac{(r\overline{V})_r}{r} \overline{u'u'} + 2 \frac{\overline{V}}{r} \overline{v'v'} + \frac{\overline{V}^2}{r} \frac{\overline{\rho'v'}}{\overline{\rho}}$$

$$A \frac{q}{\Lambda} \overline{\rho'u'} = - \overline{\rho}_r \overline{u'u'} + \frac{\overline{V}^2}{r} \frac{\overline{\rho'\rho'}}{\overline{\rho}} + 2 \frac{\overline{V}}{r} \overline{\rho'v'}$$

$$A \frac{q}{\Lambda} \overline{\rho'v'} = - \frac{(r\overline{V})_r}{r} \overline{\rho'u'} - \overline{\rho}_r \overline{u'v'}$$

$$bs \frac{q}{\Lambda} \overline{\rho'\rho'} = - \overline{\rho}'_r \overline{\rho'u'}$$

and

$$q = \sqrt{\overline{u'u'} + \overline{v'v'} + \overline{w'w'}}$$

A,b,s are model constants which have the values 0.75 , 0.125 and 1.8 , respectively. Lambda (Λ) is the integral scale parameter in the turbulent model and has the dimensions of length. Solution to the above system can be obtained by assuming

$$\overline{u'u'} = UU\Lambda^2(\overline{V}_r - \frac{\overline{V}}{r})^2$$

$$\overline{v'v'} = VV\Lambda^2(\overline{V}_r - \frac{\overline{V}}{r})^2 \qquad\qquad \overline{\rho'u'} = RU\Lambda^2\overline{\rho}_r(\overline{V}_r - \frac{\overline{V}}{r})$$

$$\overline{w'w'} = WW\Lambda^2(\overline{V}_r - \frac{\overline{V}}{r})^2 \qquad\qquad \overline{\rho'v'} = RV\Lambda^2\overline{\rho}_r(\overline{V}_r - \frac{\overline{V}}{r})$$

$$q^2 = QQ\Lambda^2(\overline{V}_r - \frac{\overline{V}}{r})^2 \qquad\qquad \overline{\rho'\rho'} = RR\Lambda^2\overline{\rho}_r^2$$

$$\overline{u'v'} = UV\Lambda^2(\overline{V}_r - \frac{\overline{V}}{r})^2$$

and substituting Eq. (25) into Eq. (24), yielding

$$QUU = \frac{Q^3}{4} + 2SRU + 4NUV$$

$$QVV = \frac{Q^3}{4} - 2(1 + 2N)UV$$

$$QWW = \frac{Q^3}{4}$$

$$QUV = 2N(VV - UU) - UU + SRV$$

$$AQRU = 2NRV + SRR - UU$$

$$AQRV = - UV - (1 + 2N)RU$$

$$bsQRR = - RU \tag{26}$$

with

$$QQ = UU + VV + WW$$

N is again defined to be

$$N = \frac{\overline{V}}{r} / (\overline{V}_r - \frac{\overline{V}}{r}) \tag{27}$$

and S is a Richardson number defined as

$$S = \frac{\overline{\rho}_r}{\rho} \frac{\overline{V}^2}{r} / (\overline{V}_r - \frac{\overline{V}}{r})^2 \tag{28}$$

The solutions to Eq. (24) are lengthy and only the solutions for Q^2 , UV and RU are displayed below.

$$Q^2 = - \frac{B + \sqrt{B^2 - 4C}}{2} \tag{29}$$

where

$$B = \frac{S}{A}\left(5 + \frac{1}{bs}\right) + 2\frac{N}{A^2}(1 + 2N) + 16N^2 + 8N - 2$$

$$C = \frac{S^2}{A^2}\left(4 + \frac{1}{bs}\right) + \frac{S}{A}\left\{(16N^2 + 8N)\left(3 + \frac{1}{bs} - \frac{1}{A}\right)\right.$$

$$\left. + \frac{2}{A} - \frac{2}{bs}\right\} + \frac{2N}{A^2}(1 + 2N)(16N^2 + 8N - 2)$$

$$UV = -\frac{\frac{Q^3}{4}\left[2 + \frac{1}{2A} + N\left(\frac{1}{A} + 2\right)\right]}{Q^2 + 16N^2 + 12N + 2 + \frac{1}{A}(S + 1 + 2N)} \tag{30}$$

$$RU = -\frac{2\left[N\left(\frac{1}{A} + 2\right) - 1\right]UV}{\left[AQ^2 + S\left(4 + \frac{1}{bs}\right) + \frac{2N}{A}(1 + 2N)\right]} \tag{31}$$

Since Q^2 must be positive definite, there is a relationship between Richardson number and N for which $Q^2 = 0$. On Fig. 22 are shown Q^2 isopleths. As can be seen, self-sustained turbulence is possible only for those values of S and N which fall below the $Q^2 = 0$ curve. Above this curve, turbulence is damped by centrifugal effects of the swirling flow.

With the radial density set equal to zero $(S = 0)$, self-sustained turbulence is possible if $-0.68 < N < 0.18$ as has been shown by Donaldson and Bilanin.[14] Simple parallel shear flow corresponds to $N = 0$. Here, the critical Richardson number above which self-sustained turbulence is not possible is approximately 0.55, which agrees with that found by Lewellen, Ref. 5.

In Figs. 23 and 24 are shown curves of constant UV and RU, respectively. As can be seen, $RU < 0$ as it must be to insure that RR is positive definite (Eq. (26)).

The values of S and N which may be attained in a hot swirling jet cover $N < 0$ and all S if both positive and negative density gradients are allowed. Negative gradients might occur in an advanced engine which exhausts hot gas through an annular region. Therefore, it appears that the presence of swirl, coupled with mean density gradients, can profoundly affect the ability of the jet to produce turbulence. We, therefore, suggest that the mechanisms which result in noise suppression by swirling the hot
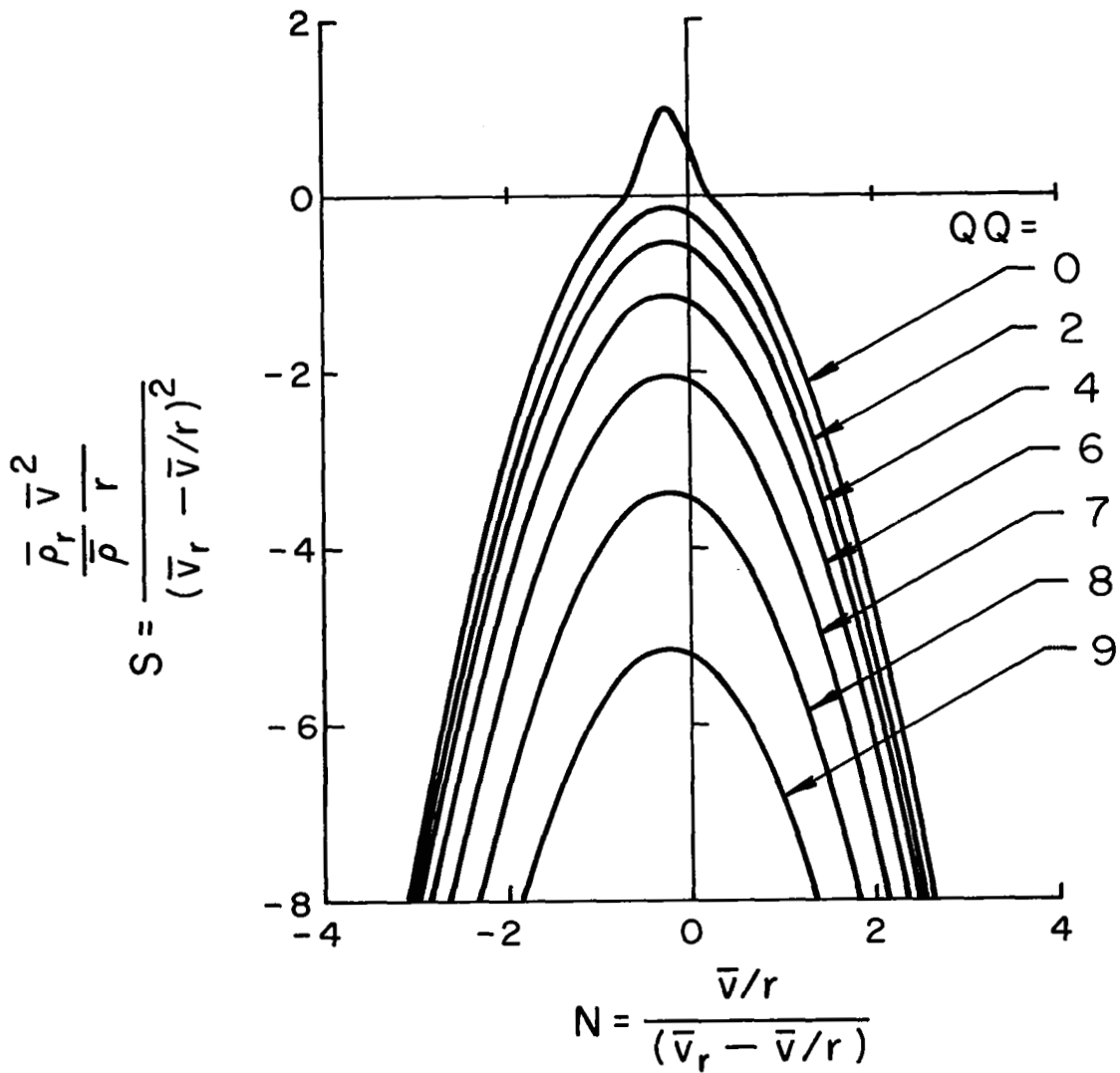
Figure 22. Isopleths for Q^2 (superequilibrium limit) as a function of swirl number N and Richardson number S.
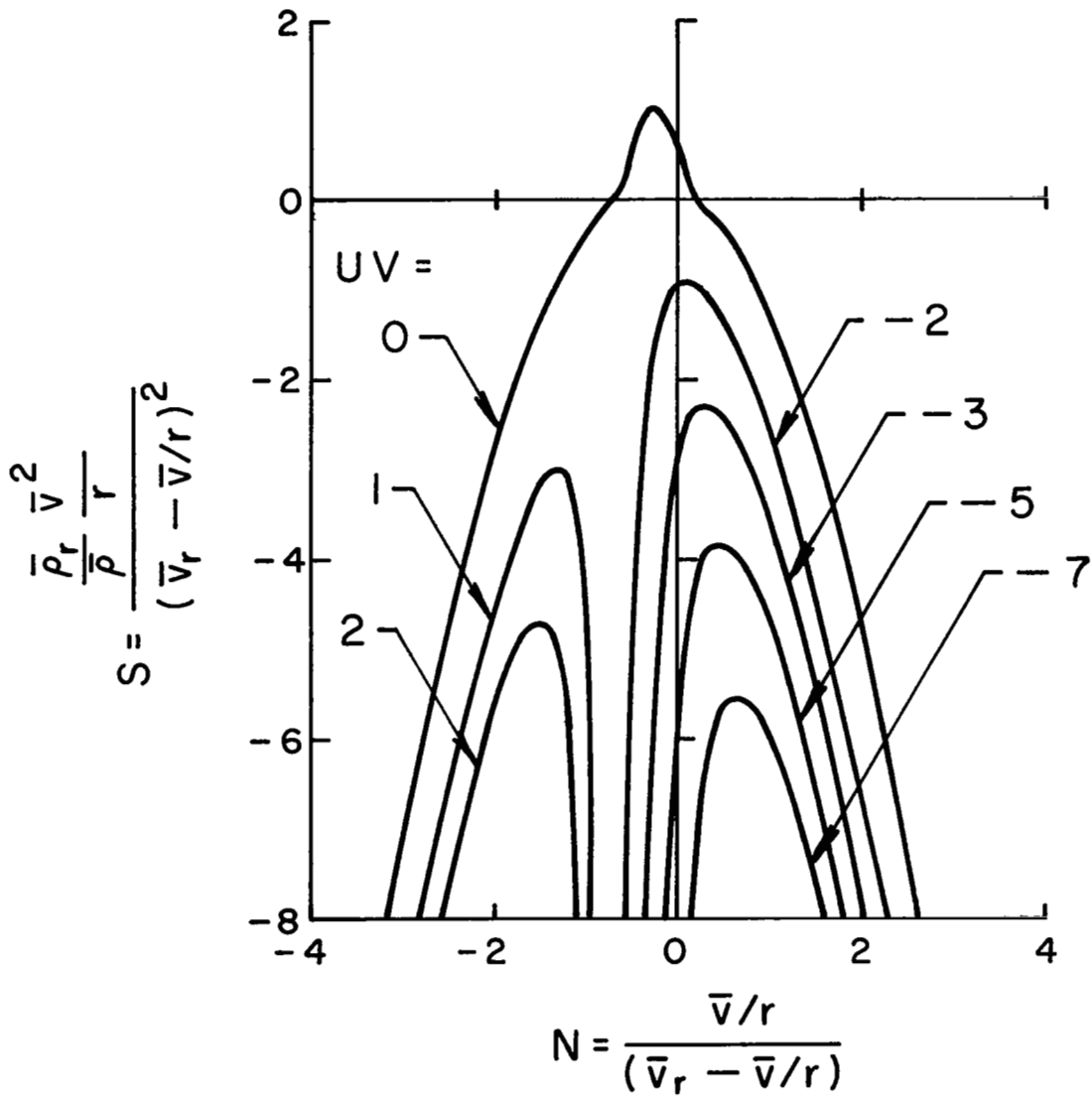
Figure 23. Isopleths for UV (superequilibrium limit) as a function of swirl number N and Richardson number S
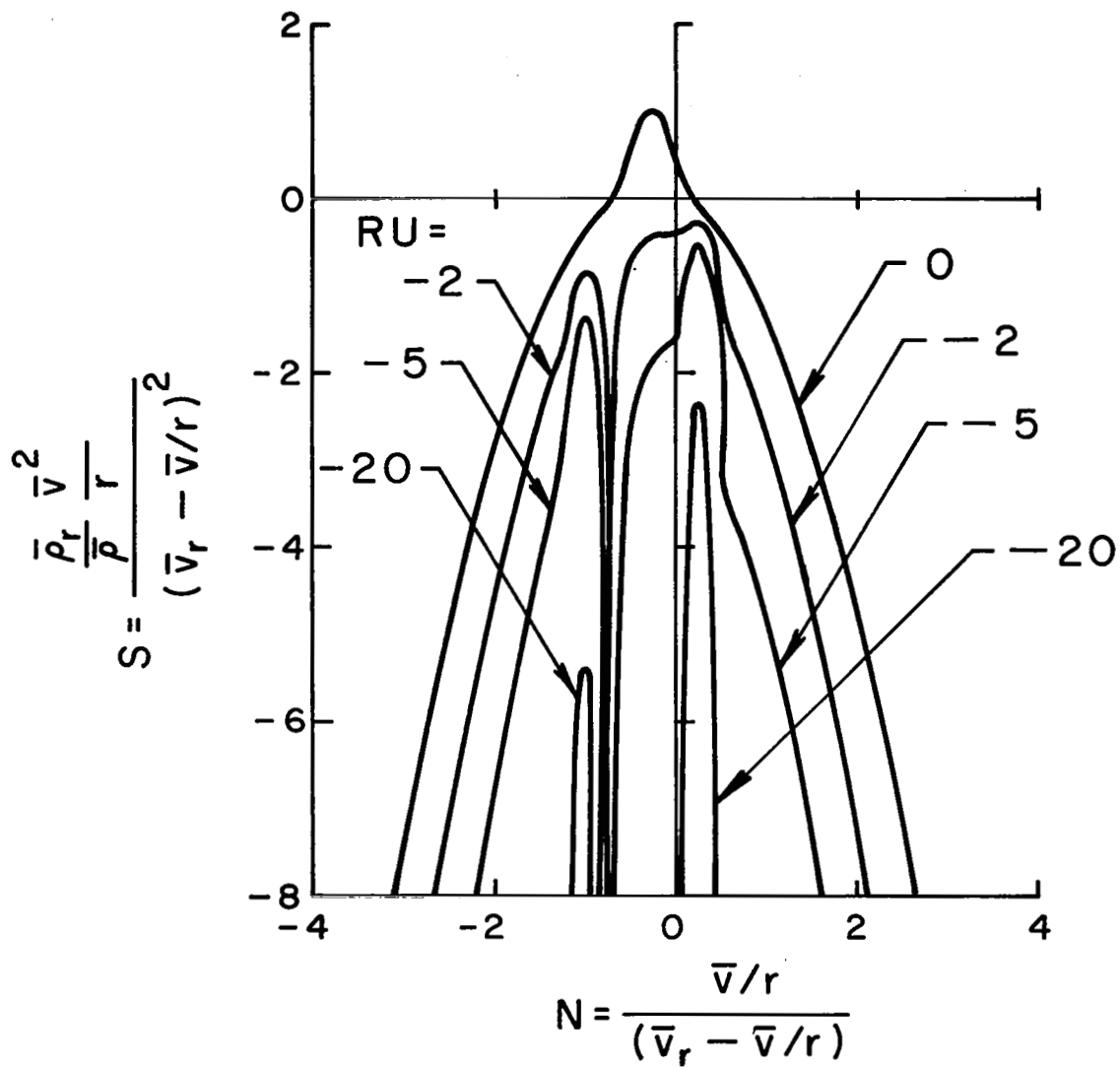
Figure 24. Isopleths for RU (superequilibrium limit) as a
function of swirl number N and Richardson number S .

exhaust flow of a jet engine may be intimately related to the modification of the turbulent stability of the jet.

VII.   CONCLUSIONS

A first look has been made at using second-order velocity correlations predicted from second-order closure turbulent transport theory to predict the generation of aerodynamic sound. It is suggested that second-order turbulent transport theory, in its present form, does contain turbulent statistical quantities which appear in several formulations of the aerodynamic sound generation problem. It is also suggested that second-order closure transport theory might be extended or modified to directly compute fluctuations which appear explicitly as source terms in current aerodynamic sound formulations.

Several calculations of complex jet flowfields have been undertaken to illustrate the versatility of second-order closure turbulent modeling. These computations include swirled and non-swirled jets and a flowfield simulating exhaust from a multitube nozzle. It has been shown, with second-order closure turbulent transport theory coupled with Ribner's formulation of the aerodynamic sound generation problem, that swirling the exhaust of a cold jet does not offer any appreciable sound power reduction over a nonswirled equal thrust jet. It is suggested that the stabilizing/destabilizing effect present when the jet flow is hot and is swirled, which is not included in our current model, may in fact explain this apparent contradiction with measured data.

VIII.   REFERENCES

1.   Ribner, H.S.: "The Generation of Sound by Turbulent Jets," *Advances in Applied Mechanics,* edited by H.L. Dryden and Th. von Karman, Academic Press, New York, 1964, pp. 103-182.

2.   Lighthill, M.J.: "On Sound Generated Aerodynamically; I General Theory," *Proceedings of the Royal Society,* Vol. A211, No. 1107, March 1952, pp. 564-587.

3.   Lilley, G.M., Morris, P.J., and Tester, B.J.: "On the Theory of Jet Noise and its Applications," *The Generation and Radiation of Supersonic Jet Exhaust Noise,* edited by H.E. Plumblee, Jr., AFAPL-TR-74-24, 1974, pp. 37-51; also *Progress in Astronautics and Aeronautics - Aeroacoustics: Jet and Combustion Noise; Duct Acoustics,* Vol. 37, edited by H.T. Nagamatsu, J.V. O'Keefe, and I.R. Schwartz, AIAA, New York, 1975, pp.3-39.

4. Yates, J.E., and Sandri, G.: "Bernoulli Enthalpy: A Fundamental Concept in the Theory of Sound," *Progress in Astronautics and Aeronautics - Aeroacoustics: Jet Noise, Combustion and Core Engine Noise,* Vol. 43, (Edited by I.R. Schwart, H.T. Nagamatsu and W.C. Strahle.) AIAA, New York, 1976, pp. 65-89.

5. Lewellen, W.S., and Teske, M.E.: "Turbulence Modeling and its Application to Atmospheric Diffusion, Part II: Critical Review of the Use of Invariant Modeling," EPA Report No. EPA-600/4-75-016b, A.R.A.P. Report No. 254, Part II. December 1975.

6. Donaldson, C. duP.: "Construction of a Dynamic Model of the Production of Atmospheric Turbulence and the Dispersal of Atmospheric Pollutants," Published in *American Meteorological Society Workshop on Micrometeorology,* 1973, pp. 313-392.

7. Bilanin, A.J., Teske, M.E., and Hirsh, J.E.: "A Look at the Deintensification that Results as a Consequence of Vortex Breakdown," Presented at the *Aircraft Wake Vortices Conference,* Department of Transportation, Transportation Systems Center, Cambridge, Mass., March 1977, DOT Report No. FAA-RD-77-68.

8. Sullivan, R.D.: "A Program to Compute the Behavior of a Three-Dimensional Turbulent Vortex," ARL-TR-74-0009, A.R.A.P. Report No. 200, June 1973.

9. Wygnanski, I., and Fiedler, H.: "Some Measurements in the Self-Preserving Jet," *Journal of Fluid Mechanics,* Vol. 38, September 1969, pp. 577-613.

10. Corrsin, S., and Uberoi, M.W.: NACA Report No. 1865.

11. Lush, P.A.: "Measurements of Subsonic Jet Noise and Comparison with Theory," *Journal of Fluid Mechanics,* Vol. 46, Part 3, 1971, pp. 477-500.

12. Lu, H.Y., Ramsay, J.W., and Miller, D.L.: "Noise of Swirling Exhaust Jets," Presented at the *3rd AIAA Aero-Acoustics Conference,* Palo Alto, California, July 1976, AIAA Paper No. 76-510.

13. Schwartz, I.R.: "Jet Noise Suppression by Swirling the Jet Flow," *Progress in Astronautics and Aeronautics - Aeroacoustics: Jet Combustion Noise, Duct Acoustics,* Vol. 37, (Edited by H.T. Nagamatsu, J.V. O'Keefe, and I.R. Schwartz) AIAA, New York, 1975, pp. 191-205.

14. Bilanin, A.J., and Donaldson, C duP.: "Vortex Wakes of Conventional Aircraft," AGARDograph No. 204, May 1975.

1. Report No. NASA CR-2994	2. Government Accession No.	3. Recipient's Catalog No.
4. Title and Subtitle "Application of Second-Order Turbulent Modeling To The Prediction of Radiated Aerodynamic Sound"		5. Report Date June 1978
		6. Performing Organization Code
7. Author(s) Alan J. Bilanin and Joel E. Hirsh		8. Performing Organization Report No.
		10. Work Unit No.
9. Performing Organization Name and Address Aeronautical Research Associates of Princeton, Inc., 50 Washington Road Princeton, New Jersey 08540		11. Contract or Grant No. NAS 2-8832
		13. Type of Report and Period Covered Contractor Report
12. Sponsoring Agency Name and Address National Aeronautics and Space Administration Ames Research Center Moffett Field, CA 94035		14. Sponsoring Agency Code
15. Supplementary Notes		

16. Abstract

Current formulations of the generation of aerodynamic sound by turbulence all require statistical information with regard to the turbulent flowfield. Second-order closure turbulent modeling in its present form is shown to provide some of this statistical information.

The Ribner[1] formulation of the generation of aerodynamic sound is coupled with predictions of second-order velocity correlations and integral scale to estimate the sound radiated from several complicated jet flows. In particular, it is shown that the sound radiated from a cold swirling jet is greater than from its nonswirling equal thrust counterpart.

The noise radiated from the flowfield of a multitube suppressor is estimated and compared with an equal thrust equal diameter Gaussian jet. It is shown that the multitube concept is indeed quieter.

17. Key Words (Suggested by Author(s)) Turbulence Modeling, Aerodynamic Sound, Jet Noise	18. Distribution Statement Unlimited Star Category - 34		
19. Security Classif. (of this report) Unclassified	20. Security Classif. (of this page) Unclassified	21. No. of Pages 73	22. Price* $5.50